SURFACE MODIFICATION OF YTTRIA-STABILISED ZIRCONIA AT NANOSCALE FOR *IN VITRO* STUDY

SOON GINNY

FACULTY OF ENGINEERING
UNIVERSITY OF MALAYA
KUALA LUMPUR

2018

SURFACE MODIFICATION OF YTTRIA-STABILISED ZIRCONIA AT NANOSCALE FOR *IN VITRO* STUDY

SOON GINNY

THESIS SUBMITTED IN FULFILMENT OF THE REQUIREMENTS FOR THE DEGREE OF DOCTOR OF PHILOSOPHY

FACULTY OF ENGINEERING
UNIVERSITY OF MALAYA
KUALA LUMPUR

2018

UNIVERSITY OF MALAYA

ORIGINAL LITERARY WORK DECLARATION

Name of Candidate: Soon Ginny

Matric No: KHA140093

Name of Degree: Doctor of Philosophy

Title of Thesis: Surface modification of yttria-stabilised zirconia at nanoscale for *in vitro* study

Field of Study: Biomaterials and Tissue Engineering

I do solemnly and sincerely declare that:

(1) I am the sole author/writer of this Work;
(2) This Work is original;
(3) Any use of any work in which copyright exists was done by way of fair dealing and for permitted purposes and any excerpt or extract from, or reference to or reproduction of any copyright work has been disclosed expressly and sufficiently and the title of the Work and its authorship have been acknowledged in this Work;
(4) I do not have any actual knowledge nor do I ought reasonably to know that the making of this work constitutes an infringement of any copyright work;
(5) I hereby assign all and every rights in the copyright to this Work to the University of Malaya ("UM"), who henceforth shall be owner of the copyright in this Work and that any reproduction or use in any form or by any means whatsoever is prohibited without the written consent of UM having been first had and obtained;
(6) I am fully aware that if in the course of making this Work I have infringed any copyright whether intentionally or otherwise, I may be subject to legal action or any other action as may be determined by UM.

Candidate's Signature Date:

Subscribed and solemnly declared before,

Witness's Signature Date:

Name:

Designation:

SURFACE MODIFICATION OF YTTRIA-STABILISED ZIRCONIA AT NANOSCALE FOR IN VITRO STUDY

ABSTRACT

This study has utilised a straightforward yet economical approach to fabricate arrays of nanoislands on miscut yttria-stabilised zirconia substrates. These self-assembled nanostructures were produced with two simple procedures: source deposition by powder-suspension-based method and annealing treatment. At varying dwell times, the nanostructures formed on the substrates were observed for their morphology, alignment, and coverage. The use of miscut surfaces has successfully improved the alignment and coverage of nanoislands, in which surfaces with different miscut angles also appeared to influence the spacing between them. Also, the introduction of miscut to the surface has demonstrated to be more effective in fabricating aligned nanostructures at a larger scale. The annealing treatment at 1100 ^{o}C for 5 h has fabricated significantly ordered nanoislands on 10-degree miscut substrates compared to other profiles in this work. Hence, these nanopatterned substrates underwent several characterisations prior to *in vitro* studies involving different types of cells. In particular, osteoblasts, primary bovine chondrocytes, and human mesenchymal stem cells have been used to explore the interaction between cells and nanostructures to ensure the good cytocompatibility of substrates. In comparison with the untreated substrates, the nanopatterned substrates were demonstrated to have a better affinity with water, in other words, a more hydrophilic surface. Their surface roughness at the nanoscale has also been enhanced due to the presence of nanostructures. Energy dispersive x-ray (EDX) and x-ray diffraction (XRD) results showed the respective elements found in the nanopatterned substrate and its phase wherein the elements contained in the substrate agreed well with the XRD results as well. In general, the cells have exhibited positive response in contact with the nanopatterned substrates. Both osteoblasts and chondrocytes have shown an

up-regulated proliferation rate over time. Enhanced cell attachment has also been observed on the nanopatterned substrates, which was attributed to the surface qualities and the availability of extensive anchorage points. The osteoblast differentiation was also believed to be improved by the imposed nanostructures as the ALP activity and mineralisation process were more active compared to those on the control group. On the other hand, it is suggested that further measures are required to facilitate the functionality of cartilage tissue as the enhancement of chondrocyte function was not evident with the use of surface nanofeatures alone. The immunofluorescence staining has also illustrated an outstanding focal adhesion of human adiposed-derived mesenchymal stem cells (ADMSCs) on the nanopatterned samples. As expected, the ADMSC proliferation rate was significantly enhanced at different time intervals in comparison with the untreated samples. The osteogenic potential of nanostructures has also been highlighted in this study.

Keywords: zirconia, ceramic, surface modification

PENGUBAHSUAIAN PERMUKAAN YTTRIA-STABIL ZIRCONIA DI NANOSCALE UNTUK KAJIAN *IN VITRO*

ABSTRAK

Kajian ini telah menggunakan pendekatan yang mudah tetapi ekonomik untuk mengarang susunan nanoislands pada substrat zirkonia yang distabil yttria. Struktur nano berkumpul diri dihasilkan dengan dua prosedur mudah: pemendapan sumber oleh kaedah berasaskan suspensi serbuk dan rawatan penyepuhlindapan. Pada tahan masa yang berlainan, struktur nano yang terbentuk pada substrat diperhatikan untuk morfologi, penjajaran, dan liputan mereka. Penggunaan permukaan vicinal telah berjaya meningkatkan keselarasan dan liputan nanoislands, di mana permukaan dengan sudut yang berbeza juga mempengaruhi jarak di antara mereka. Juga, pengenalan pemotongan ke permukaan telah menunjukkan keberkesanan dalam menyusun struktur nanoisland sejajar pada skala yang lebih besar. Rawatan penyepuhlindapan pada 1100 ^{o}C selama 5 jam telah direka dengan ketara mengarahkan nanoislands pada substrat 10 darjah berbanding dengan profil lain dalam karya ini. Oleh itu, substrat nanopattern ini menjalani beberapa ciri sebelum kajian *in vitro* yang melibatkan pelbagai jenis sel. Khususnya, osteoblas, chondrocytes bovine primer, dan sel stem mesenchymal manusia telah digunakan untuk meneroka interaksi antara sel dan struktur nano untuk memastikan ketoksikan sitokompatibiliti yang baik. Sebagai perbandingan dengan substrat yang tidak dirawat, substrat nanopattern mempunyai pertalian yang lebih baik dengan air, dengan kata lain, permukaan yang lebih hidrofilik. Kekasaran permukaan mereka di nanoscale juga telah dipertingkatkan kerana kehadiran struktur nano. Keputusan X-ray dispersi sinar-x (EDX) dan X-ray diffraction (XRD) menunjukkan unsur-unsur yang terdapat di substrat nanopattern dan fasa di mana unsur-unsur yang terkandung di dalam substrat itu dipersetujui dengan baik dengan hasil XRD juga. Secara umum, sel-sel telah menunjukkan tindak balas positif dalam hubungan dengan

substrat nanopattern. Kedua-dua osteoblas dan chondrocytes telah menunjukkan kadar percambahan yang dikawal selia dari semasa ke semasa. Lampiran sel yang dipertingkatkan juga telah diperhatikan di substrat nanopattern, yang disebabkan oleh kualiti permukaan dan ketersediaan kepatuhan yang luas. Perbezaan osteoblast juga dipercayai diperbaiki oleh struktur nano yang dikenakan kerana aktiviti ALP dan proses mineralisasi lebih aktif berbanding dengan kumpulan kawalan. Sebaliknya, adalah dicadangkan langkah-langkah selanjutnya diperlukan untuk mengfungsikan fungsi tisu tulang rawan kerana peningkatan fungsi chondrocyte tidak dapat dilihat dengan penggunaan nanofeatures permukaan sahaja. Pewarnaan imunofluoresen juga menggambarkan lekatan fokus yang luar biasa dari sel stem mesenchymal yang berasal dari adiposed manusia pada sampel nanopattern. Seperti yang dijangkakan, kadar proliferasi ADMSC meningkat dengan ketara pada selang masa yang berlainan berbanding dengan sampel yang tidak dirawat. Potensi osteogenic nanostructures juga telah diketengahkan dalam kajian ini.

Kata kunci: zirkonia, seramik, pengubahsuaian permukaan

ACKNOWLEDGEMENTS

First and foremost, I would like to express my sincere gratitude to my supervisor, Assoc. Prof. Ir. Dr. Belinda Murphy for her guidance, patience, and continuous support have significantly encouraged my postgraduate journey. I would like to thank my co-supervisors, Prof. Dr. Sheikh Ali Akbar and Dr. Chong Pan Pan for their insightful advice and feedback that greatly assisted the study.

I would like to pay my regards to the staff members and technicians in the faculty for their services. I am also grateful to my lab mates for their support and help in getting results of better quality.

Lastly, I would like to show my appreciation for the encouragement from my family and friends throughout this journey.

TABLE OF CONTENTS

LIST OF FIGURES

LIST OF TABLES

LIST OF SYMBOLS AND ABBREVIATIONS

EDX	:	Energy dispersive x-ray
XRD	:	X-ray diffraction
ADMSCs	:	Adiposed-derived mesenchymal stem cells
ZrO_2	:	Zirconia
Al_2O_3	:	Alumina
PSZ	:	Partially stabilised zirconia
NIH	:	National institute of health
TCP	:	Tricalcium phosphate
OCI	:	Osteoclast
FBGC	:	Foreign body giant cells
SBF	:	Simulated body fluid
PLGA	:	Polylactide-*co*-glycolide
CaO	:	Calcia
MgO	:	Ceria
Y_2O_3	:	Yttria
PSZ	:	Partially stabilised zirconia
Ti	:	Titanium
TZP	:	Tetragonal zirconia polycrystal
UV	:	Ultraviolet
CP	:	Calcium phosphate
YSZ	:	Yttria-stabilised zirconia
HA	:	Hydroxyapatite
EPD	:	Electrophoretic deposition
YTZP	:	Yttria-tetragonal zirconia polycrystals

HGF	:	Human gingival fibroblast
HDMEC	:	Human dermal microvascular endothelial cell
L-DOPA	:	3,4-dihydroxy-L-phenylalanine
TiO_2	:	Titanium oxide
RGD	:	Arginine-glycine-aspartate
ECM	:	Extracellular matrix
GDC	:	Gadolinia-doped ceria
FESEM	:	Field emission scanning electron microscopy
AFM	:	Atomic force microscopy
hFOB	:	Human fetal osteoblastic cell
DMEM	:	Dulbecco's modified eagle's medium
FBS	:	Fetal bovine serum
G418	:	Geneticin
PBS	:	Phosphate buffer saline
DMSO	:	Dimethyl sulfoxide
AA	:	Antibiotic-antimycotic
ALP	:	Alkaline-phosphatase activity
GAGs	:	Glycosaminoglycan
EDTA	:	Ethylenediaminetetraacetic acid
DMMB	:	1,9-dimethylmethylene blue
SSC	:	Saline sodium citrate
RT-qPCR	:	Quantitative reverse-transcription polymerase chain reaction
Gd	:	Gadolinium
Ce	:	Cerium
O	:	Oxygen

Y	:	Yttrium
Zr	:	Zirconium
DNA	:	Deoxyribonucleic acid
MSCs	:	Mesenchymal stem cells
ISCT	:	International society for cellular therapy

LIST OF APPENDICES

CHAPTER 1: INTRODUCTION

1.1 Introduction

Bioceramics refer to various forms of ceramic materials with special compositions that are mainly used in orthopaedics and dentistry. Rising failure rates experienced by metallic and polymeric prosthesis have contributed to the rapid development of bioceramics for clinical use (Tiwari & Nordin, 2014). Zirconia (ZrO_2) and alumina (Al_2O_3) are both representative examples of first generation bioceramics, which are characteristically bioinert ceramics (Planell, Best, Lacroix, & Merolli, 2009). The use of zirconia for biomaterial applications was restricted to hip joint replacement, yet in recent years it has been commonly used as a restorative material for dental applications as well (Ko et al., 2007). Alumina has been a popular material for dental applications, but some alumina implants, for example, Tübingen implants, have become obsolete in the market due to the problems of mechanical failure (Sennerby, Dasmah, Larsson, & Iverhed, 2005). The assessment of zirconia dental implants has revealed several advantages over alumina dental implants, such as comparable strength with higher fracture toughness and also a lower cost of production. Besides, partially stabilised zirconia (PSZ) was also suggested to replace alumina for ceramic femoral head prosthesis due to its superior mechanical properties (Planell et al., 2009).

Although zirconia has a superior wear performance to alumina, zirconia has a fatal weakness in that aging phenomena appear in the presence of water. Consequently, the transformation of tetragonal to monoclinic phase leads to surface roughening and cracking (Chevalier, 2006). Hence, partially stabilised zirconia, such as yttria-stabilised zirconia, has been introduced to overcome the issue of phase transformation. For instance, yttria is used to stabilise the tetragonal or cubic phase. Yttria-stabilised tetragonal zirconia polycrystals are of high interest in clinical application owing to their

good fracture resistance and flexural strength (Stadlinger, Hennig, Eckelt, Kuhlisch, & Mai, 2010).

The interaction between cells and materials is also an important aspect of successful *in vitro* and *in vivo* studies. Material biocompatibility can be improved through surface modification. A number of surface modification techniques have been developed and applied to investigate and improve the biological response of tissue. The influence of surface characteristics including surface topography, surface chemistry, and surface energy on cellular response has often been studied as reported in the literature (Att et al., 2009; Liu et al., 2007). For example, surface roughness has been demonstrated to affect cell growth and activity (Faia-Torres et al., 2014; Liu, Wu, Ai, Han, & Hu, 2015).

The topological and physicochemical properties manipulate the osteoconductivity of implants; meanwhile, the level of osteoconductivity is represented by the peri-implant osteogenesis (Kono et al., 2015; Ueno, Tsukimura, Yamada, & Ogawa, 2011). Surface topographies have also been demonstrated to regulate and alter cell morphology in several studies (Ghrebi, Hamilton, Douglas Waterfield, & Brunette, 2013; Kiang, Wen, del Álamo, & Engler, 2013). Additionally, surface pattern on the material can be used to guide cell growth and orientation (Laranjeira et al., 2014). The physicochemical properties of the biomaterials are also of vital importance as enhanced cell adhesion and proliferation results in a higher bone-implant contact and strengthening of the biomechanical interaction (Gehrke, 2013). The process of inflammation, bone remodelling activities, and bone formation response can also be regulated by altering the physicochemical properties (Omar et al., 2010; Wennerberg & Albrektsson, 2009).

Advances in surface modification technologies have also contributed to the reduced healing time before loading the implant (Lazzara, Testori, Trisi, Porter, & Weinstein, 1999). The healing time is a period in which the implant is not subjected to loading,

estimated at 3 to 6 months (Šimůnek, Kopecká, & Strnad, 2004). The healing process is affected by the interaction between materials and cells in the biological environment and can be accelerated by rapid tissue integration (Helmus, Gibbons, & Cebon, 2008; Zheng et al., 2011).

Development of emerging nanotechnology has brought significant impact to society and environment due to its wide-ranging application to biomedical science, electrical engineering, and the material industry. Surface patterning is one of the techniques used in surface modification, as it can be applied to alter the surface by creating or transfer a pattern on the surface of the material (Govindarajan & Shandas, 2014). Surface patterning, a process able to fabricate structures at nanoscale, has been implemented for different applications such as miniaturization of integrated semiconductor devices (Crnogorac et al., 2007), DNA separation (Ogawa, Ogawa, Oki, Hashioka, & Horiike, 2007), tissue engineering (Gadegaard, Martines, Riehle, Seunarine, & Wilkinson, 2006), and biosensors (Lim & Donahue, 2007). Surface nano-patterning can be achieved by several methods such as laser irradiation, e-beam lithography, ion beam sputtering, and self-assembly (Gago et al., 2002; Hong, Huang, Luk’yanchuk, & Chong, 2003; MacManus‐Driscoll, 2010; Mendes et al., 2004). Lithography, which is one of the approaches used in patterning, is capable of fabricating pattern feature sizes from nanoscale up to microscale. Complex patterns can be produced with ease by combining other techniques including etching and deposition. However, these techniques are costly and have low throughput, making them incompatible for mass production (Pimpin & Srituravanich, 2011). Hence, there is a need to explore alternative processes that are inexpensive and suitable for industrial production.

Surface modification has also been conducted using self-assembly approaches as observed in different types of materials (Foston et al., 2012; Shu, Ou, Wang, Zou, & Li,

2011). Nanoscale self-assembly, one of the important branches of nanotechnology, is defined as "the autonomous organization of components into patterns or structures without human intervention" (Whitesides & Grzybowski, 2002). Self-assembly occurs via direct interaction such as interparticle force or indirect method with the use of template or external field. A certain degree of control is necessary in order to prepare an efficient build-up of nanoparticles for advanced applications (Grzelczak, Vermant, Furst, & Liz-Marzán, 2010). A self-assembly technique has been adopted in the semiconductor industry for quantom dot application (Lu & Sastry, 2007). Although islands formed on semiconductor systems show uniform size and shape, their self-ordering is not significant without guidance through lithography or other techniques (Rauscher, Boyne, Dregia, & Akbar, 2008).

Rauscher et al. (2008) first discovered self-assembly in a whole new class of materials (gadolinia-doped ceria/yttria-stabilised zirconia system) where spontaneous self-assembled nanoislands with consistent orientation relationship were observed. The properties of these nanoislands are different from the usual self-assembled semiconductor islands, such as high oxygen conductivity, good chemical stability under extreme temperature, high hardness and good transparency to the visible light, rendering possible new applications (Rauscher et al., 2008). Ansari et al. (2013) further investigated the mechanism of formation of self-assembled nanoislands, in which the breakup of surface layer into nanostructures occurred due to stress buildup. Additionally, a simple yet versatile powder-suspension-based method was proven to produce arrays of nanoislands. This provides an alternative to conventional lithography techniques in the fabrication of nanopatterns (Ansari et al., 2013).

Cell-substrate interaction is one of the crucial factors in determining biocompatibility, whether for designing medical implants or developing tissue

engineering applications. Surface features at nanoscale provide direct mechanical interactions with cell receptors and components, in turn regulating the cells to fulfil the intended purpose. In particular, nano-features in tissue engineering applications allow cells to perceive them as microenvironment-like substances or cell microenvironments (An, Chua, Yu, Li, & Tan, 2013). Nanofeatures have been applied to dictating stem cell fate (Griffin, Butler, Seifalian, & Kalaskar, 2015), biomolecule interaction at interfaces (Psarra et al., 2015), fabrication of biomimetic scaffold (Wan et al., 2015), and modulation of protein adsorption and cellular response (Ercan, Khang, Carpenter, & Webster, 2013).

The present research was divided into three parts:

1. Study of the effect of annealing hour and miscut angles on the formation of self-assembled nanostructures. Throughout the entire study, the powder-suspension-based method was used to deposit the gadolinia-doped ceria (GDC) source on the substrates. The formation of nanostructures was observed and optimisation based on annealing hour was conducted.
2. Choice of the optimal annealing profile based on the formation and alignment of nanoislands for subsequent characterisation study. The nanostructured substrates fabricated by the optimised profile were subjected to a series of characterisation including X-ray diffraction analysis, energy-dispersive spectroscopy analysis, surface wettability, and surface roughness prior to *in vitro* studies. The untreated substrates acted as a control group in the *in vitro* studies.
3. Investigation of cell behaviour on the nanostructured samples in comparison with the unmodified/control samples. Different cell sources (human foetal osteoblast, primary bovine chondrocytes, and human adiposed-derived mesenchymal stem cell) were used in the *in vitro* study for evaluating various cellular responses.

1.2 Problem Statement

Although zirconia is known to be the first generation of bioceramic, as mentioned by Planell et al. (2009), there is still a continuous need to improve the cell and material interaction. This improvement is necessary to further reduce the long healing time before loading the implant as mentioned by Simunek et al. (2004). With the growing demand to enhance cell and material interaction, surface patterning was introduced. One of the techniques introduced to address this issue was lithography which was widely known to produce very systematic structures with nanoscale to microscale features. However, Pimpin & Srituravanich (2011) had reported that lithography method was not suitable for a mass scale production due to its low output and high cost.

Self-assembly method was introduced and implemented in the semiconductor industry first, then found to be viable in gadolinia-doped ceria/yttria-stabilised zirconia system by Rauscher et al. (2008). This method was found to be simplistic and versatile to be implemented in a larger scale unlike lithography. One of the limitations of self-assembly is that lithography is still needed to assist the ordering of nanostructures. However, the self-assembled nanostructures produced in the GDC/YSZ system has demonstrated significant ordering without the use of lithography.

1.3 Objectives

This study focuses on the fabrication of self-assembled nanostructures via powder-suspension-based approach followed by *in vitro* studies using different types of cells, to study the biocompatibility of the materials and the influence of the nanostructures on the cell growth and behaviour.

The objectives of this study are as follow:

i. To investigate the formation of YSZ/GDC nanoislands by varying the annealing time and miscut angle.

ii. To improve the alignment of nanostructures by using miscut surface.

iii. To examine the effect of nanostructures on the behaviour of osteoblasts.

iv. To evaluate the morphology and functions of chondrocytes elicited by nanostructures.

v. To investigate the growth and osteogenic differentiation of mesenchymal stem cells on nanostructures.

1.4 Thesis Structure

In chapter 2, a brief review of the types of biomaterials is presented, followed by a study of the background of zirconia ceramics. An intensive review of various surface modification techniques that have been conducted on zirconia for *in vitro* and *in vivo* studies is included, in which the cellular response to the surface-modified zirconia and biological response of animal model are discussed thoroughly. Finally, the mechanism of self-assembly of YSZ/GDC nanostructures is explored.

Chapter 3 presents the fabrication of self-assembled nanostructures and characterisation methods used in this study. The cell culture techniques and culture conditions are provided in detail; meanwhile, the cell isolation method and cell characterisation protocol are also included. Lastly, the procedures conducted to measure the growth and behaviour of different cells will be laid out in this chapter.

Results and discussion are presented in Chapter 4. The effect of miscut angles and annealing time on the formation of nanostructures are examined. A thorough discussion is also presented to study the cell behaviour in response to the nanostructures, in which

the biocompatibility of the nanostructured materials is indicated by the overall cellular response as revealed by the *in vitro* studies.

Lastly, Chapter 5 concludes with the findings and provides suggestions for future work.

CHAPTER 2: LITERATURE REVIEW

2.1 Introduction

The National Institute of Health (NIH) defined a biomaterial as:

> "any substance (other than drug) or a combination or substances, synthetic or natural in origin, which can be used for any period of time, as a whole or a part of a system which treats, augment, or replaces any tissue, organ, or function of the body" (NIH, 1982, p. 1).

In 2009, William redefined biomaterial as:

> "a substance that has been engineered to take a form which, alone or as part of a complex system, is used to direct, by control of interactions with components of living systems, the course of any therapeutic or diagnostic procedure, in human or veterinary medicine" (Williams, 2009, p. 5908).

An ideal biomaterial should have good mechanical properties and biocompatibility. A biomaterial should not evoke an inflammatory response in the host (Tiwari & Nordin, 2014). The intensity and duration of inflammatory response are the benchmarks for the biocompatibility of a biomaterial.

Biomaterials are further classified into four categories: metals, polymers, ceramics, and composites. Metals and alloys are commonly used for orthopaedic and dental applications such as hip and knee joint replacement, and dental restoration (Goriainov, Cook, Latham, Dunlop, & Oreffo, 2014; Knosp, Holliday, & Corti, 2003; Sansone, Pagani, & Melato, 2013). The common use of metals for biomedical applications is due to their reliable mechanical strength and toughness. The typical biometals used are stainless steel, cobalt alloys, titanium, and titanium alloys (Hanawa, 2002; Niinomi, 2008). In general, all biometals are corrosion-resistant. This is an important

characteristic, as the release of metal ions, corrosion products, and wear debris can cause toxicity in a biological environment (Hanawa, 2002).

Compared to metal, ceramics possess superior compressive strength, corrosion and wear resistance, good electric and thermal insulators. These are some of the important characteristics for biomaterials. However, due to the ionic bonding in ceramics, it is difficult for ceramics to be sheared plastically and this contributes to their brittleness and low tensile strength (Munz & Fett, 2013). The details of bioceramics will be discussed in Section 2.2.

In comparison with metals and ceramics, polymers are the most versatile biomaterials as they can be tailored to fulfil the mechanical, electrical, chemical, and interfacial requirements of various biomedical applications. Their ease of fabrication also allows the polymers to be made into different shapes and structures (Teo et al., 2016). Polymers can be made artificially or found in nature. Synthetic polymers are more cost-effective and commercially available, but they are lacking biodegradability, an important quality of a natural polymer (Angelova & Hunkeler, 1999; Teo et al., 2016). However, natural polymers are not suitable for mass production due to the difficulty in purification and modification (Angelova & Hunkeler, 1999). Representative naturally occurring polymers include collagen and chitosan, the two most abundant natural polymers, which have been studied in detail due to their biocompatibility and ease of processing (Shoichet, 2009). Despite that, it is difficult to obtain natural polymers in bulk and process them for application. Moreover, the degradation rate of natural polymers is inconsistent (Sabir, Xu, & Li, 2009).

Lastly, composite materials are a heterogeneous combination of two or more distinctly different constituent materials. The characteristics of composites material vary highly depending on the structure, most notably the shape of the heterogeneities (Park &

Lakes, 2007). The advantage of composite biomaterials is that they can exhibit the desirable properties of their constituent materials or even express certain properties that do not belong to the single constituent material (Salernitano & Migliaresi, 2003). Composites materials are gaining popularity because of the above advantage.

2.2 Bioceramics

Bioceramics consist of a class of inorganic non-metallic materials which are popular choices in hip-joint applications, dental implants, and bone replacements (Burdick & Mauck, 2010). The clinical use of bioceramics began with the use of porcelain in dental crowns in the late eighteenth century while gypsum was used for orthopaedics applications in the late nineteenth century (Chevalier & Gremillard, 2009). Bioceramics comprise several types of materials including ceramics, bioglasses, and glass-ceramics, and are in general classified into three classes: bioinert, bioresorbable and bioactive ceramics. *In vivo* reactivity is a key factor in classifying the bioceramics (Planell et al., 2009).

2.2.1 Bioinert

Bioinert ceramics are first generation bioceramics, characterised by the possibility of soft tissue interplay at the bone-implant interface inhibiting the bone from forming a bond with the bioinert material (Planell et al., 2009). Bioinert ceramics barely experience chemical changes when they are placed in physiological environments. Hence, their physical and mechanical properties are retained in the *in vivo* situation (De Aza, De Aza, & De Aza, 2005). However, due to their bioinertness, these ceramics trigger a foreign body reaction after implantation. The formation of fibrous tissue surrounding the implant isolates it from the host (Castner & Ratner, 2002). In consequence, a thick layer of fibrous tissue would cause implant failures due to worsening interfacial micromovement (Planell et al., 2009).

Representative examples of bioinert ceramics include alumina, zirconia, alumina-ziconia, and carbonaceous materials (De Aza et al., 2005). The use of alumina as a biomaterial was first reported in the sixties as bone substitute and dental implant (Sandhaus, 1967; Smith, 1963). Today, alumina bioceramics have been widely used for orthopaedic applications, especially total hip prostheses because of their biocompatibility and good resistance to corrosion and wear. However, to avoid loosening of acetabular component, alumina is only used for the femoral head as a alumina/ultrahigh-molecular-weight polyethylene pair has shown to reduce wear debris significantly in clincal studies in comparison with a alumina/alumina pair (De Aza et al., 2005).

Tübingen implants were one of the most popular alumina dental implants that were used for the tooth replacement in the maxilla and mandible area (Albrektsson, Zarb, Worthington, & Eriksson, 1986). However, the failure of these implants was due to the low flexural strength that caused cross-sectional fracture (De Aza et al., 2005). The use of single crystal alumina as dental implant was attributed to its flexural strength (13,000 kg/cm^2) which is 3 times higher than that of polycrystalline alumina (3800 kg/cm^2). Despite that, the mechanical strength of single crystal alumina would be a concern as lattice imperfections on the surface could cause brittle fracture of the material (Kawahara, Hirabayashi, & Shikita, 1980).

2.2.2 Bioresorbable/biodegradable

Bioresorbable ceramics are the second generation bioceramics, characterised by dissolving after a specific period. They are specially designed to promote self-repair of tissue and degrade to avoid complications associated with synthetic material in the host (Planell et al., 2009). In general, these materials serve as a scaffold for the living cells to grow and encourage tissue regeneration, at the same time as providing mechanical

support, and degrading so as to be eventually removed from the body. However, the rate of ceramic degradation and the formation of living tissue are required to be in control to avoid undesirable decrease in mechanical properties of the materials which would eventually affect the functionality of the material (Sheikh et al., 2015).

Typical examples of resorbable bioceramics include calcium sulphate and calcium phosphate. Calcium phosphate-based materials are chemically similar to the nature bone tissue and allow integration with the bone remodelling process (Su et al., 2014). The use of tricalcium phosphate was first reported in 1920 to fill the bone gaps in rabbit, and faster bone growth was observed (Albee, 1920). Tricalcium phosphate has been commonly used to fill bone defects in dental and orthopaedic applications because they are capable for forming a bone with the bone (Su et al., 2014).

Several studies have demonstrated active resorption of tricalcium phosphate causes rapid new bone formation (Bohner, 2001; Cutright, Bhaskar, Brady, Getter, & Posey, 1972). Osteoconduction is a phenomenon in which the integration of a biomaterial with bone takes place and allows ingrowth of tissue (Khan, Rayan, Dhinsa, & Marsh, 2011). A successful graft-bone remodelling process relies on good osteoconductivity and resorption of the material (Sheikh et al., 2015). A recent study has sought to control the osteoclast resorption of tricalcium phosphate by tuning the surface architecture of the material. It was observed that osteoclasts survived on submicrostrucured tricalcium phosphate instead of microstructured tricalcium phosphate, and resorption of tricalcium phosphate could not take place without osteoclast-specific machinery. As seen in figure 2.1, the surface microstructure of tricalcium phosphate which was resorbed by osteoclast appears to have smaller grains and enhanced microporosity (Davison et al., 2014).

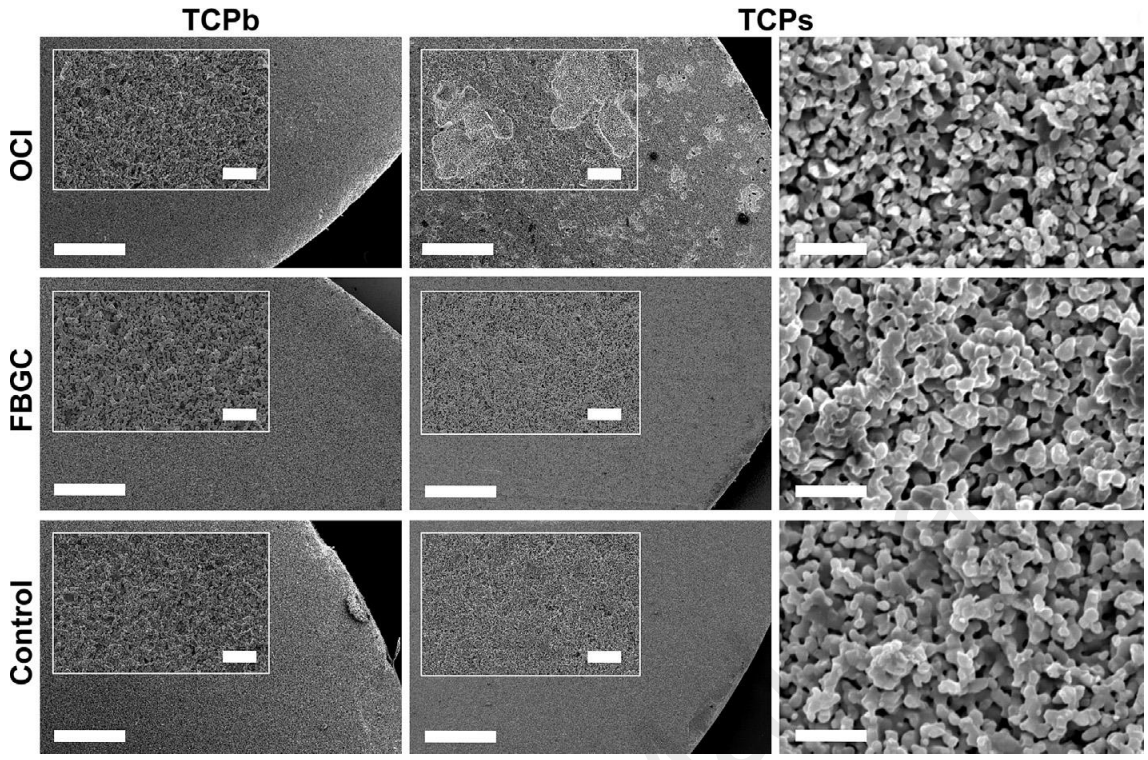

Figure 2.1: Scanning electron micrographs of tricalcium phosphate on microstructured (TCPb) and submicrostructured tricalcium phosphate (TCPs) after removal of osteoclast (OCI) and foreign body giant cells (FBGC). The control reference was incubated without cells. Overview scale = 500 µm; inset scale = 50 µm (Davison et al., 2014).

2.2.3 Bioactive

Bioactive ceramics are also known as second generation bioceramics. Their surface reactivity allows ingrowth of new bone to take place and form a tight bond between the implant and tissues. Reaction with physiological fluids takes place on the surface of bioactive materials, forming an apatite layer, which can form new bone in the presence of living cells. Bioactive ceramics are ideal candidates for prosthetic applications, in which the bond between tissue and prosthesis is crucial, as successful development of biomaterial is highly reliant on the interaction at the cell-material interface. Bioglasses, which are bioactive ceramics, present several advantages, including their degradability and ability to stimulate the formation of new tissue. The best known bioglass is Bioglass

45S5, which was discovered in 1969 by Hench. The bioglasses of the second generation bioceramics are known to form bonding with the host tissue; meanwhile, the bioglass of the third generation bioceramics possess gene activation properties for the tissue regeneration process. The next generation of bioactive ceramics is expected to stimulate tissue regeneration through the ceramics being loaded with biologically active molecules (Planell et al., 2009). The concept of "smart" bioactive orthopaedic implants has also been described as producing "smart" materials which have excellent biocompatibility, in situ sensing, and are able to promote growth of tissue (Tran, Sarin, Hurt, & Webster, 2009).

Bioactivity can also be divided into two classes which are osteoproductive and osteoconductive materials. Osteoproductive materials elicit both intracellular and extracellular responses at the interface, whereas osteoconductive materials only obtain extracellular responses (Tran et al., 2009). Osteoproduction has also been introduced as osteoinduction, due to its ability to induce bone production without direct contact with bone (Jones, Gentleman, & Polak, 2007). Kokubo and Takadama (2006) have concluded an efficient approach to investigate osteoproductivity to screen biomaterial by soaking the materials in simulated body fluid (SBF) and observe the apatite formation (Figure 2.2). This could also help to reduce experimentation involving animals (Kokubo & Takadama, 2006).

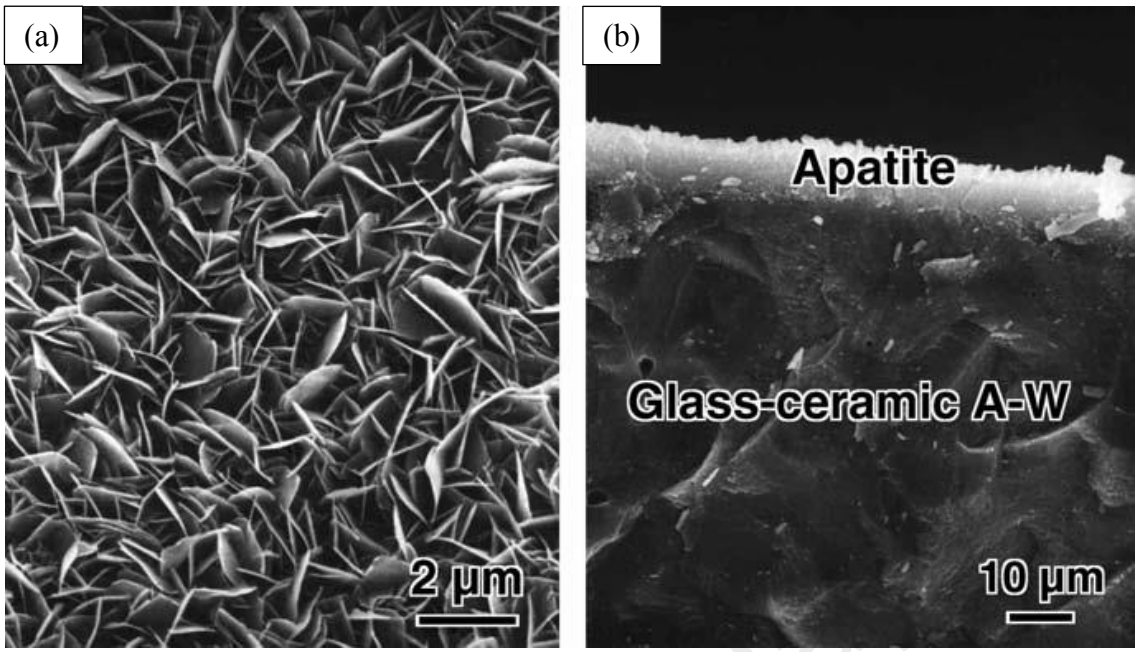

Figure 2.2: (a) Scanning electron micrograph showing the formation of apatite on the surface of glass-ceramic apatite–wollastonite; (b) Cross-sectional image of apatite layer (Kokubo et al., 1990).

According to Langer and Vacanti (1993), "Tissue engineering is an interdisciplinary field that applies the principles of engineering and the life science toward the development of biological subsitutes that restore, maintain, or improve tissue function" (p. 920). Three key aspects are included in designing a tissue-engineered construct: cells, scaffold, and regulatory signals (Langer & Vacanti, 1993). Scaffolds seeded with cells and growth signals serve as a template for the formation of tissue. They can be implanted at the site directly or later after being cultured *in vitro* (O'Brien, 2011).

Hydroxyapatite, tricalcium phosphate, and bioactive glass are among the popular materials for bone tissue engineering as they can form a direct bond with living tissue after implantation. Although bioactive ceramics have been proven to improve osteoblast growth and differentiation, their brittleness and slow degradation rate has limited their clinical application. Load bearing applications require support from the ceramic scaffold to sustain the mechanical loading. The fracture toughness and compressive strength of

weight-bearing bone in the human body are 2-12 MPa·$m^{1/2}$ and 130-180 MPa respectively (Gao et al., 2014). However, conventional sintered dense hydroxyapatite has been reported to possess fracture toughness of 0.61-1.06 MPa·$m^{1/2}$ whereas three-dimensional printed tricalcium phosphate scaffolds have a compressive strength of 1.75-5.48 MPa, which is much lower than that of weight-bearing bone (Fielding, Bandyopadhyay, & Bose, 2012; Wang & Shaw, 2009). Hence, further improvements are required to enhance the respective mechanical strength of ceramics in favour of meeting the demand of load bearing applications.

2.2.4 Methods to Improve Mechanical Properties of Bioceramics

Other than controlling the crack growth, second phase additions including fibre, whisker, and particles have also been applied to enhance the toughness of bioceramics. For example, the structural integrity and the material strength of polylactide-*co*-glycolide (PLGA) fibre-reinforced calcium phosphate bone cement were greater in comparison with non-reinforced calcium phosphate bone cement (Losquadro, Tatum, Allen, & Mann, 2009). Filamentary growths of single crystals, also known as whiskers, have been used as reinforcements to strengthen different ceramic materials, including calcium phosphate cement and hydroxyapatite, due to their superior tensile strength (Becher, Hsueh, Angelini, & Tiegs, 1988; Bose, Banerjee, Dasgupta, & Bandyopadhyay, 2009; P. Zhao et al., 2012). Despite the enhanced strength and toughness of ceramics, the second-phase additions impose limitations due to the toxicity of whisker and diminished biocompatibility (Gao et al., 2014).

Recent advancements in nanotechnology have brought revolutionary changes to the research of biomaterials in terms of mechanical and biological performance. Compared to conventional materials, nanomaterials possess enhanced strength and toughness due to the reduced defects in materials, as the crystalline grains are nanometres in size

(Meyers, Mishra, & Benson, 2006). The fracture toughness of nanoceramics can be improved by the decrease in lattice dislocation slip as the grain size is smaller, and also enhanced grain boundary sliding and migration (Chokshi, 1990). Owing to the smaller grain size and larger surface area with stronger interfacial interactions, nanomaterials also gained superior torsion and tensile modulus. Thus, nanoceramics have been put forward as a promising solution to the brittleness of bioactive ceramics (Gao et al., 2014).

2.3 Background Study of Zirconia Bioceramic

Zirconium oxide (ZrO_2), also known as zirconia was discovered by a German chemist known as Martin Heinrich Klaproth in 1789. Desirable mechanical strength, toughness and chemical stability have made zirconia an interesting biomaterial (Piconi & Maccauro, 1999). Zirconia offers several advantages over alumina in terms of higher fracture toughness, lower friction and wear. It is also reported to have high bending and compression strength, and shares similar mechanical properties to those of stainless steel (Piconi & Maccauro, 1999; Planell et al., 2009). The biomedical application of zirconia was first reported by Helmer and Driskell in 1969, in which zirconia was used for the total hip replacements as ball heads (Helmer & Driskell, 1969).

Figure 2.3: Zirconia screw implant (bar = 10 mm) (Akagawa, Ichikawa, Nikai, & Tsuru, 1993).

Zirconia was first applied for dental applications in 1993 (Figure 2.3) (Akagawa et al., 1993). An important characteristic of zirconia is its white or tooth colour which makes it greatly valued in terms of its dental aesthetics. Tooth-coloured zirconia has been used to address the problems of implant discoloration, which otherwise causes a bluish-grey colour on a patient's overlying skin (Figure 2.4) (Langhoff et al., 2008; Park, Shin, Choi, & Kim, 2013). This aesthetical characteristic has also provided an alternative to solving the problem of insufficient soft tissue for covering up the greyish titanium implant (Kimura, Matsuzaka, Yoshinari, & Inoue, 2012). Besides, zirconia dental implants can be fabricated at a lower cost and provides higher fracture toughness than single crystalline alumina dental implants (Planell et al., 2009).

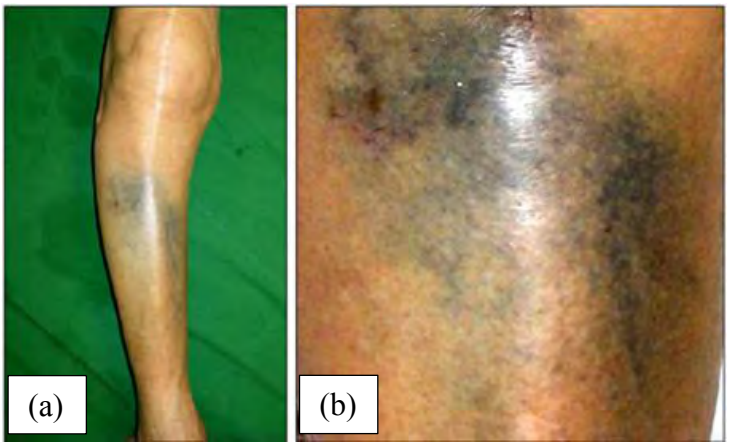

Figure 2.4: Bluish discoloration caused by titanium alloy prosthesis is observed on the right shin of patient (Park et al., 2013).

Zirconia presents in polymorphs which are known as monoclinic, tetragonal, or cubic- phase. Pure zirconia is in monoclinic phase at room temperature (Planell et al., 2009). The cubic-to-tetragonal and tetragonal-to-monoclinic phases take place below 2370 ^{o}C and 1170 ^{o}C respectively. The transformation of tetragonal to monoclinic phase induces high internal compressive stress, which is caused by the 3-5% volume expansion (Chevalier, 2006; Conrad, Seong, & Pesun, 2007). The stresses crack pure zirconia into pieces at room temperature after sintering at 1500-1700 ^{o}C. Hence, additives such as calcia (CaO), magnesia (MgO), ceria (CeO_2), or yttria (Y_2O_3) are added to stabilise the tetragonal or cubic phases of zirconia. These multiphase materials are known as partially stabilised zirconia (PSZ) (Piconi & Maccauro, 1999).

In general, cubic zirconia constitutes the microstructure of PSZ as the major phase at room temperature, whereas the tetragonal and monoclinic precipitates make up the minor phase. When a crack happens, the transformation of tetragonal precipitates into monoclinic phase is accompanied by expansion, in which the stress field generated acts opposite to the stress field, thus discouraging crack propagation (Piconi & Maccauro, 1999). In other words, the compressive stresses caused by the volume expansion

counteract the external tensile stresses at the crack tip. This phenomenon of detaining crack propagation is known as transformation toughening (Conrad et al., 2007). Yttria-stabilized tetragonal zirconia polycrystals are of immense interest for medical applications due to their fracture resistance and flexural strength, which reduce the risk of mechanical failure of the materials (Stadlinger et al., 2010).

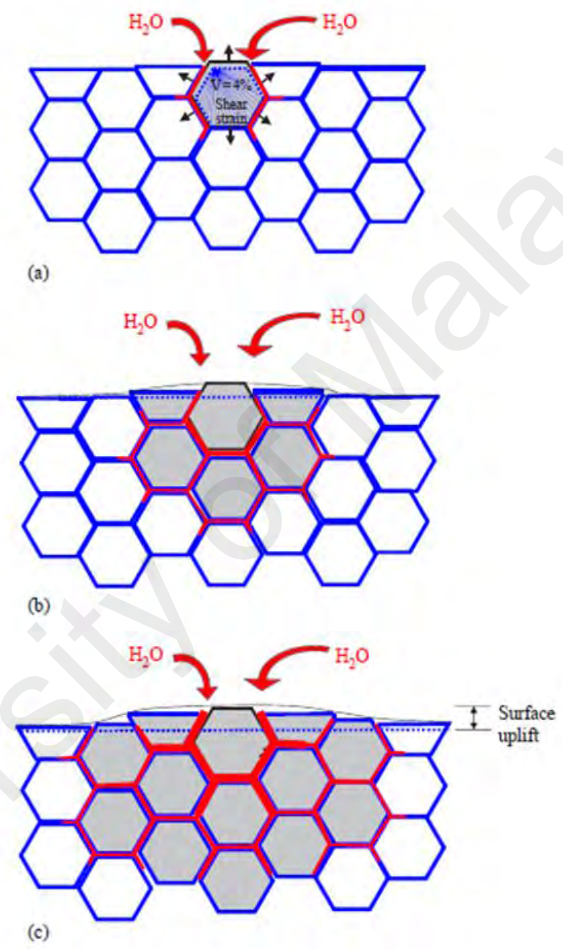

Figure 2.5: Schematic diagram of aging process of zirconia ceramics (Chevalier, 2006).

The use of zirconia for biomedical applications is limited mainly due to degradation and radiation. Radioactive impurities have been found in some zirconia materials (Planell et al., 2009). However, the radioactive potential of zirconia ceramics has been concluded to be less significant compared to the radioactive appliances in the

surroundings (Bavbek, Ozcan, & Eskitascioglu, 2014). Degradation caused by the phase transformation, which was accelerated in the aqueous environment, especially under dynamic loading, has been a long-term concern in the clinical application of zirconia biomaterials (Planell et al., 2009). Figure 2.5 illustrates the aging process of zirconia ceramics. In the presence of water or vapour, surface transformation to the monoclinic phase takes place and the transformation of one grain causes stress to the neighbouring grains due to the volume expansion. This leads to microcracking and allows water to penetrate into the material (Chevalier, 2006). To date, the study of the mechanism of zirconia degradation is still on-going. Doping is one of the methods used to improve the hydrothermal stability of zirconia (Tredici et al., 2016). Nevertheless, there is huge room for improvement to resolve the long term degradation issue of zirconia.

2.4 Surface Modification of Zirconia for In Vitro Studies

The surfaces of materials are uniquely reactive with properties that are different from the bulk materials. Altering the surface properties through surface modification techniques has always aimed to enhance the biological performance of the material's surface and retain the bulk properties at the same time. According to Liu et al., surface properties including surface energy, surface charge, wettability, surface chemistry, and surface topography, have great impact on the biological performance of a biomaterial. The mechanism of cell adhesion has been actively researched for over 50 years. This is due to the attachment and adhesion of anchorage-dependent cells are of crucial importance in the early stage of cell-material interactions, which eventually determine the success of implanted biomaterials (Liu et al., 2007).

Plenty of studies have been conducted to investigate the influence of surface modified zirconia on cellular response and its performance in in vivo studies. According to Depprich et al. (2008), the clinical use of zirconia bioceramics is limited as it is

challenging to produce modified surface. Different approaches have been applied to modify and improve the surface properties of biomaterials. Milling and sandblasting are two common techniques used to modify the surface of zirconia bioceramics. Nevertheless, technology advance in recent years allows exploration of several novel approaches such as laser-irradiation and coating for the surface treatment of zirconia (Aboushelib, Osman, Jansen, Everts, & Feilzer, 2013).

2.4.1 Sandblasting

Two main approaches; optimisation of roughness, and application of bioactive coating, are often applied to improve the surface properties. Optimisation of roughness can be achieved by sandblasting and acid-etching (Langhoff et al., 2008). Machined surfaces which are often classified as unmodified surfaces, and sandblasted surfaces have thus far been commonly observed in the studies of zirconia for biomaterial application (Soon, Pingguan-Murphy, Lai, & Akbar, 2016). Sandblasting, which is also known as airborne particle abrasion, produces a rougher surface compared to a machine and polished surface as shown in Figure 2.6. This technique results in a surface with micro-roughness (Aboushelib et al., 2013).

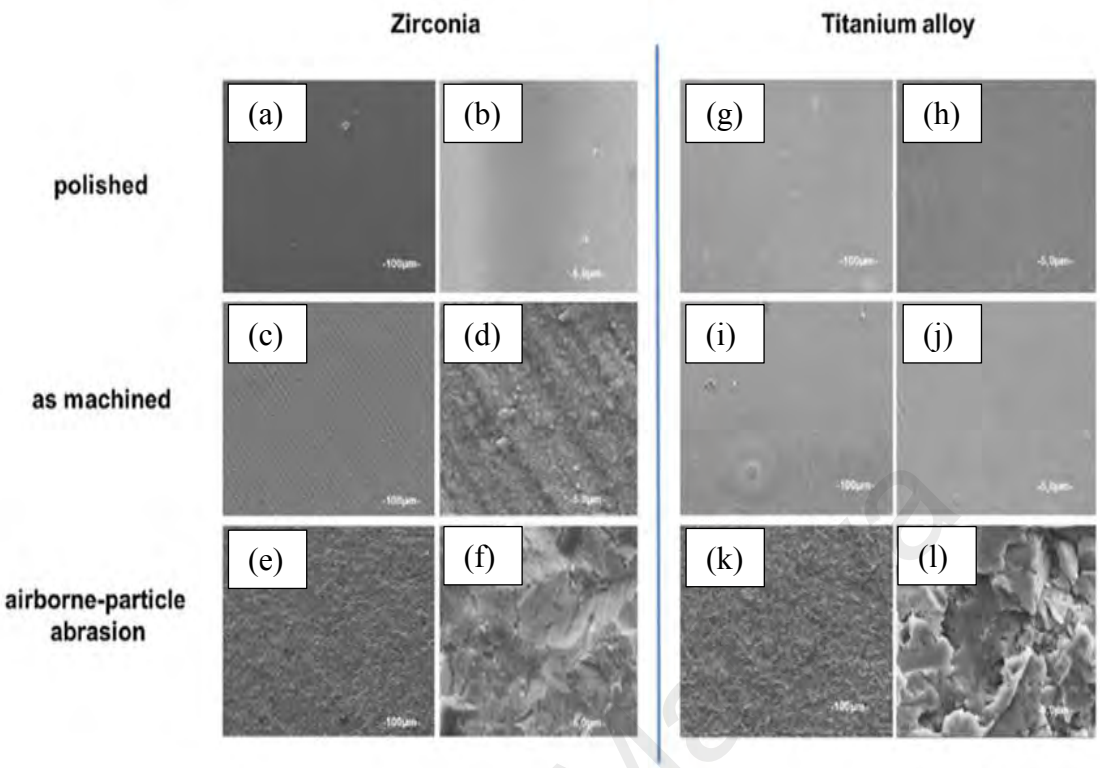

Figure 2.6: Scanning electron microscopic image of zirconia and titanium alloy with machined, polished, and sandblasted surface (Nothdurft et al., 2015).

Several parameters including size, shape, and kinetic energy of the particles during sandblasting process affect the outcome of the surface roughness. During sandblasting, air pressure generates impulse to eject the particles, in which the kinetic energy gained relies on the density, volume, and velocity of the particles (Balza et al., 2013). The advantage of using sandblasting is due to its homogenous and anisotropic abrasion which allows surface modification to be performed on hard materials. The surface of materials such as ceramic, glass, and silicon can be easily modified with sandblasting (Dubotzky & Kruger, 2001). In addition, alumina particles are commonly used as abrasive for sandblasting attributed to its hardness and needle-like shape. Their low production cost and inert behaviour also made them favoured over the other abrasive materials. However, the fragile nature of alumina and the increase kinetic energy of the particle might cause fractures of the particles. The rupture of alumina particles would

decrease the surface roughness of materials as particles generated are smaller (Balza et al., 2013).

A recent study has investigated behaviour of fibroblasts and epithelial cell on zirconia with different surface topographies including machined, polished, and sandblasted surfaces. It was observed that the rougher sandblasted surface has enhanced the fibroblast adhesion and proliferation. Epithelial cells showed a highest proliferation rate on machined surface, which corresponded well with observations in previous studies, where epithelial cells favour smooth surfaces for proliferation (Nothdurft et al., 2015). Nothdurft et al. (2015) has also raised the disadvantage of using alumina particles as abrasives for a sandblasting process as the alumina contamination would alter the surface chemistry. However, acid-etching treatment can be applied to clean alumina residues caused by sandblasting (Chrcanovic, Leão, & Martins, 2013).

Rough zirconia surfaces has been suggested to be beneficial for osseointegration applications in which previous study has illustrated outstanding behaviour of osteoblast-like SAOS-2 cells on both sandblasted and sandblasted/etched zirconia in terms of adhesion, proliferation, and differentiation. Both surface topographies showed similar surface roughness but the microstructure was less pronounced on the sandblasted zirconia viewed under scanning electron microscope. A highest amount of calcium was found on sandblasted/etched zirconia. The immunofluorescence staining illustrated well-organized actin fibres (green) on both zirconia surfaces but a better focal adhesion contacts (red) on sandblasted zirconia (Figure 2.7). Sandblasted zirconia showed a higher cell attachment but lower metabolic activity in comparison with the sandblasted/etched zirconia (Hempel et al., 2010).

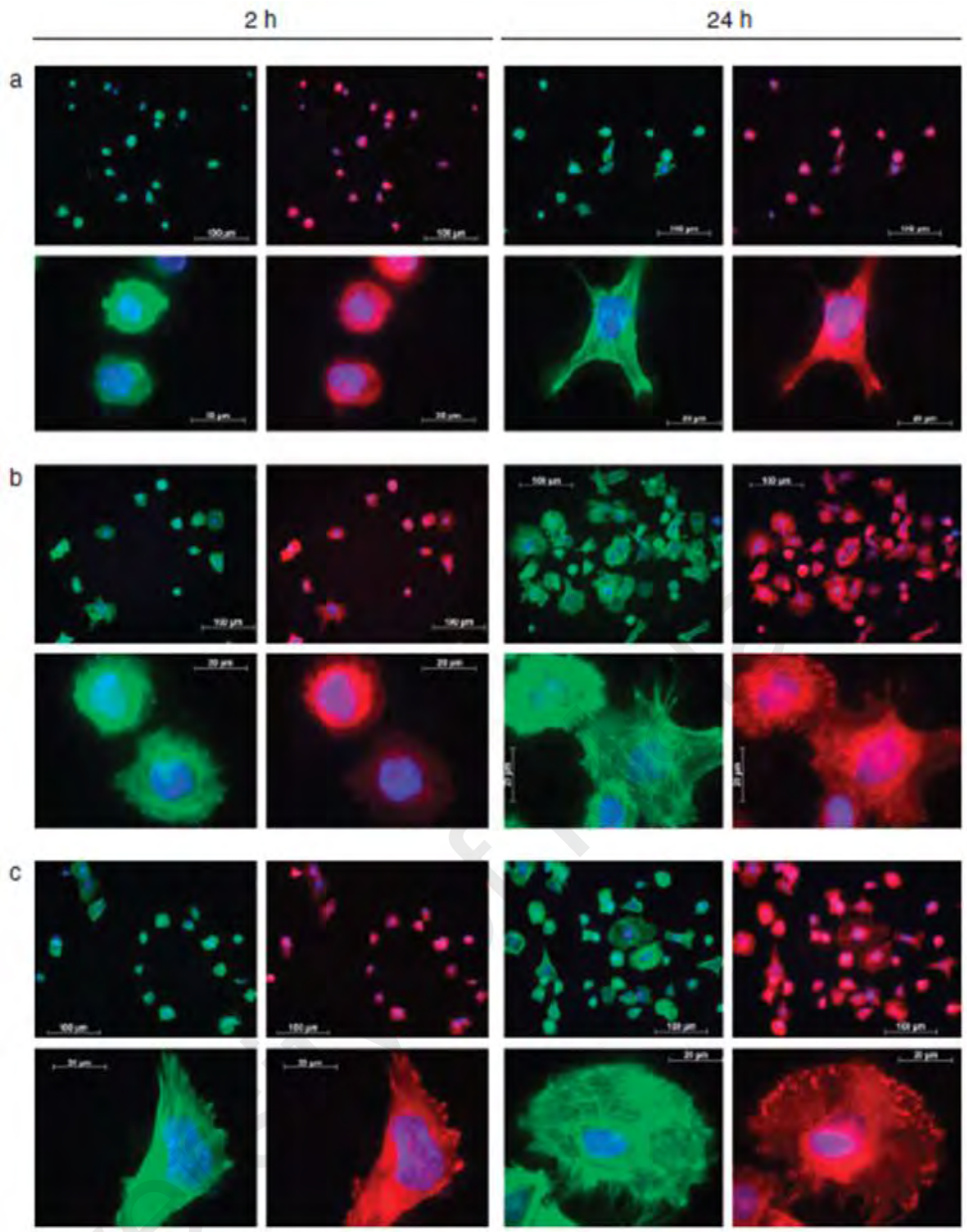

Figure 2.7: Immunofluorescence staining of cells on (a) sandblasted/etched titanium, (b) sandblasted/etched zirconia, and (c) sandblasted zirconia. Nuclei, actin filaments, and focal adhesion were indicated by blue, green, and red fluorescence respectively (Hempel et al., 2010).

In the *in vivo* study by Stadlinger et al. (2010), sandblasted zirconia implants were implanted submerged and non-submerged in minipigs in order to investigate the formation of soft and hard tissue. This study has reported the absence of signs of inflammation in general, except for the lost implant which was unavailable for

examination. Hence, the implants were concluded to be clinically stable. The non-submerged zirconia has shown a good biocompatibility due to soft tissue adaptation. Despite the higher bone implant contact of submerged zirconia implants, no significant difference was found for the osseointegration between submerged and non-submerged zirconia implants (Stadlinger et al., 2010).

Dental implant testing is challenging as choosing the suitable animal model can be difficult. This is primarily due to the different teeth morphology between humans and animals. In the study of Langhoff et al. (2008), ovine was chosen for testing the dental implants for its human-like remodelling rate, bone structure, and proportions. The zirconia implants used in this study were modified by a combination of sandblasting and etching. All the zirconia implants have shown good biocompatibility and osseointegration, with the formation of bone around the implants and remodelling of cortical bone. Additionally, there were no signs of inflammation, fracture or bone resorption (Langhoff et al., 2008).

2.4.2 Etching

Other than sandblasting, acid-etching has also been applied commonly to roughen zirconia surface. Different types of acid including hydrofluoric acid, nitric acid or sulphuric acid have been used for acid-etching process. After acid-etching, heat treatment can be applied to smoothen the sharp edges resulting from the etching process (Kohal et al., 2013). Acid-etching provides several advantages such as homogenous roughing of the materials with any shape and size, and the absence of delamination of material attributed to its chemical texturing approach which does not exert stress on the materials (Chrcanovic & Martins, 2014; Iwaya et al., 2008). However, acid-etching might cause undesirable chemical changes of the materials (Hoshing, Suvarna Patil, & Bandekar, 2014).

Several parameters affect the topography formed using acid etching approach. These include prior treatment, composition of acid mixture, temperature, and treatment time. Acid etching is an appropriate approach when producing a microscale surface texture as interlocking the bone and implant is desirable (Chrcanovic & Martins, 2014). Previous studies have applied a combination approach of sandblasting and acid-etching to further enhance the degree of micro-roughness of zirconia surface (Hempel et al., 2010; Kohal et al., 2013; Langhoff et al., 2008). A material surface with optimised micro-roughness fabricated using this method has been shown to improve osteoblast attachment and proliferation (Sammons, Lumbikanonda, Gross, & Cantzler, 2005).

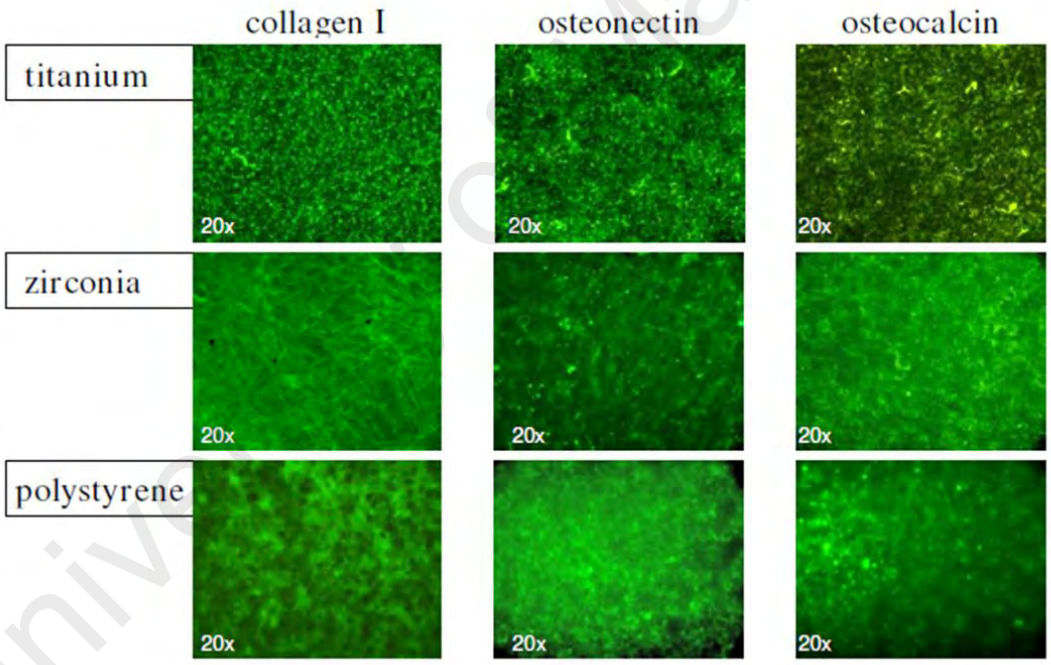

Figure 2.8: Expression of collagen I, osteocalcin, and osteonectin on acid-etched titanium, zirconia, and polystyrene surfaces (Depprich et al., 2008).

Extensive researches have been conducted to study the behaviour of osteoblast on different surface topographies. Acid-etched zirconia was suggested to be an appropriate material for dental applications due to its superior biocompatibility with good attachment, proliferation, and differentiation of primary osteoblasts in the *in vitro* study

by Depprich et al. (2008). Besides that, denser collagen fibrils were also observed on zirconia surfaces compared to that on titanium surfaces, in which both materials were acid-etched (Figure 2.8) (Depprich et al., 2008). However, in contrast to the good cell attachment and proliferation on rougher surfaces as observed in previous studies, Hauser-Gerspach et al. (2012) has illustrated a reduction of cell-spreading on rougher acid-etched zirconia surfaces due to cell adaptation to the macro and micro holes of the samples.. (Hauser-Gerspach et al., 2012)

An *in vivo* study has placed acid-etched zirconia implant surfaces in rat cranium with created bone defect to study the biocompatibility and osseointegration of materials. There was no sign of inflammation found in the study. Development of blood vessels, bone implant contact and bone regeneration were also observed in this study. After 56 days, a direct bridging of the bone defects was detected and the areas between zirconia discs and bone were enriched with connective tissue (Mai et al., 2012).

Besides acid-etching treatment, a relatively new etching treatment which is known as selective infiltration etching has been reported to enhance the nanoscale surface roughness without altering the surface chemistry of material. This technique does not change the microscopic surface roughness nor cause material losses. Selective infiltration etching has been applied to produce nanoporous zirconia surface for *in vitro* study in which enhanced osteoblast cell spreading and the fusion of cell membrane with the nanoporous surface were observed (Figure 2.9) (Aboushelib et al., 2013). Selective infiltration etched surface can be prepared by coating the material with a specific infiltration glass. The coated material is then heated above its glass transition temperature and the infiltration of molten glass would take place between the grains. This technique is termed selective because the surface grains in contact with the glass

alone are involved in the process, which allows only certain area to be treated (Aboushelib, Kleverlaan, & Feilzer, 2007).

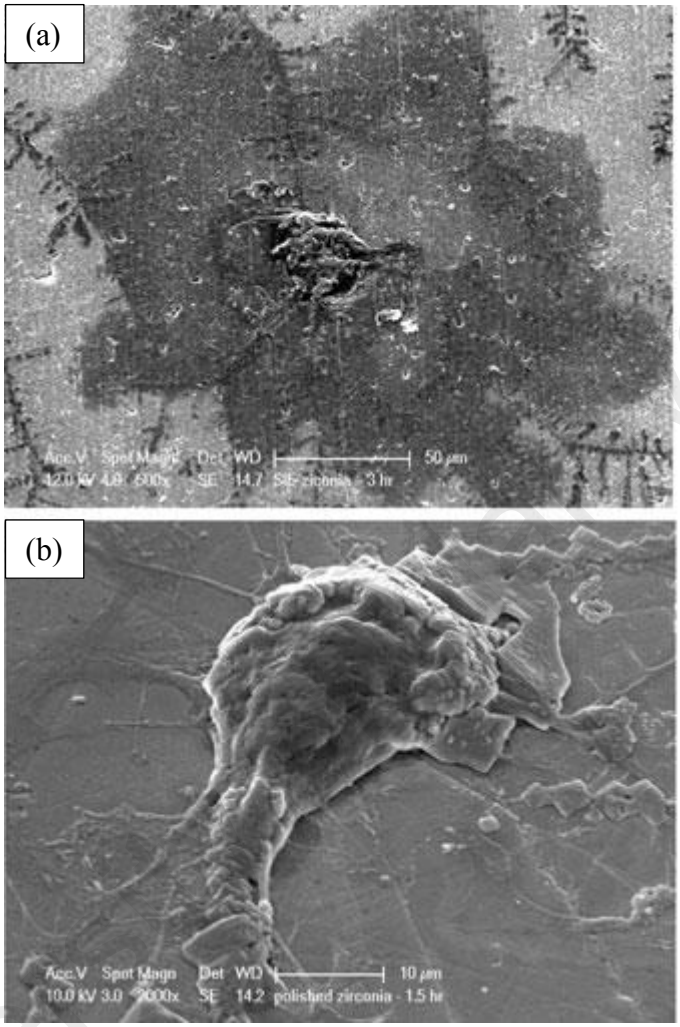

Figure 2.9: Scanning electron microscopic images of osteoblast cultured on (a) etched zirconia and (b) polished zirconia. There was a visible gap between the osteoblast and polished zirconia (Aboushelib et al., 2013).

2.4.3 Polishing

Unlike sandblasting or acid-etching, polishing gives a smooth texture to the surface (Figure 2.6). Previous studies have concluded that epithelial cells are highly likely to adhere to a smoother polished surface than to a rougher acid-etched or sandblasted surface, whereas fibroblasts adhere well to both surface textures (Klinge & Meyle, 2006). Additionally, osteoblasts adhere and proliferate better on rougher surfaces (Brett

et al., 2004). The surface of zirconia is commonly polished by silicon carbide polishing paper and diamond or silica suspension with a polishing machine (Aboushelib et al., 2013; Kimura et al., 2012; Nothdurft et al., 2015). The advantage of mechanical surface treatment methods, for example, polishing, is that the surface texture or finish can be altered without changing the surface chemistry (Nothdurft et al., 2015).

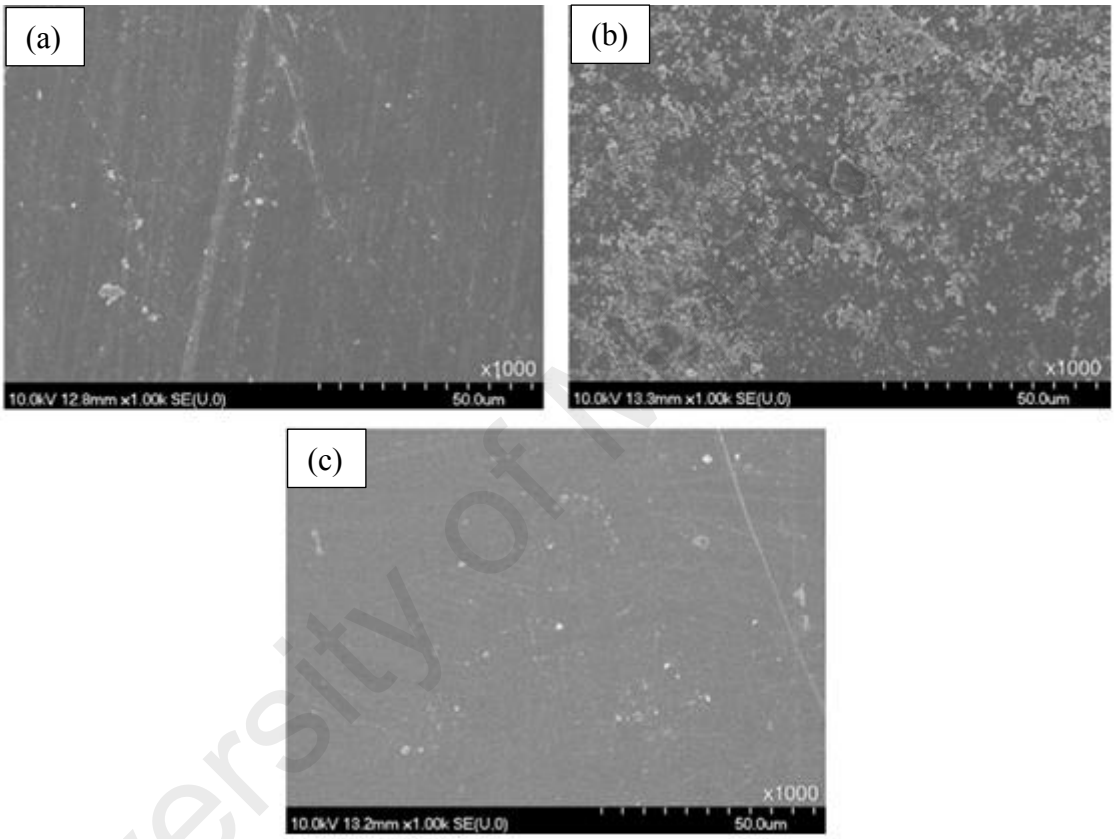

Figure 2.10: Scanning electron microscopic images of polished (a) lithium-disilicate, (b) zirconia, and (c) cobalt-chromium (Forster et al., 2014).

Nevertheless, according to the findings from previous studies, the polishing treatment done on zirconia surface is limited due to its macromolecular structure. For instance, Forster et al. have shown that polished zirconia possessed the highest roughness (R_a) which was 25.3 nm, in comparison with the other polished materials, lithium-disilicate (14.7 nm) and cobalt-chromium (4.6 nm), attributed to the granulated structure (Figure 2.10) (Forster et al., 2014). It is known that smooth polished or

machined surfaces provide a more favourable surface for epithelial cells to proliferate (Linkevicius & Apse, 2008). According to Forster et al. (2014), the evaluation of biological response of epithelial cells is important when the materials will be in contact with the gingival sulcus which is covered with epithelial tissue. The epithelial cells had the least attachment and proliferation on the roughest polished zirconia in comparison with polished cobalt-chromium and lithium-disilicate (Forster et al., 2014). This finding was also supported by Nothdurft et al. (2015) where epithelial cell showed a higher proliferation rate on the smoother zirconia surfaces.

Kimura et al. (2012) was the first to study the adhesion of human oral keratinocytes on polished zirconia. However, it was reported that no significant difference was observed in cell attachment between polished titanium and zirconia (Figure 2.11). Additionally, their mRNA expression and protein expression in laminin γ_2 and integrin β_4, and cell morphology were also not significantly different. The similar cell viability on both materials was claimed to be caused by the similar surface roughness of the two materials. Zirconia biomaterial in this study was concluded to have comparable potential as titanium for the development of epithelial attachment (Kimura et al., 2012).

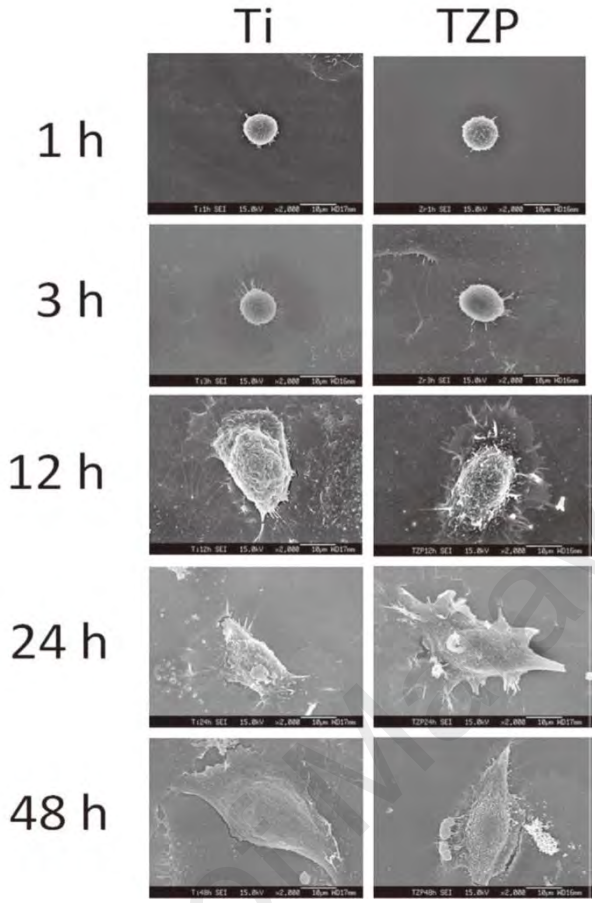

Figure 2.11: Scanning electron microscopic images of keratinocytes adhesion to polished titanium (Ti) and tetragonal zirconia polycrystal (TZP) at 1, 3, 12, 24, and 48 h of culture (Kimura et al., 2012).

2.4.4 Laser Treatment

Laser treatment has been a popular surface treatment in modifying the surface properties for a variety of materials. Laser treatment has demonstrated its versatility in altering the surface properties of biomaterials and also its advantage over other treatments such as sandblasting and etching. For example, there was no risk of surface contamination with laser treatment as the laser is not in contact with the material (Yasuno, Kakura, Taniguchi, Yamaguchi, & Kido, 2014). In addition, this surface processing method has also intrigued researchers with its ability to improve and control material wettability since the wettability is often interrelates with cell adhesion (Hao &

Lawrence, 2003b). A wide range of materials including metal, polymer, and fibre has reported the use of laser processing to modify the surface properties (Soon et al., 2016).

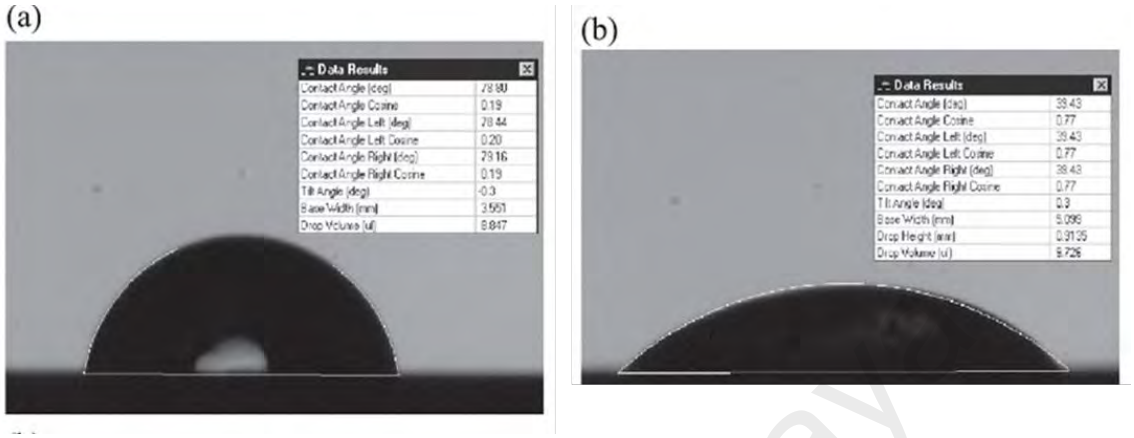

Figure 2.12: Contact angle of sessile drops on (a) untreated and (b) laser-treated magnesia partially stabilised zirconia (Hao & Lawrence, 2003b).

Several studies have investigated the changes in wettability in response to the types of laser used (Lawrence & Li, 1999, 2001; Lawrence, Li, & Spencer, 1999). The wettability of magnesia partially stabilised zirconia was significantly improved by the laser treatment owing to altered surface topography, composition, and energy (Hao & Lawrence, 2003a; Lawrence & Li, 2002). Hao and Lawrence (2003b) have investigated the correlation between laser parameters, wettability, and cell attachment by enhancing the surface wettability of zirconia with laser treatment. As seen in Figure 2.12, the laser treatment has significantly improved the surface wettability of zirconia in which the contact angle of sessile drop was highly reduced on laser-treated surface. The surface energy and surface oxygen were also claimed to influence the wettability to some extent. This study showed enhancement of human skin fibroblasts on the magnesia partially stabilised zirconia surfaces with different laser parameters. Also, the fibroblasts were not observed on the untreated surface (Figure 2.13). This has further proven that the laser-treated zirconia has produced a more favourable surface for the cell attachment

and the wettability was the key factor in influencing the cell adhesion on the magnesia partially stabilised zirconia (Hao & Lawrence, 2003b).

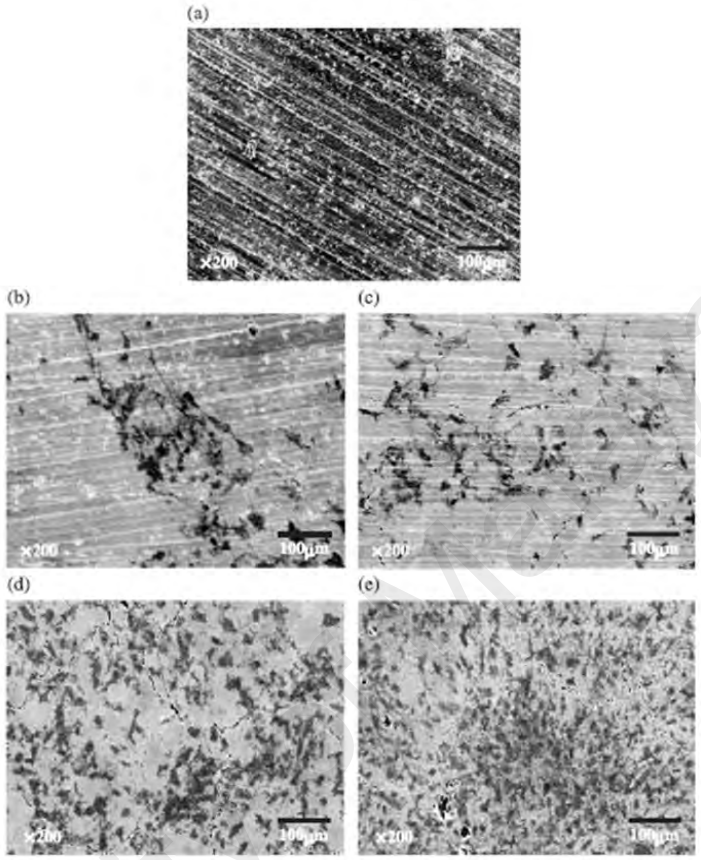

Figure 2.13: Scanning electron microscopic images of fibroblasts on (a) untreated and (b-e) laser-treated magnesia partially stabilised zirconia (Hao & Lawrence, 2003b).

The influence of wettability is an important area of study as it affects cell function, protein adsorption, and also cell adhesion. The nature of the protein-bearing aqueous solution rules the adsorption of protein, and cells react differently in response to the organised protein layers (Hao, Ma, Lawrence, & Zhu, 2005). Hence, the adsorbed protein layer plays an important role as it dictates the cellular interaction eventually. Hao and Lawrence (2004) have reported the influence of surface nature on the protein adsorption in which a large amount of fibronectin was detected on the laser-treated zirconia surface. In contrast to fibronectin, the albumin adsorption was reduced by the

surface roughness and wettability (Hao & Lawrence, 2004). Not only did a number *of in vitro* studies on laser-treated zirconia bioceramics show good cellular response and cell adhesion, but an *in vivo* study also reported a significantly improved bone-implant contact and removal torque value for laser-treated implant (Yasuno et al., 2014).

2.4.5 Ultraviolet (UV) Light Treatment

Previous studies have demonstrated that bone implant contact can be highly improved after the implants were treated with UV light. This was attributed to the effect of superhydrophilicity (Aita et al., 2009; Ogawa, 2014; Shetty, Puthukkat, Bhat, & Shenoy, 2014). Superhydrophilicity of a material is defined by the immensely low water contact angle that is less than 5 degrees (Mills & Crow, 2008). Hydrophilicity is involved in the initial interaction with proteins and cells, in which a hydrophilic surface is beneficial for the wound healing and osseointegration at early stage (Sawase et al., 2008).

The formation of hydroxyl (-OH) and oxygen ($-O_2$) groups takes place on the outermost layer when the hydrophilic oxide surface forms bonds with water (Tengvall & Lundström, 1992). The formation of hydoxylated oxide surface is useful for the enhancement of surface reactivity of materials with the surrounding ions, amino acids, and proteins in the tissue fluid (Sawase et al., 2008). For instance, osteoblasts have shown a higher level of differentiation markers on hydrophilic surfaces in comparison with hydrophobic surfaces (Zhao et al., 2005). In addition, the process of osseointegration was also improved by hydrophilic surfaces through enhanced bone implant contact and bone anchorage during bone healing (Sartoretto et al., 2015).

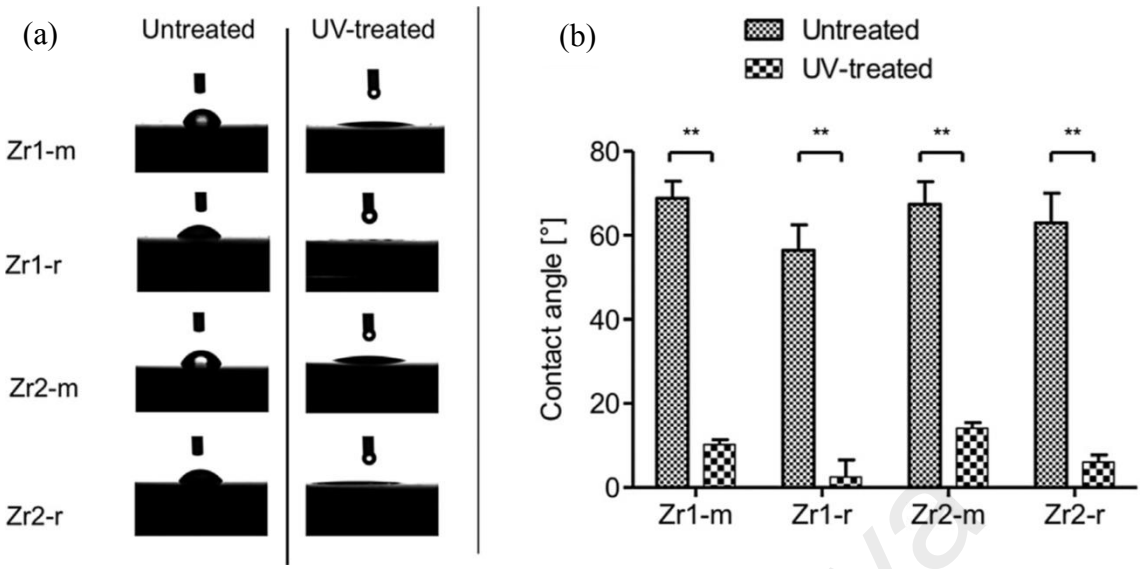

Figure 2.14: (a) Contact angle of water droplets on samples with and without UV-treatment (b) The average water contact angle before and after UV-treatment (Tuna, Wein, Swain, Fischer, & Att, 2015).

Tuna et al. has studied the effect of UV treatment on zirconia-based samples with different composition and surface topography whereby all the samples turned hydrophilic or even superhydrophilic after the UV treatment (Figure 2.14). UV treatment has significantly altered the physiochemical properties of the zirconia samples. The changes in wettability are often attributed to the reduction of carbon content in the material surface, which is manipulated by two mechanisms: direct decomposition of carbon using UV treatment, and photocatalytic activity of zirconia (Tuna et al., 2015). Another study by Att et al. (2009) has supported the finding of Tuna et al. (2015) where enhancement of surface hydrophilicity was observed with the decrease in water contact angle on UV-treated zirconia samples. Besides, the enhancement of hydrophilicity is proportional to the time of UV treatment. UV light treatment has been shown to enhance the osteoblasts attachment, spreading, and proliferation on zirconia surface, as shown in Figure 2.15. According to Att et al. (2009), the hydrophilicity and reduction of hydrocarbons helped to improve the

bioactivity in terms of attachment, proliferation, and mineralisation. Nevertheless, UV light treatment did not regulate the osteoblast gene expression such as osteopontin and osteocalcin (Att et al., 2009).

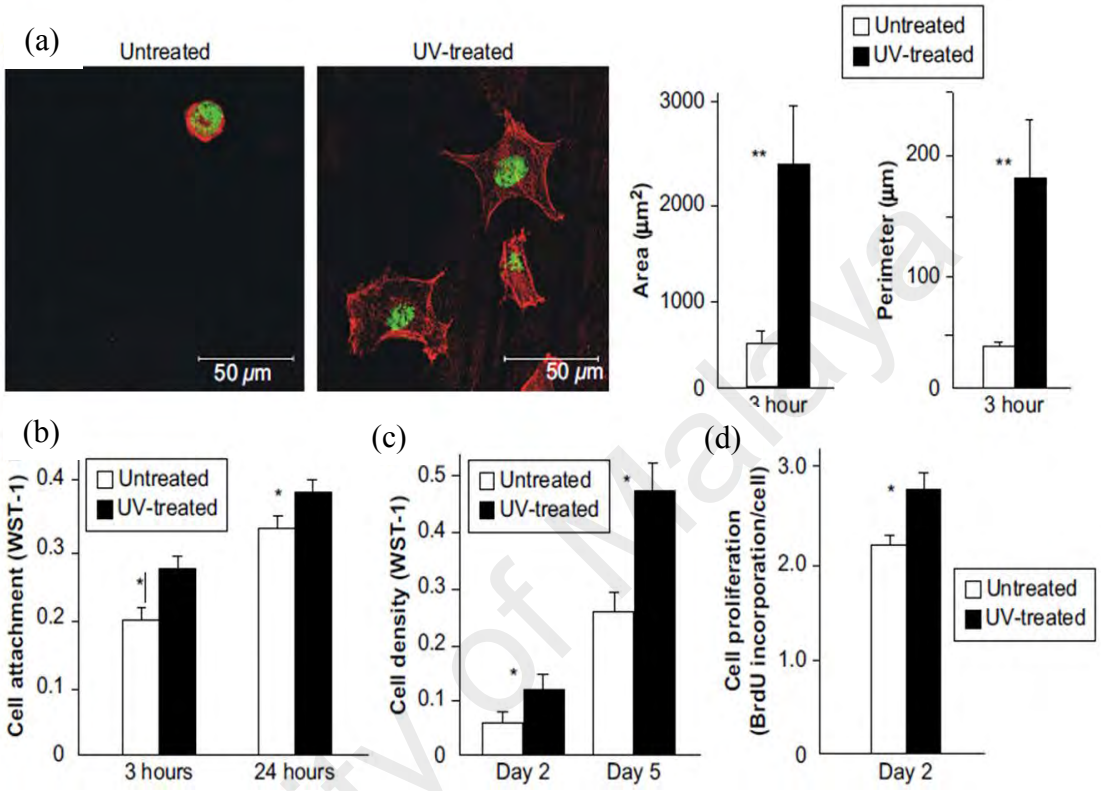

Figure 2.15: (a) Immunofluorescence staining images of osteoblasts on untreated and UV-treated zirconia after 3 h of culture. Nuclei were indicated by green fluorescence while actin filaments were indicated by red fluorescence. (b-d) The cell attachment, density and proliferation on untreated and UV-treated zirconia at different time points. The statistical significance between the untreated and UV-treated zirconia was denoted by * and ** at $p<0.05$ and $p<0.01$ respectively (Att et al., 2009).

The benefit of hydrophilicity for biological enhancement has been controversial owing to the inconsistency of results in previous studies. Other than hydrophilicity, the hydrocarbon content has to be taken into consideration as well, as the atomic percentage of hydrocarbon can be altered by the UV treatment (Tuna et al., 2015). Based on a

previous finding, the amount of protein adsorption and cell adhesion are inversely correlated with the atomic percentage of carbon (Aita et al., 2009). However, a recent study has reported that UV-treated samples did not improve the cell adhesion as compared to that on plasma-treated samples, despite the fact that UV-treated samples were superhydrophilic with reduced carbon content. It was suggested that other factors such as surface energy and surface hydroxyl groups were associated with the observation (Kobune, Miura, Sato, Yotsuya, & Yoshinari, 2014). In conclusion, in order to study the effect of UV treatment on zirconia biomaterials, further research should be conducted to resolve the contradictory results in previous studies.

2.4.6 Coating

For biomaterials which are mainly used to provide mechanical support, coating has been commonly applied to resolve their need of enhanced surface properties (Stanic et al., 2002). A phenomenon known as "the race for the surface" takes place when bacterial colonisation and tissue integration occur following the implantation of an orthopaedic device. Hence, surface modification can be applied to inhibit bacterial colonisation and to prepare an adhesive surface for proper cell attachment (Gristina, 1987). Coating is strategically used to enhance the biocompatibility and osseointegration of an implant for a successful clinical test (Torricelli et al., 2001). In order to increase the competitiveness of zirconia as a favourable implant candidate, surface modification techniques should be developed to guide the formation of tissue (Pelaez-Vargas et al., 2011).

Calcium phosphate (CP)-based material has been a popular biological fixation which is used to replace cemented fixation. This approach allows formation of rigid bond between the implant and host tissue without the use of cement (Jaffe & Scott, 1996). Although CP-based material is bioactive, pure CP coating leads to poor stability and

weak bond strength. Hence, it is a challenge to control the adhesion strength of the coating and maintain the bulk properties of the substrate (Dorozhkin, 2013; Pardun, Treccani, Volkmann, Streckbein, et al., 2015).

The strength of the coating stability and the adhesion to the substrate are key factors in an effort to reduce the chances of failure and delamination (Barnes, Johnson, Snell, & Best, 2012). For example, yttria-stabilised zirconia (YSZ) reinforced hydroxyapatite (HA) coating with enhanced coating stability and adhesive strength has been fabricated to overcome the aforementioned issues (Pardun, Treccani, Volkmann, Li Destri, et al., 2015; Yugeswaran, Yoganand, Kobayashi, Paraskevopoulos, & Subramanian, 2012). Plasma spraying technique is commonly used in industry to fabricate CP-based coatings due to its versatility, high deposition rate, and low cost. However, this technique has several flaws including variation in coating/implant bond strength and also modification of HA structure. Thus, development of new techniques to deposit CP-based coating on the implants is required to address the limitation of plasma spraying technique (Herman, 1988; Yang, Kim, & Ong, 2005).

Despite the stability issue, studies have shown that CP-based coating with a higher dissolution rate enhanced the cellular response of osteoblasts owing to its dissolution (De Groot, De Putter, Smitt, & Driessen, 1981; Zeng & Lacefield, 2000). Pardun et al. (2015) have studied the effect of coating composition on mechanical and biological properties of the coating by mixing YSZ with CP in different ratios. It was found that a higher ratio of YSZ improved the coating adhesion whereas a higher ratio of CP improved the bioactivity of the coating (Pardun, Treccani, Volkmann, Streckbein, et al., 2015). On the other hand, another study claimed that the influence of microstructure on osteoblast activity was more significant than that of CP-based coatings as observed on porous zirconia scaffolds (Song & Cho, 2014). A recent study by Pae et al. (2014) also

suggested that CP only influenced the cell differentiation at an early stage. Despite the fact that the ALP activity of CP-coated zirconia was the highest in comparison with smooth zirconia and HA-coated zirconia, there was no significant difference in their cellular activity, proliferation, and differentiation (Pae, Lee, Noh, & Woo, 2014).

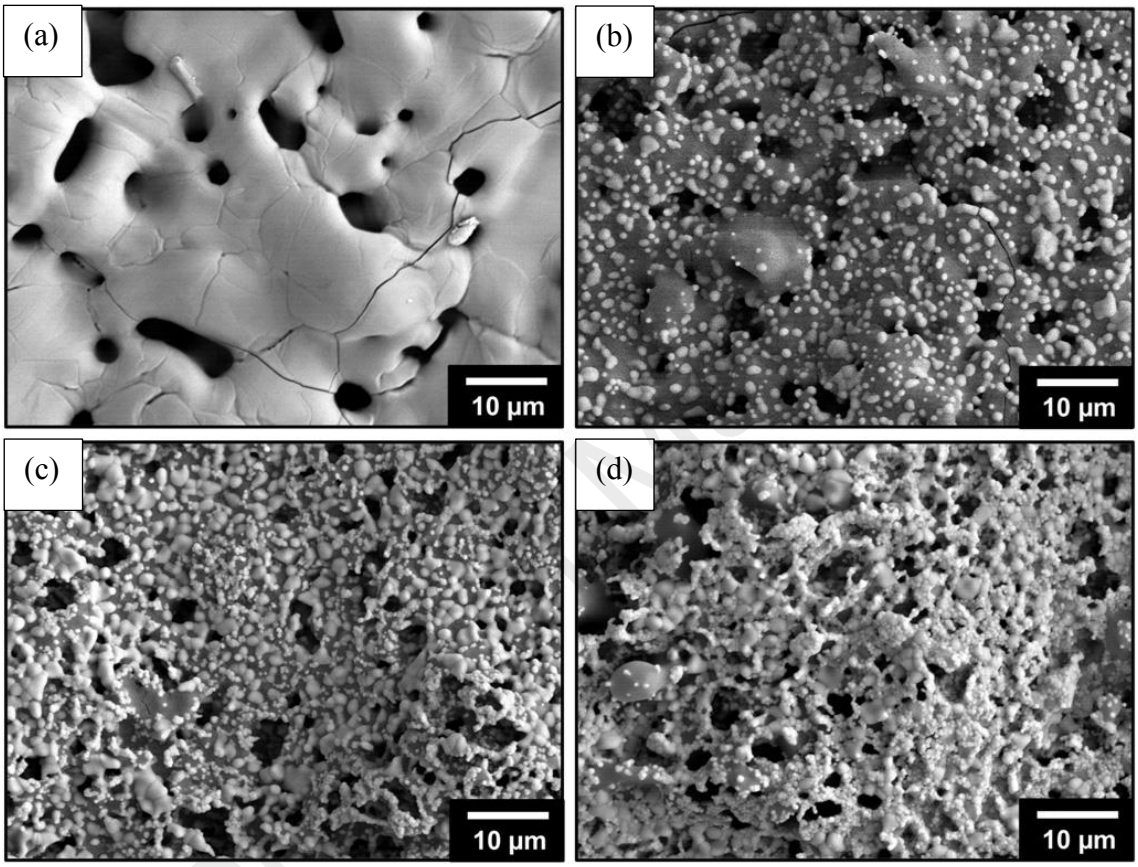

Figure 2.16: Scanning electron microscopic image of (a) pure CP coating and (b-d) YSZ/CP coatings with different ratios (Pardun, Treccani, Volkmann, Streckbein, et al., 2015).

Wet powder spraying has been applied to fabricate YSZ/HA coatings using a double-action airbrush spray (Pardun, Treccani, Volkmann, Streckbein, et al., 2015). The advantage of this technique is its versatility in coating planar or curved surfaces with varying thickness. However, the long term stability of the coating produced by this technique has yet to be discovered (Pardun, Treccani, Volkmann, Li Destri, et al., 2015). The bioactivity of the coating in simulated body fluid was enhanced by the

increased content of CP, but the opposite effect was observed for the mechanical and chemical stability of the coating. Although YSZ/HA coatings with different composition shared similar morphologies as seen in Figure 2.16, their cellular responses were different. Immunofluorescence staining demonstrated enhanced adhesion, proliferation, and spreading of cells on coatings with higher YSZ content while coating with higher CP content appeared to impede cell spreading (Figure 2.17). The difference in cellular responses was attributed to the dissolution of coating, in which an alkaline pH of the culture medium has affected the initial cell viability due to the coating dissolution (Pardun, Treccani, Volkmann, Streckbein, et al., 2015). Several *in vitro* studies have the dissolution behaviour of CP-based materials using bone cells (Pae et al., 2014; Pardun, Treccani, Volkmann, Streckbein, et al., 2015; Song & Cho, 2014). A higher dissolution rate of coating would release more Ca^{2+} that are beneficial for cell response and also enhance the process of osseointegration (Zeng & Lacefield, 2000). However, the dissolution behaviour of coating would affect the stability of implants (De Groot et al., 1981).

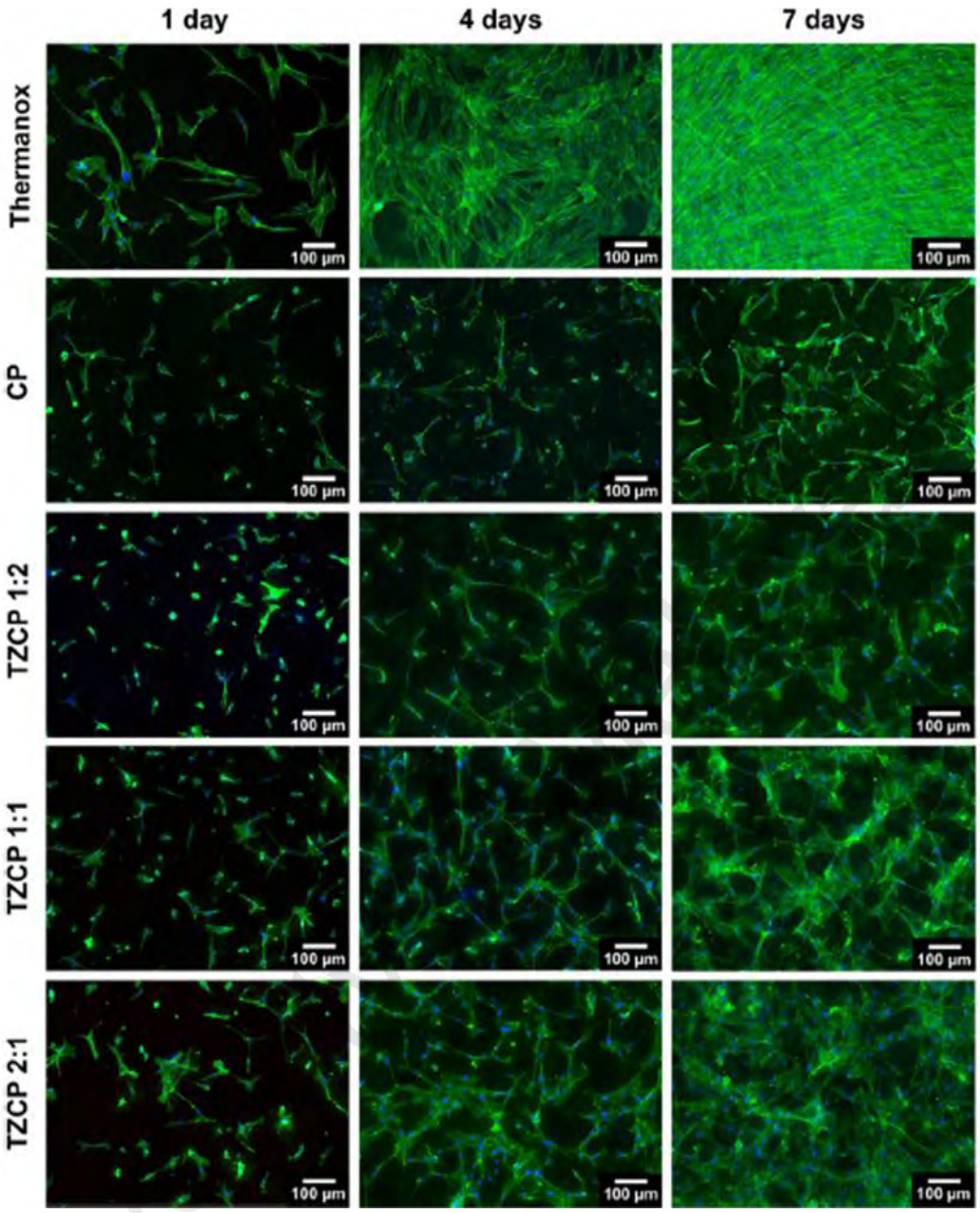

Figure 2.17: Fluorescence images of osteoblasts cultured on different coatings in comparison with thermanox. Actin filaments were indicated by the green fluorescence while nuclei were indicated by the blue fluorescence (Pardun, Treccani, Volkmann, Streckbein, et al., 2015).

Zirconia/HA composite film was designed to enhance the bioactivity and corrosion resistance of zirconia. Plasma spraying is a common fabrication method used to fabricate this composite film but the coating is not reliable as a result of residual stress. In addition, the fabrication of a uniform coating for implants with complex geometry is

difficult (Sandhyarani, Rameshbabu, & Venkateswarlu, 2014). Hence, electrophoretic deposition (EPD) has been proposed to replace traditional techniques because it is simple and versatile (Zhang, Kwok, Cheng, & Man, 2011). A novel method has combined both plasma electrolytic oxidation and electrophoretic deposition to produce and coat zirconia/HA film on zirconium, in which good biocompatibility, corrosion resistance, and bioactivity obtained by the material have broaden its potential applications (Sandhyarani et al., 2014).

Other than HA, silica is also a common coating material for zirconia. RKKP, which is a popular bioactive silica-based glass, has been studied for cell response and also ossseointegration. The overall outcome based on previous studies has been positive. RKKP coating can be produced with either enamelling and firing technique or thermal treatment (Bosetti, Vernè, Ferraris, Ravaglioli, & Cannas, 2001; Stanic et al., 2002; Torricelli et al., 2001). An optimised coating of RKKP on zirconia is defined by a continuous amorphous coating without defects and also the absence of Zr^{4+} diffusion into the glass (Torricelli et al., 2001). AP40 which is also a type of silica bioactive glass, has been reported to have comparable reactivity with RKKP (Bosetti et al., 2001).

Good reactivity is required for the enhancement of osteoconductivity when a material is placed in bone tissue (Zhong & Greenspan, 2000). The bioactivity of a material is often assessed by the formation of a hydroxyapatite layer on the surface after immersing it in simulated body fluid (Kokubo, Kushitani, Ohtsuki, Sakka, & Yamamuro, 1992). A higher proliferation rate of osteoblast-like cells has been observed on both AP40 and RKKP coated zirconia. Also, it was observed that the surface of both glass-coated zirconia samples was covered with self-grown apatite layer (figure 2.18). In comparison with the uncoated zirconia, a higher amount of protein was bound on the coated zirconia (Bosetti et al., 2001).

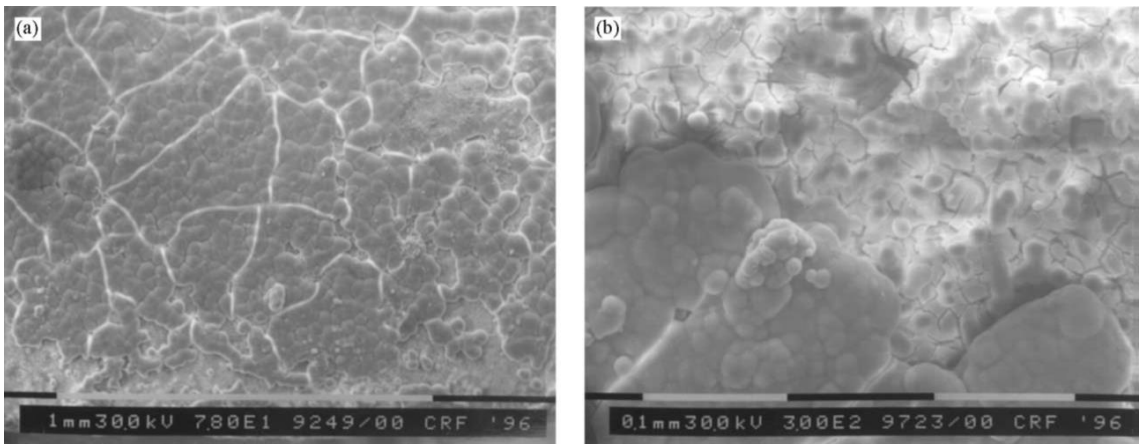

Figure 2.18: Scanning electron microscopic images of globular morphology of apatite on (a) AP40- and (b) RKKP-coated zirconia (Bosetti et al., 2001).

Successful *in vitro* study of bioactive coatings has broadened the potential applications for bone reconstruction and orthopaedic implants. Torricelli et al. (2001) have demonstrated improved osteoblast proliferation and differentiation on RKKP-coated alumina and zirconia. The cell proliferation and ALP activities were not restricted by the coating whereby a good biocompatibility was also reported in the study (Torricelli et al., 2001). In addition, the use of a silica coating is not only beneficial for the growth of osteoblast and osteoblast-like cells. It has also been shown to enhance fibroblast behaviour. According to Bosetti et al. (2001), similar responses from both fibroblasts and osteoblasts were observed in which the cell proliferation was significantly enhanced on the AP40- and RKKP-coated zirconia compared to that on uncoated control. However, there was no significant difference in the cell attachment on the coated and uncoated samples (Bosetti et al., 2001).

Besides uniform coating, micropatterned silica fabricated by soft lithography and the sol-gel method has also been coated on zirconia to guide tissue regeneration. Further, these micropatterned have demonstrated the influence of surface topography on cell behaviour (Laranjeira et al., 2014; Pelaez-Vargas et al., 2011). The micropatterned

silica coating developed by Pelaez-Vargas et al. (2011) has demonstrated its ability to guide tissue regeneration on zirconia. This silica coating also showed good biocompatibility and induced early alignment of osteoblast-like cells on the surface (Figure 2.19). The lamellopodia extensions were seen to be aligned towards the micropillars in comparison with the flat silica coating and bare zirconia surfaces. This study has also suggested the potential of surface-modified ceramic biomaterials for guidance of periodontal tissue regeneration (Pelaez-Vargas et al., 2011).

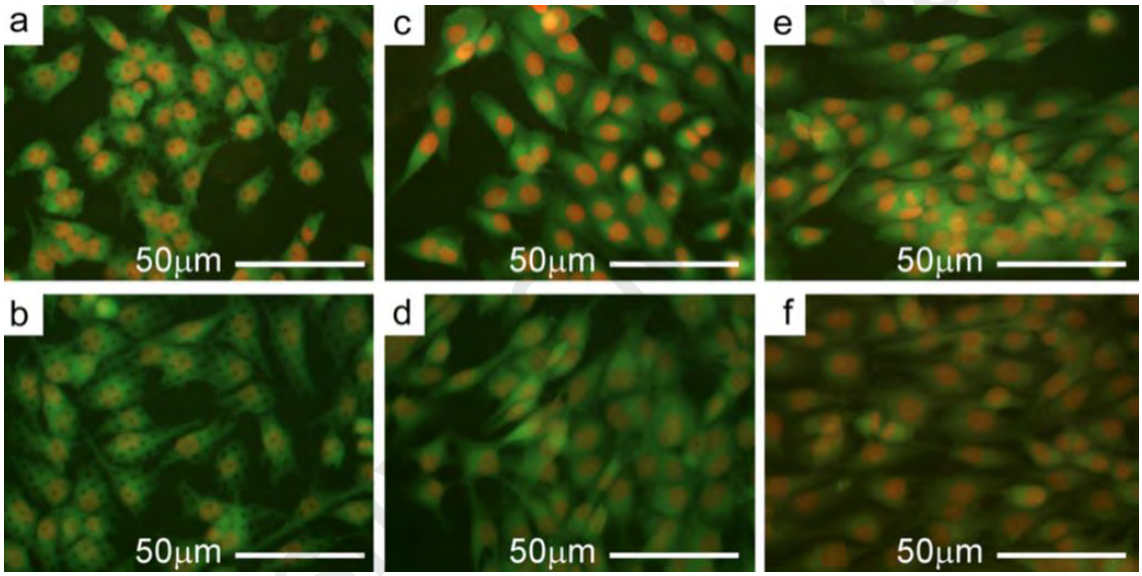

Figure 2.19: Cell adhesion and spreading on (a,b) micropatterned, (c,d) flat silica coating, and (e,f) bare zirconia after 1 day (a,c,e) and 4 days (b,d,f) of culture (Pelaez-Vargas et al., 2011).

A phenomenon known as "contact guidance" happens when the alignment of cells are guided by the surface grooves (Weiss, 1945). A recent study by Laranjeira et al. (2014) has also demonstrated that the growth of fibroblast and endothelial cells was guided by the micropatterned silica-coated zirconia with grooves (Figure 2.20). It can be seen that both types of cells showed a unidirectional alignment on the surface with parallel grooves. On the other hand, the gene expression levels of fibroblast-specific protein-1 and collagen type I were higher on the surface with pillars. These observations

have suggested that surfaces with grooves and pillar are more suitable for guided tissue regeneration and specific protein stimulation respectively (Laranjeira et al., 2014). Previous studies have also revealed that endothelial cells demonstrated improved alignment, elongation and migration in response to ridge-groove surfaces (Anselme et al., 2010; Bettinger, Zhang, Gerecht, Borenstein, & Langer, 2008). A study by Pae et al. (2009) also showed that fibroblasts were more likely to attach to yttria-tetragonal zirconia polycrystals (YTZP) with grooves but no difference was seen in the level of mRNA for laminin and fibronectin for smooth YTZP and YTZP with grooves.

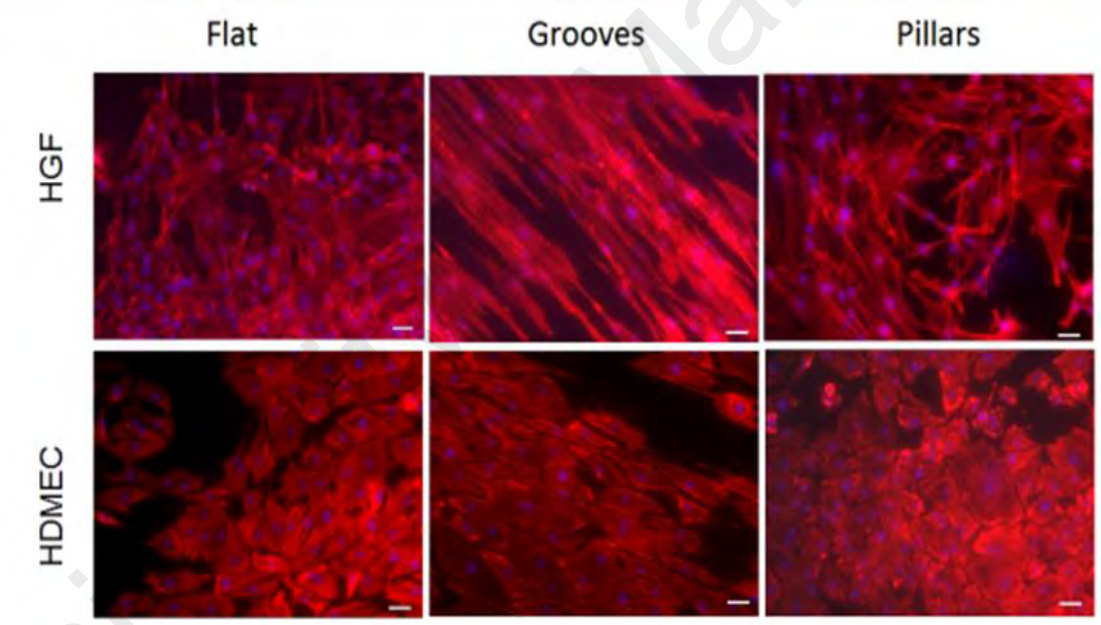

Figure 2.20: Fluorescence microscopic images of human gingival fibroblast (HGF) and human dermal microvascular endothelial cell (HDMEC) cultured on flat and micropatterned surfaces with grooves and pillars for 7 days (Laranjeira et al., 2014).

Mussels' adhesive properties have inspired a new surface modification approach in which L-DOPA (3,4-dihydroxy-L-phenylalanine), a compound that can be found in the adhesive structure of mussels, was coated on zirconia as a means to improve the

biocompatibility of the material. The L-DOPA was coated on zirconia through an oxidative polymerization technique by immersing the zirconia disc in a solution of L-DOPA which was dissolved in tris-hydrochloride. L-DOPA coating is cost-effective and it is able to cover implants with complex geometry. This method also allows conjugation with multiple biomolecules. *In vitro* study has shown flattened, polygonal osteoblast-like cells on the surface of L-DOPA coated zirconia. Also, actin stress fibres were also seen to be well-organised on the treated surfaces. This indicated that the L-DOPA has resulted in good cell adhesion at the interface. The ALP activity was significantly enhanced on the coated specimen, although the difference may be due to unequal cell numbers between samples as suggested by the normalization of ALP activity based on total protein content (Liu, Lee, & Lui, 2013).

Titanium oxide (TiO_2) nanotubes were coated on a commercial zirconia implant in a recent *in vitro* study by Frandsen et al. (2013). The zirconia implants were first sputter coated with a film of titanium before anodisation was conducted to produce TiO_2 nanotubes on the implant surface. Other than enhanced osteoblast behaviour, the treated implants also showed an outstanding surface wettability with a zero water contact angle, indicating a superhydrophilic surface. The osteoblasts also demonstrated superior adhesion and integration on the treated surface of zirconia implants in comparison with the bare implants, as seen in Figure 2.21 (Frandsen, Noh, Brammer, Johnston, & Jin, 2013).

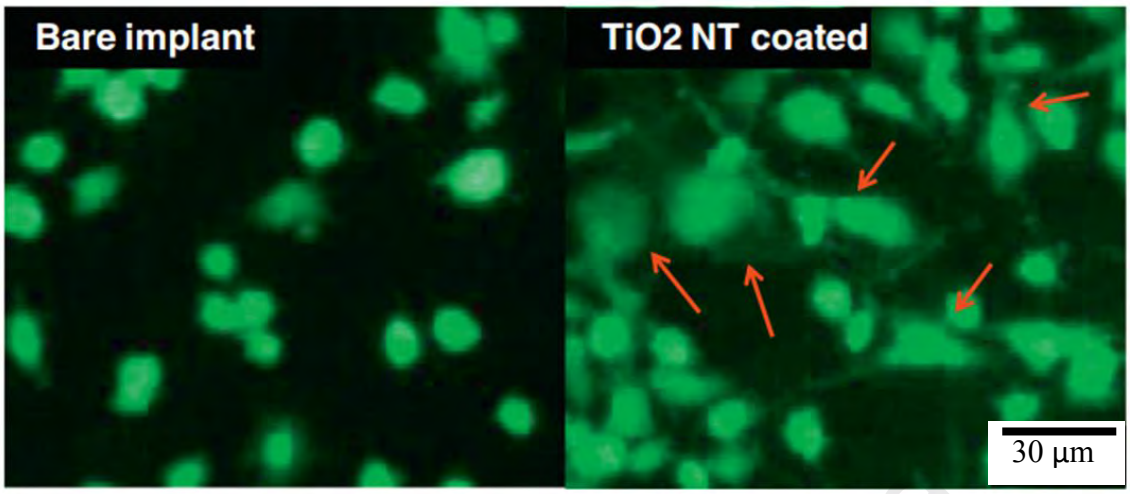

Figure 2.21: Fluorescence microscopic images of osteoblast cell spreading on (a) bare implant and (b) nanotube-coated implant after 24 h of culture (Frandsen et al., 2013).

An *in vivo* study has investigated the influence of zirconia implant with different surface topographies (machined surface and surfaces coated with different pore-formers). All the implants showed good integration with the surrounding tissue due to the ingrowth of bone from the neighbourhood. It was found that direct formation of bone occurred on the zirconia implants with modified surface. In general, all the implants have displayed intact surface layers and no significant difference was observed for the bone-implant contact (Sennerby et al., 2005).

2.4.7 Biofunctionalisation

Biofunctionalisation refers to the immobilisation of biomolecules on the material surface which subsequently changes the biochemical properties of the surface and biological responses at the interface. This approach is also known as biomimetic surface modification (Hsu et al., 2014). Compare to the conventional calcium phosphate based coating, this technique allows anchorage of proteins, enzymes, peptides, and other organic components on the implant surface (Morra, 2006). The anchorage of these

components which possess specific composition decides the types of tissue to be developed at the implant-tissue interface (Schwarz et al., 2007).

Arginine-glycine-aspartate (RGD) is a widely utilised adhesive peptide, whereby many adhesive proteins such as fibronectin, fibrinogen, and collagen, contain RGD as their cell recognition sites. The RGD sequences are identified by at least one of the integrins, which constitute a recognition system with the adhesion proteins to provide cell adhesion, differentiation, and growth signal. Previous study has successfully immobilised RGD on YTZP to improve the biocompatibility of the material (Ruoslahti & Pierschbacher, 1987).

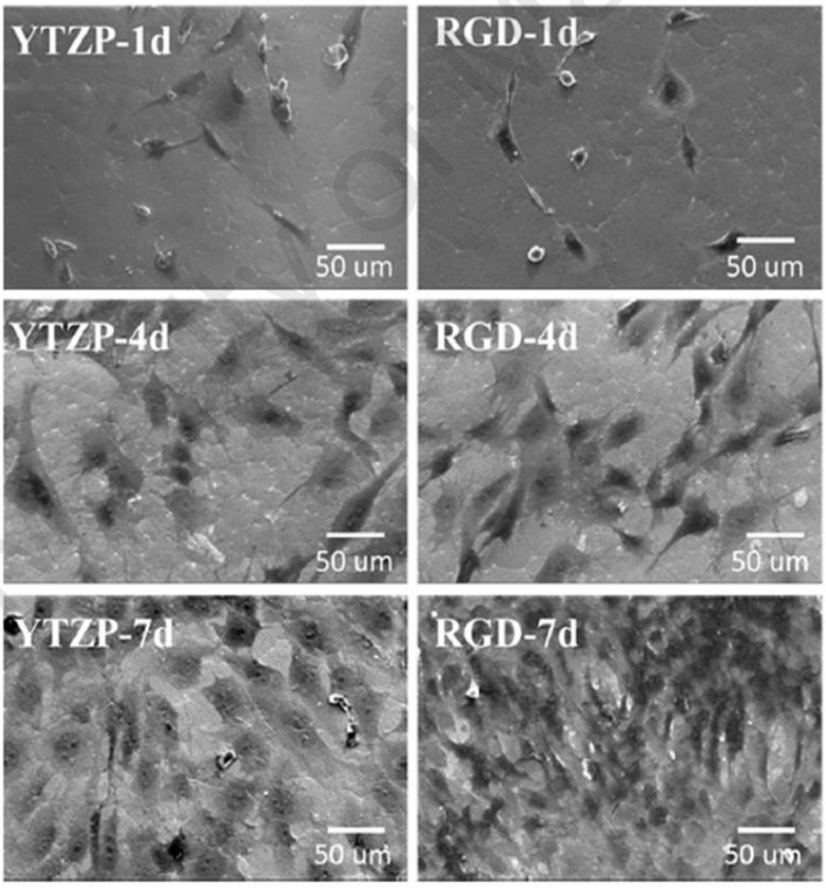

Figure 2.22: Scanning electron microscopic images of MG-63 cells on YTZP with and without RGD after 1, 4, 7 days of culture (Hsu et al., 2014).

A recent study by Hsu et al. (2014) has applied a novel approach to improve the bioactivity of YTZP by immobilising RGD peptide through covalent bonds. The samples were subjected to hydrothermal treatment at first to produce hydroxyl group on the surface prior to covalent immobilisation of peptide through silanisation. MG-63 osteoblast-like cells were cultured on specimens with and without RGD. The cells showed a superior adhesion and growth on the specimens with RGD in comparison with the specimens without RGD (Figure 2.22). The cell proliferation and activity also demonstrated a positive correlation with the culture time. A higher ALP activity on specimen with RGD at day 14 showed that the biofunctionalisation treatment has induced cell differentiation and proliferation (Hsu et al., 2014).

Previous studies have concluded that cell adhesion is mediated by extracellular matrix (ECM) proteins including fibronectin and vitronectin. It is important to understand the mechanism of ECM proteins in regulating the cell adhesion because the biocompatibility and integration of implants with the surrounding tissues are depending on the process of cell adhesion. For instance, fibronectin serves as a precursor for cell adhesion and bone formation at the implant surface (Wilson, Clegg, Leavesley, & Pearcy, 2005). Rubinstein et al. (2014) immobilized fibronectin dimers on a zirconia implant and activated them through a nanostructure-induced electrostatic mechanism. The activation was completed by selective electrostatic interactions between the zirconia surface patches with negative charge and fibronectin domains with positive charge. Dense fibronectin matrix was also observed to form throughout the grown cells (Figure 2.23). The treated zirconia surface has encouraged not only the production of ECM but also focal cell adhesion based on immunohistochemistry analysis (Rubinstein, Sabirianov, & Namavar, 2014).

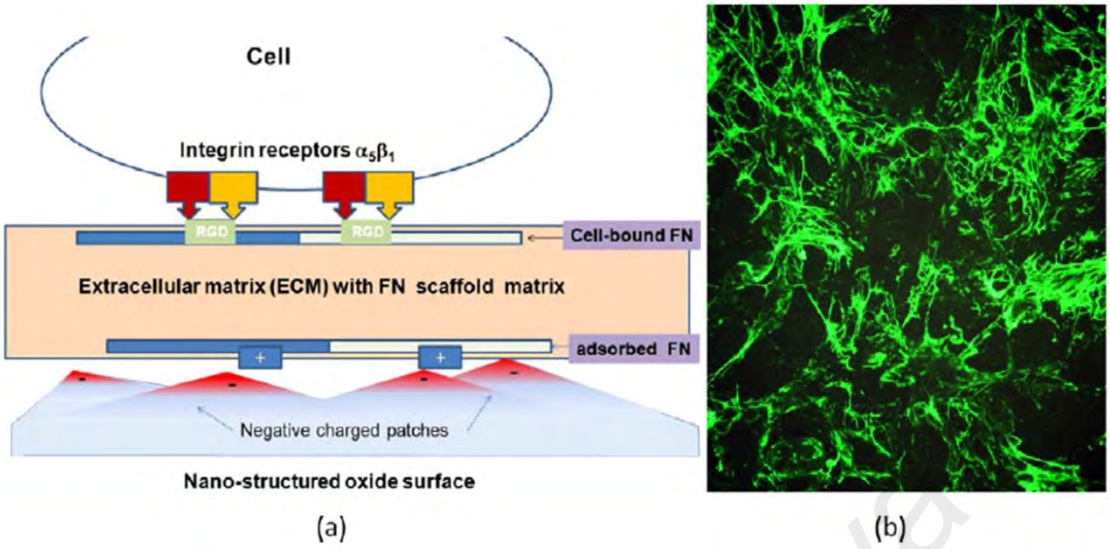

Figure 2.23: (a) Schematic diagram of cell attaching to fibronectin adsorbed on the surface (b) Optical microscopic image of dense fibronectin matrix (Rubinstein et al., 2014).

2.4.8 Self-Assembly of Nanostructures on Yttria-stabilised Zirconia

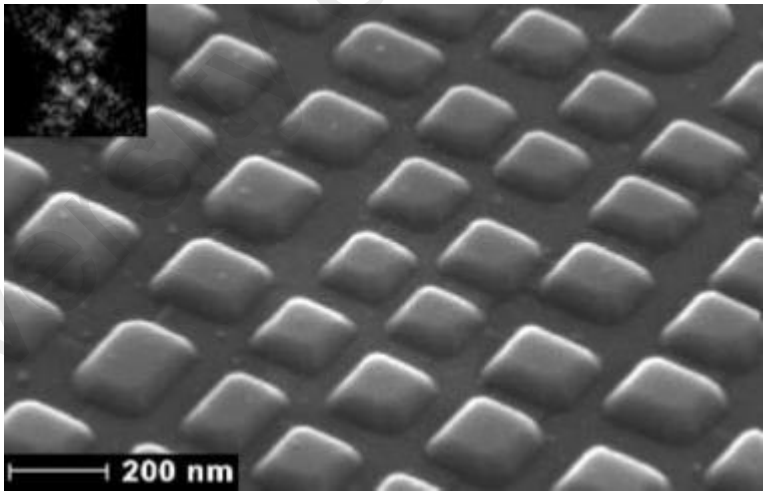

Figure 2.24: Scanning electron microscopic image of self-assembled nanostructures on (001)-YSZ (Rauscher et al., 2008).

Rauscher et al. (2008) discovered spontaneous ordering of nanostructures in oxide ceramics, in which self-assembly of nanoislands were observed on the surface of YSZ. Based on the study, the deposition of GDC film on the (100) surface of single crystal

YSZ broke up into nanoislands and this was attributed to a stress-driven instability (Figure 2.24). The self-assembly of islands was found in a new class of material which is oxide ceramic. In addition, the alignment and ordering of the nanoislands took place without guidance by lithography or multiple depositions (Rauscher et al., 2008).

On the other hand, these self-assembled nanostructures formed in the GDC-YSZ system could open up a new range of applications due to their oxygen conductivity, good chemical stability at high temperature, and transparency in the visible spectrum. As observed in Figure 2.24, the alignment of nanostructures was oriented with pseudoperiodicity. The islands formed in the GDC/YSZ system are ranging from 100 to 200 nm with a gap space of 10-75 nm as reported (Rauscher et al., 2008).

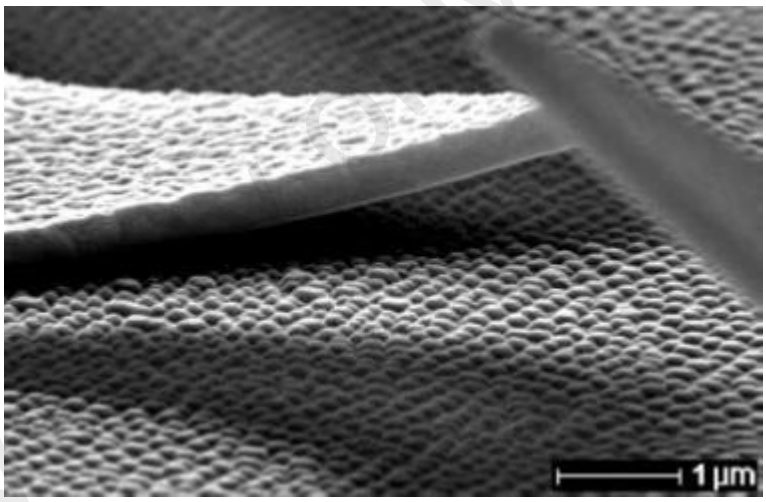

Figure 2.25: Scanning electron microscopic image of spalled GDC film with arrays of nanoislands formed during annealing (Rauscher et al., 2008).

In the early stage of the study, the formation of self-assembled nanoislands was studied by depositing a GDC film on the (100)-oriented YSZ in which the deposited film was spalled prior to annealing due to internal stresses in the film, and the nanoislands were formed on the exposed surface at varying annealing hours (Figure 2.25). The alignment of nanoislands along the <110> direction suggested that the

islands were governed by the elastic anisotropy of the substrate; meanwhile, the YSZ substrate has the lowest modulus along <110> on the (001)-surface. Hence, nanostructures have strong intrinsic to follow the most compliant axis and were aligned along this elastically favoured direction (Rauscher et al., 2008).

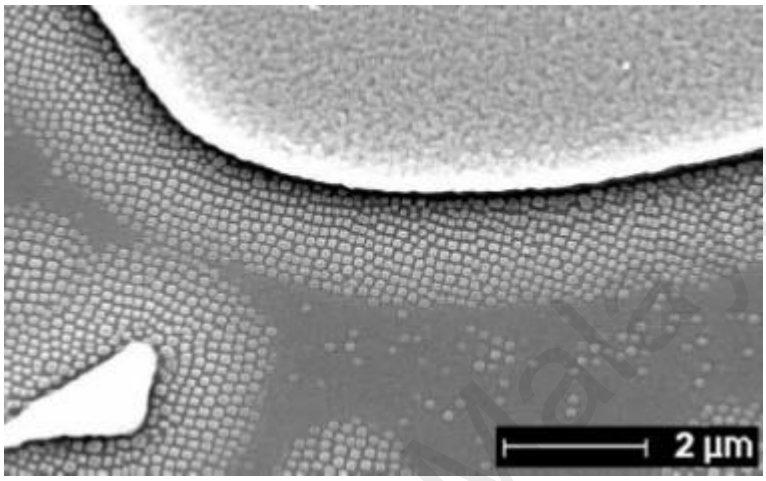

Figure 2.26: Formation of nanoislands on YSZ annealed at 1150 ^{o}C for 2 h with a ramping rate of 1 ^{o}C/min (Rauscher et al., 2008).

The formation of nanostructures in Figure 2.26 has suggested the contribution of stress state as a catalyst for the breakup of nanostructures, and the role of the unspalled patch as a diffusion source. The stress state at the spallation edge was claimed to be a favourable location for the formation of nanostructures, and this explained the outward growth of islands from the edge of spalled patches. The growth of the self-assembled islands was considered self-catalytic as the islands formed at a further distance had sharp facets and yet to achieve equilibrium shape (Figure 2.27). The formation of the newest islands was governed by the strain field of the existing islands. (Rauscher et al., 2008).

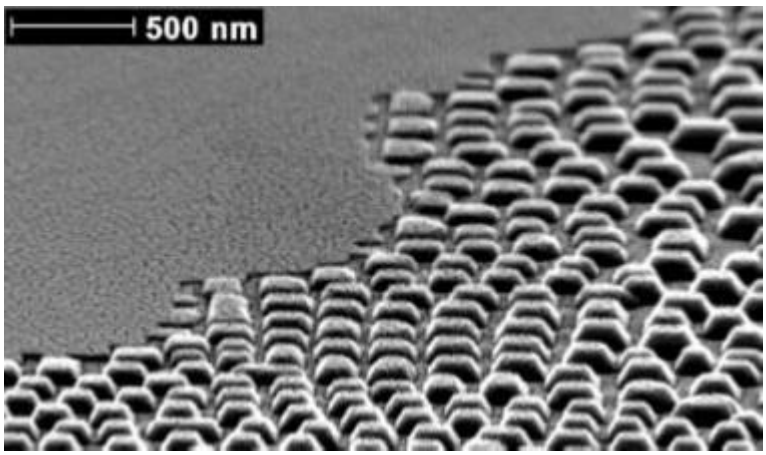

Figure 2.27: Scanning electron microscopic image of tilted YSZ substrates annealed at 1150 ^{o}C for 20 h with a ramping rate of 1 ^{o}C/min (Rauscher et al., 2008).

Ansari et al. (2013) have further investigated the mechanism of the formation of YSZ/GDC nanoislands by depositing the GDC source through different approaches, which are photolithography technique and the powder-suspension-based method. The formation of nanoislands were also found to be aligned along the <110> direction, which is in a good agreement with the finding by Rauscher et al. (2008). Furthermore, the use of photolithography has demonstrated that there was no contact between the GDC and the YSZ substrates between the patches prior to annealing treatment, as the surface was masked during the deposition of GDC (Figure 2.28a) (Ansari et al., 2013).

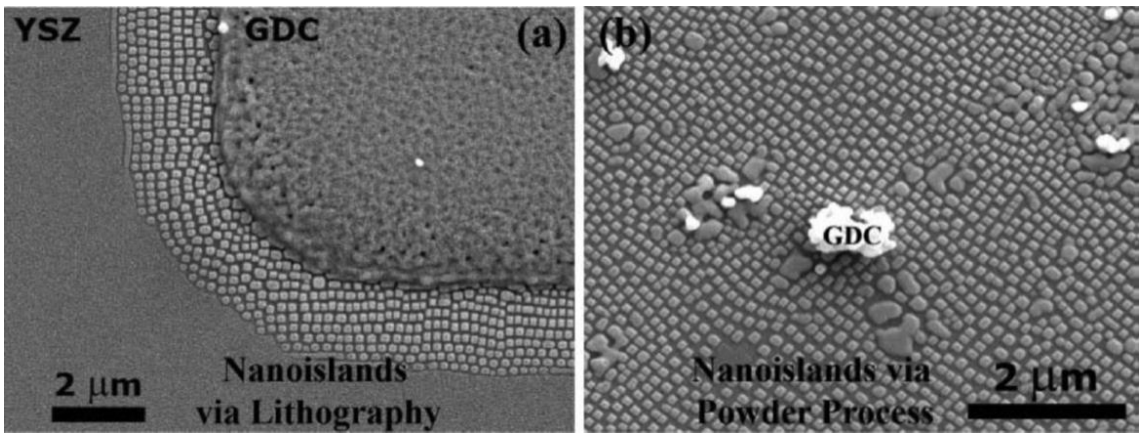

Figure 2.28: The formation of nanoislands via (a) lithography and (b) powder-suspension method (Ansari et al., 2013).

According to Boyne et al. (2011), although the GDC patches can initiate the formation of nanoislands next to the patches due to induced-stress, a local source of stress is necessary so that further formation of nanoislands can be sustained. Also, this local source of stress could be a chemical inhomogeneity (Boyne, Rauscher, Dregia, & Wang, 2011). This indicated that any means of GDC deposition would be able to cause the formation of nanoislands. Hence, a powder-suspension-based approach was taken to deposit the GDC source on the surface. As expected, arrays of nanoisland were formed on the substrate as seen in Figure 2.28b. The role of local stresses which was deemed necessary for a long-range formation of nanostructures, has been opposed by the experiments with powder-suspension-based approach, as the physical contact of powder with the surface was insufficient to yield a stress state comparable with those of GDC patches (Ansari et al., 2013).

Additionally, by increasing the ramp rate of annealing treatment, limited formation of nanoislands indicated that the islands were formed during or after the annealing treatment. This observation was further studied by a quenching experiment which allowed the YSZ substrates to be cooled immediately instead of usual cooling process. It was found that the formation of nanoislands occurred during the annealing treatment,

but not during the cooling process. Also, the formation of nanostructures on the quenched sample was similar to those on samples with normal cooling process (Ansari et al., 2013).

Parikh et al. (2012) reported the cellular behaviour of SK-N-SH neuroblastoma cells in response to nanofeatures fabricated by the GDC/YSZ system. The GDC thin film was sputter-coated on the YSZ substrates prior to annealing. Varying annealing profiles have resulted in different nanofeatures including islands, connected islands, and pits (Figure 2.29). The islands and pits shared similar average heights, 36.0±1.54 nm and 36.6±2.13 nm respectively. However, the feature spacing for the pits was much higher (124±53.5 nm) than that of the islands (55.3±35.0 nm); Meanwhile, the connected islands possessed an average feature height of 56.9±1.84 nm with an average feature spacing of 65.7±33.5 nm. The cells on connected islands and pits showed a better cell spreading while the cells on islands were more rounded. The stronger cell attachment on the connected islands and pits was attributed to the greater feature area (Parikh et al., 2012).

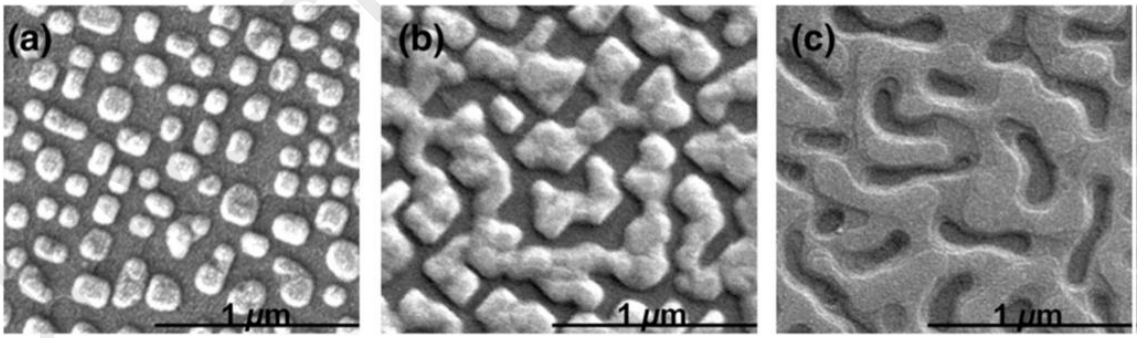

Figure 2.29: Scanning electron microscopic images of (a) islands, (b) connected islands, and (c) pits (Parikh et al., 2012)

2.5 Summary

This chapter discussed the literature in a chronological arrangement. Firstly, a brief review of biomaterials including different classifications of bioceramics and their

appplications, and secondly the background of zirconia. Finally, the various surface modification techniques that have been performed on zirconia biomaterials for the evaluation of *in vitro* and *in vivo* biological response.

In summary, the variety of techniques performed to produce surface-modified zirconia is still limited according to the literature. However, technological advances have introduced new approaches for the surface modification of zirconia, such as biofunctionalisation, laser treatment, and coating. The YSZ/GDC system for the fabrication of self-assembled nanofeatures is indeed a revolutionary change as it has brought the surface modification of zirconia to another level. The potential applications which may result from this discovery should be explored wider and further in future.

CHAPTER 3: METHODOLOGY

3.1 Introduction

This chapter provides detailed procedures on the fabrication and characterisation of nanostructures. Also, the protocols of cell culture and *in vitro* studies are stated thoroughly. A brief workflow of the study is illustrated in Figure 3.1.

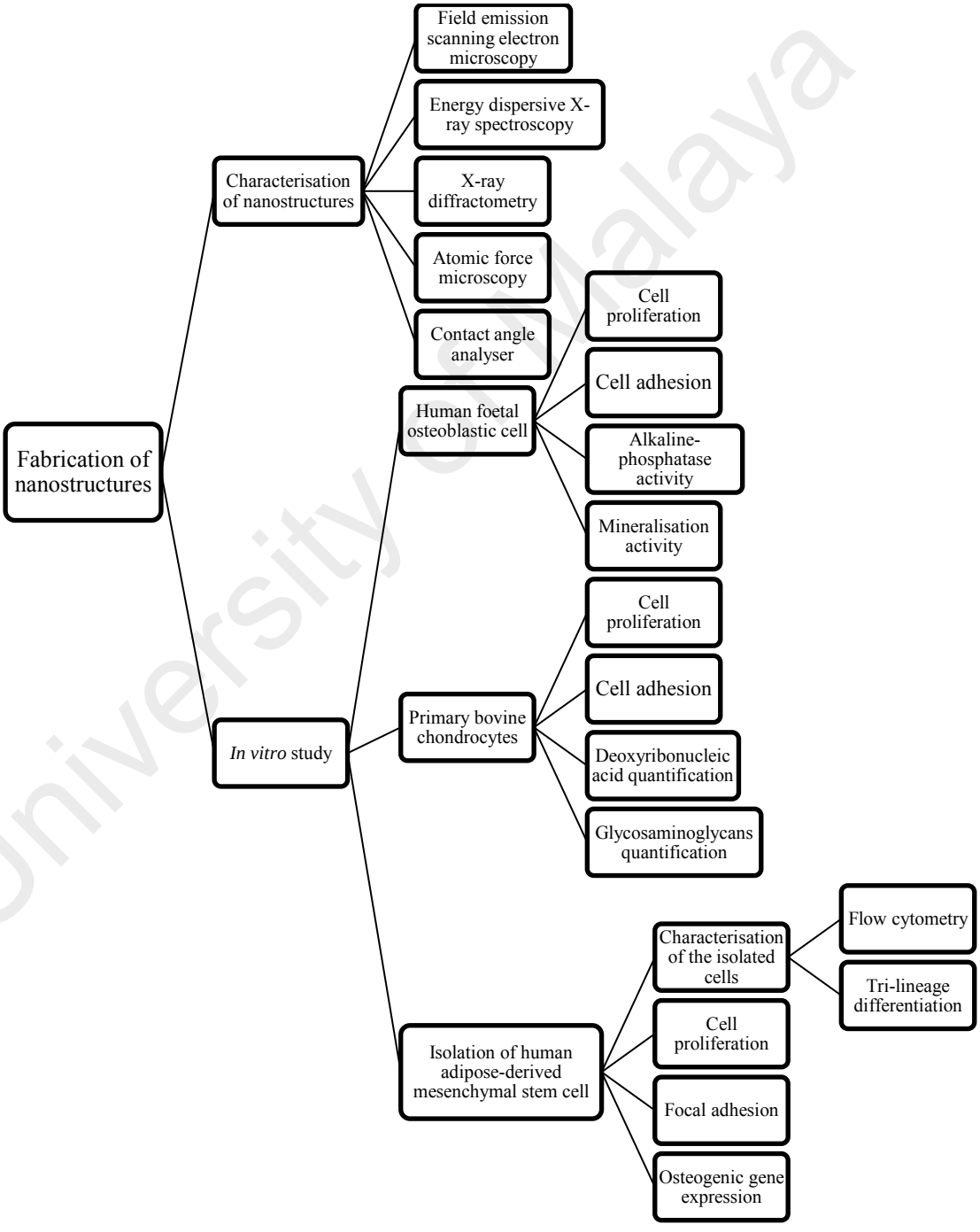

Figure 3.1: Workflow diagram

3.2 Fabrication of Self-assembled Nanoislands on Miscut YSZ-(001)

Single-crystal YSZ-(001) substrates with no miscut and different miscut angles (6 ^{o} and 10 ^{o}) toward [110] were purchased from MTI Corporation (USA). 10 mol% GDC powders used in this study were obtained from Nextech Materials (USA). All substrates were 5 mm x 5 mm x 0.5 mm (width x length x thickness) in dimensions and chemically polished before delivery. 0.1 g/L GDC powder suspension was prepared by dissolving 0.01 g of GDC powder into 100 mL of ultrapure water (membrapure Aquinity, Scientech, Taiwan). The powder suspension was ultrasonicated (Vibra-Cell VCX 500, Sonics & Materials, USA) for 5 min at 70% amplitude. The pulse effect was set to 5 s on and 1 s off. The ultrasonicated suspension was applied to the surfaces of substrates using pipette. The substrates with deposited GDC suspension were left to dry overnight, followed by annealing in a box furnace (Nabertherm, Germany) at different annealing profiles respectively (Table 3.1).

Table 3.1: **Annealing profiles.**

Profile	**Annealing temperature**	**Annealing hour(s)**	**Ramp rate**
Profile 1	1100 ^{o}C	1	10 ^{o}C/min
Profile 2		3	
Profile 3		5	
Profile 4		10	
Profile 5		15	

3.2.1 Characterisation of YSZ/GDC Nanoislands

3.2.1.1 Evaluation of Surface Morphology of Nanopatterned Substrates

Nanostructures were gold or platinum coated prior to observation using field emission scanning electron microscopy (FESEM; JSM 7600-F, JEOL, Japan; INCA-TOUCH software). The surface morphology of nanopatterned substrates formed by different annealing profiles was observed and compared.

3.2.1.2 Evaluation of Composition and Phase of Materials

Energy dispersive X-ray spectroscopy (EDX; ProX, Phenom) and X-ray diffractometry (XRD; Empyrean, PANalytical, Netherlands) were used to check the composition of the nanostructures and the phase purity of the materials respectively. Cu-Kα was used as the radiation source for the XRD which was operated at 45 kV and 40 mA. Step scan and scan speed were set at 0.02 ^{o} and 0.5 ^{o}/min respectively, with a 2 Θ scanning ranging from 20 ^{o} to 50 ^{o}.

3.2.1.3 Evaluation of Surface Roughness and Hydrophilicity of the Nanopatterned Surface

The surface roughness and the wettability of the surface were investigated by atomic force microscopy (AFM; Ambios Technology, USA; Gwyddion software) in contact mode (beam shaped cantilever) under ambient condition and contact angle goniometer (Kruss, Germany) (n=6). Wettability is indicated by the water contact angle, in which the higher the water contact angle, the lower the wettability of the surface.

3.3 Cell Culture

3.3.1 Culture of Human Foetal Osteoblastic Cell Line (hFOB)

A human fetal osteoblastic cell line was obtained commercially from ATCC (hFOB 1.19, ATCC No: CRL-11372). Complete growth medium was used to culture osteoblast, and consisted of Dulbecco's Modified Eagle's Medium: Ham's F12 (DMEM

F-12; #D8900, Sigma-Aldrich) supplemented with 10% fetal bovine serum (FBS; #FB-1001/500, Biosera), 1.2 g/L sodium bicarbonate (#S5761, Sigma) and 1% penicillin-streptomycin (#15140-122, Gibco, Life Technologies). 0.3 g/L geneticin (G418; #10131-035, Gibco) was also added to the medium according to the manufacturer's product sheet.

Thawing of the frozen cells should be conducted quickly, to reduce the damage to cells due to exposure to ice crystals. The vial was thawed in a clean water bath at 37 ºC and then centrifuged at 1500 rpm (K3 series, Centurion Scientific) for 5 min. The cell pellet was resuspended in complete growth medium and dispensed into a 75 cm^2 culture flask (T75 flask). The culture was kept in an incubator (Memmert, Germany) at 34 ºC under 5% CO_2. The culture medium was replaced every 3 days.

When the culture reached 70-80% confluence, subculturing was conducted by following procedures: Culture medium was discarded and the culture was rinsed three times with phosphate buffer saline (PBS; #P4417-100TAB, Sigma) as incomplete removal of medium would inhibit the action of trypsin. For each T75 flask, 5 mL of TryPLE express (#12604-021, Gibco, Life Technologies) was added to the flask, followed by incubation at 37 ºC for 5 min. When the cells were observed to be detached from the culture surface, 5 mL of complete growth medium was added to inactivate the trypsin. The cell suspension was centrifuged at 1500 rpm to form a cell pellet and the supernatant was discarded.

Cell counting is required before distributing the appropriate number of cells to new culture vessels. 1 mL of complete growth medium was added to resuspend the pellet. A uniform single-cell suspension is of importance for accurate cell counting. This can be achieved by pipetting the cell suspension several times using a 1 mL pipette (Eppendorf). Depending on the estimated number of cells, different dilutions can be

produced for ease of counting cells using a hemacytometer (Neubaeur, Optik Labor). If a 1:1 dilution is performed (a dilution factor of 2), the cells are diluted 1:1 (vol:vol) with 0.4% Trypan Blue in PBS (#F-7378, Sigma). 10 µL of the dilute was loaded to the chamber, carefully avoiding the appearance of bubbles in the chamber.

Under a microscope, unstained and illuminated dots (representing viable cells) in the 5 big squares of the chamber were counted. Concentration (cell/mL) of the cell suspension can be calculated by multiplying the average counts per square by dilution factor and 10,000. The cells were subcultured in new T75 flasks based on a seeding density of 5000 cells/cm^2.

For cryopreservation of hFOB, freezing medium was prepared by supplementing complete culture medium with 20% FBS and 8% dimethyl sulfoxide (DMSO; #2650, Sigma). After trypsinization and cell counting, the cell pellet was resuspended in freezing medium at a concentration of $1x10^6$ cells/mL. 1 mL of the mixture was aliquoted into each cryovial (Corning) to make up $1x10^6$ cells per cryovial. The cryovials were placed in Mr. Frosty freezing containers (Nalgene) and kept at -80 ^oC overnight before being transferred to a nitrogen tank.

3.3.2 Isolation and Culture of Bovine Chondrocyte

The metacarpal-phalangeal joints of cattle (18 to 24 months old Bos indicus calf) were washed in warm water and soaked in 70% alcohol for 30 min. The isolation of cartilage explants was conducted in a biosafety cabinet. The dissected cartilage was minced with sterile scalpels until a sludge-like appearance was observed, followed by digestion in 20 U/mL protease dissolved in PBS (#P8811, Sigma-Aldrich) for 1 h at 37 ^oC. After 1 h, the protease solution was replaced by 200 U/mL collagenase type II (#C6885, Sigma-Aldrich) in PBS and incubated for 16 h at 37 ^oC. The solution was then passed through a 70 µm cell strainer to generate a single-cell suspension. The

suspension was centrifuged at 2000 rpm for 5 min prior to removal of the supernatant. PBS was added to wash the cell pellet. The centrifugation process was repeated to remove the remaining proteolytic enzymes. The cell pellet was resuspended in culture medium and cultured in a 5% CO2 at 37 ^{o}C. The culture medium for isolated chondrocytes was a low glucose-DMEM (#D5523, Sigma-Aldrich) supplemented with 20% foetal bovine serum (Biosera), 3.7 g/L sodium bicarbonate (#S5761, Sigma), 2% antibiotic-antimycotic (AA; #15240-062, Gibco, Life Technologies), 2% HEPES (Lonza), 1% L-glutamine (#0374, Amresco, USA) and 0.0075 g/L L-ascorbic acid (#0764, Amresco, USA). The experiments in this study were conducted using primary bovine chondrocytes at an early passage to avoid dedifferentiation.

3.3.3 Isolation and Culture of Adipose-derived Human Mesenchymal Stem Cell (ADMSC)

Infrapatellar fat pad samples were obtained from donors (with written consent) at the University Malaya Medical Centre (UMMC). This study received ethical approval from the Medical Ethics Committee of the University of Malaya (MECID NO: 20163-2231, Appendix A). Donors were patients who underwent knee surgeries, at which the adipose tissue is usually discarded. The collected adipose tissue samples were washed several times with PBS supplemented with 5% AA (#15240-062, Gibco, Life Technologies), until the blood and blood vessels appeared to be removed completely. Autoclaved scissors were used to mince the tissue samples into small pieces prior to enzymatic digestion using 0.3% (w/v) collagenase type I enzyme (#LS004196, Worthington, New Jersey) in PBS. Minced samples in enzymatic solution were constantly rotated and agitated in the hybridization oven (ProBlot, Labnet) which was set at 37 ^{o}C for 1 h.

When the digested tissues were observed to be smooth, the samples were centrifuged (K3 series, Centurion Scientific) at 1500 rpm for 5 min. After centrifugation, the

samples were shaken to disrupt the pellet and to completely separate the stromal cells from the primary adipocytes. The centrifugation step was repeated and the supernatant was discarded. ADMSCs basal medium consisted of DMEM Low Glucose (#31600-034, Gibco) supplemented with 3.7 g of sodium bicarbonate (#S5761, Sigma), 10% FBS (#FB-1001/500, Biosera), and 5% AA (#15240-062, Gibco, Life Technologies). The pellet was resuspended in culture medium before being transferred to T75 flasks. If the tissue was not digested completely, the residual fat tissue would be collected and plated into culture flasks together with the resuspended cell pellet. After 7 days, the medium was discarded and the flasks were washed with PBS to remove residual tissue fragments and blood cells. Medium was changed every 3 days until 80% confluence was achieved. Subculturing and cell counting procedures were the same as previously described, except that ADMSCs basal medium was used.

3.3.3.1 Characterisation of ADMSC

(a) ***Tri-lineage Differentiation***

The StemPro chondrogenesis, osteogenesis, and adipogenesis differentiation kits (#A10071-01, #A10072-01, #A10070-01, Gibco, Life Technologies) were purchased for the tri-lineage differentiation study of isolated ADMSC. The basal medium and supplements in the kits were mixed according to the manufacturer's protocol. In brief, to prepare complete medium, 5% AA (#15240-062, Gibco, Life Technologies) was added to the complete medium. Cells at passage 2 were used in this study.

i Osteogenic Differentiation

ADMSCs were seeded into the wells of 12-well plate at $5x10^3$ cells/cm^2. The cells were initially incubated in ADMSC culture medium for 3 days, and then incubated in an osteogenic differentiation medium, which was changed every 3 days. After 21 days, the cells were washed with PBS prior to fixation with 10% formalin solution (#HT501128,

Sigma) for 10 min. The formalin was removed and the cells were rinsed with distilled water twice. Alizarin red S, 2% (w/v) solution was preprepared by dissolving 2 g of Alizarin Red S powder (#A5533, Sigma) into 100 mL of distilled water, followed by adjusting the pH to 4.1-4.3 with ammonium hydroxide (#AC458690010, Acros Organics). The cells were stained with 2% alizarin red S for 10 min, then rinsed with distilled water prior to visualisation under microscope for qualitative analysis. For negative control, ADMSCs basal medium was used instead of differentiation medium.

ii Chondrogenic Differentiation

A total of $1x10^6$ cells were centrifuged and cultured in pellet form with complete chondrogenic differentiation medium. After 21 days, the pellet was resuspended in chondrogenic differentiation medium, followed by incubation in 6-well plate with differentiation medium for 7 days. Safranin O staining, 0.1% (w/v) solution was preprepared by dissolving 1 g of Safranin O powder (#S2255, Sigma) into 1 L of distilled water. The cells were washed with PBS prior to fixation with 10% formalin solution (#HT501128, Sigma) for 10 min. The formalin was removed and the cells were rinsed with distilled water for 2 times. The cells were then stained with 0.1% Safranin O solution for 5 min, followed by rinsing with PBS prior to visualisation under microscope for qualitative analysis.

iii Adipogenic Differentiation

The cells were seeded into each well of 6-well plate at a density of $1x10^4$ cells/cm^2. The cells were incubated with stromal medium for 3 days, and then incubated with complete adipogenic differentiation medium which was changed every 3 days. After 21 days, the cells were washed with PBS prior to fixation with 10% formalin solution (#HT501128, Sigma) for 10 min. The formalin was removed and the cells were rinsed

with distilled water for 2 times. Oil red O staining, 0.3% (w/v) solution was preprepared by dissolving 0.7 g of oil red O (#O0625, Sigma) in 200 mL of isopropanol (#I9516, Sigma). Oil red O powders were added in addition. The cells were incubated with 60% isopropanol for 5 min, and then stained with freshly filtered 0.3% oil red O in 60% isopropanol for 5 min. The cells were rinsed with distilled water to wash off residual oil red O prior to visualisation under microscope for qualitative analysis.

(b) ***Flow Cytometry Assay***

The ADMSCs were detached and counted as described in the previous section (3.3.1). Stain buffer (#MAB554656, BD Biosciences) was used to resuspend the cells at a concentration of $1x10^7$ cells/mL. 100 µL of the cell suspension was transferred to each microcentrifuge tube. A human MSC analysis kit (#PMG562245, BD Biosciences) was purchased for the flow cytometric characterisation of isolated ADMSCs.

Commercial ADMSC (ATCC No: PCS-500-011) (passage 2, $1x10^6$) was used as positive control for flow cytometric characterisation of isolated ADMSC. Mesenchymal stem cell basal media supplemented with growth kit (#PCS-500-030, #PCS-500-040, ATCC) were purchased for the initial culture of admsc line. In addition, the medium was supplemented with 1% antibiotic-antimycotic (#15240-062, Gibco, Life Technologies). The cells were seeded into T75 flasks at a seeding density of 5000 cells/cm^2. The cultures were incubated at 37 ^oC under 5% CO_2 atmosphere. Subculturing and cell counting procedures were the same as previously described except that mesenchymal stem cell complete medium was used. At a later stage (passage 4), stromal medium which consisted of DMEM low glucose (#31600-034, Gibco) supplemented with 3.7 g of sodium bicarbonate (#S5761, Sigma), 10% FBS (#FB-1001/500, Biosera), and 5% AA (#15240-062, Gibco, Life Technologies), was used for the culture.

The fluorescent antibodies (FITC mouse anti-human CD90, PE mouse anti-human CD44, PerCP-Cy 5.5 mouse anti-human CD105, APC mouse anti-human CD73, hMSC positive isotype control cocktail, PE hMSC negative isotype control cocktail, hMSC positive cocktail, and hMSC negative cocktail) were added into each tube accordingly based on the technical data sheet. An unstained tube with only cells was prepared as a negative control. The tubes were incubated in the dark for 30 min. The cells were washed twice with stain buffer and resuspended with 500 µL of stain buffer. The samples were analysed on a BD accuri C6 cytometer (BD Biosciences, USA).

3.4 *In Vitro* Study

3.4.1 hFOB

On Day 0, osteoblasts were seeded on substrates at a density of $1x10^4$ cells/cm^2. At prescribed periods (Day 1, Day 3, and Day 7), the cell proliferation, differentiation, and mineralization were investigated by different assays. Culture medium was changed every 3 days. Complete medium for the culture of osteoblasts was used unless otherwise stated.

3.4.1.1 Cell adhesion

The cell adhesion study was conducted at day 1, 3, and 7. FESEM was used to observe the cell adhesion and morphology. The cells were washed thrice with PBS and fixed with 10% neutral buffered formalin solution (#HT501128, Sigma) for 1 h. The cells were dehydrated in a graded series of ethanol (30%, 50%, 70%, 90% and 100%) for 10 min each. Lastly, the samples were freeze dried (Labconco, USA) overnight.

3.4.1.2 Cell Proliferation

A resazurin reduction assay (alamar blue assay) was used to investigate the cell proliferation rate. The resazurin stock solution was prepared by dissolving resazurin sodium salt powder (#R7017, Sigma) into PBS at a concentration of 140 mg/L,

followed by sterile-filtration with a 0.2 μm bottle top filter (Corning). A 10% working solution was prepared freshly by diluting the stock solution with PBS. The substrates were rinsed twice and transferred into each well of a new 24-well plate. 1 mL of working solution was added into each well and the plate was incubated for 4 h. Triplicates of 100 μL of the mixed solution were pipetted to a 96-well plate (Nunc). The absorbance was measured at 570 nm and 595 nm using plate reader (FLUOstar OPTIMA reader, BMC LABTECH). The percentage of resazurin dye reduction was calculated by the manufacturer's formula (Pettit et al., 2005):

$$\frac{(\varepsilon_{OX})\lambda_2 \, A\lambda_1 - (\varepsilon_{OX})\,\lambda_1 \, A\lambda_2}{(\varepsilon_{RED})\lambda_1 \, A'\lambda_2 - (\varepsilon_{RED})\lambda_2 \, A'\lambda_1} \times 100 \qquad (3.1)$$

Where:

ε_{OX} = molar extinction coefficient of alamar blue oxidized form

ε_{RED} = molar extinction coefficient of alamar blue reduced form

A = absorbance of test wells

A' = absorbance of negative control well

A standard curve of percentage of resazurin reduction against cell concentration was prepared. Linear regression analysis was conducted and only assays with correlation coefficient $R^2 \geq 0.95$ were accepted for downstream analysis.

3.4.1.3 Alkaline-phosphatase Activity (ALP)

The cell differentiation was investigated through its ALP activity, which was measured by a Quantichrom ALP assay kit (#DALP-250, Bioassay Systems). In order to measure intracellular ALP, the cells were washed by PBS and lysed with 0.5 mL of 0.2% Triton X in 24-well plate. The plate was placed on a shaker for 20 min at room temperature (N-Biotek, Inc.). Working solution for each well was prepared by mixing 200 μL of assay buffer, 5 μL of magnesium acetate, and 2 μL of ρ-nitrophenyl phosphate. 50 μL of lysate was transferred into each well of 96-well plate and 150 μL

of working solution was added. 200 µL of distilled water and 200 µL of calibrator were added into separate wells respectively for control. The plate was read immediately (t=0 min) and read again after 15 min (t=15 min) at 405 nm using a plate reader (FLUOstar OPTIMA reader, BMC LABTECH). The ALP activity (IU/L) was calculated using the formula provided by data sheet:

$$\frac{(\text{OD sample}_{t=15\ \text{min}}\text{-OD sample}_{t=0\ \text{min}}) \text{ x reaction volume}}{(\text{OD calibrator-OD distilled water}) \times \text{sample volume} \times t} \times 35.3 \qquad (3.2)$$

3.4.1.4 Mineralisation Activity

To visualize the mineralisation activity, alizarin red S staining was performed to stain the extracellular calcium deposits. The cells were washed with PBS prior to fixation with 10% formalin solution (#HT501128, Sigma) for 10 min. The formalin was removed and the cells were rinsed with distilled water for 2 times. The cells were stained with 2% alizarin red S for 10 min and rinsed with distilled water prior to visualisation under a microscope for qualitative analysis.

3.4.2 Primary Bovine Chondrocyte

On Day 0, primary bovine chondrocytes were seeded on substrates at a density of $2.5x10^4$ cells/cm^2. At prescribed periods (Day 1, Day 3, and Day 7), the cell proliferation and glycosaminoglycan (GAGs) production were investigated by their respective assays. Culture medium was changed every 3 days. Complete medium for chondrocytes was used unless otherwise stated.

3.4.2.1 Cell adhesion

The cell adhesion at day 7 was observed under FESEM. The procedures for fixing and dehydrating the samples were as described in the previous section (3.4.1.1).

3.4.2.2 Cell Proliferation

A resazurin reduction assay was conducted to determine cell proliferation. The procedures were the same as described in the previous section (3.4.1.2) except that complete medium for chondrocytes was used. The growth of chondrocytes was also observed using a scanning electron microscope (SEM; Pro X, Phenom).

3.4.2.3 GAGs Quantification

The cells were collected and subjected to papain digestion. Papain digest buffer was prepared in advance with the following ingredients: 0.1576 g of L-Cysteine hydrochloride (#C1276, Sigma), 0.0806 g of ethylenediaminetetraacetic acid (EDTA; #E6758, Sigma), and 100 mL of PBS. 3 µL of papain (#P5306, Sigma) and 1 mL of digest buffer were added to each tube containing cells, and then incubated in an oven set at 65 ^{o}C for at least 1 hr with intermittent vortex-mixings. The digested samples were centrifuged at 10,000 rpm for 10 min. The supernatant was kept for the following GAG and DNA quantification.

The 1,9-dimethylmethylene blue (DMMB) assay was used to quantify intracellular GAG content. DMMB solution was prepared by dissolving 16 mg DMMB salt (#341088, Sigma) in 5 mL of ethanol in a clean glass container which was wrapped with aluminium foil, and then stirred with magnetic stirring bar. 950 mL of distilled water and 2 g of sodium formate (#K975, Sigma) were added to the dissolved DMMB. The solution was adjusted to pH 3 using formic acid (#0961, Amresco). To prepare a GAG standard curve, serial dilutions of bovine chondroitin-4-sulphate (#27042, Sigma) stock solution (1 mg/mL) were performed (Figure 3.2). Linear regression analysis was conducted and only assays with correlation coefficient $R^2 \geq 0.95$ were accepted for downstream analysis.

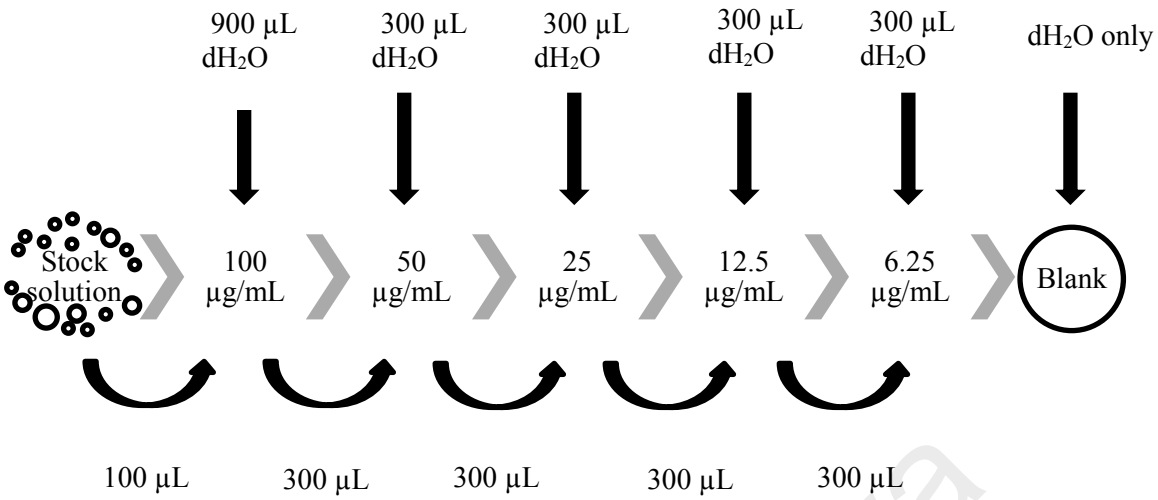

Figure 3.2: Schematic diagram of serial dilutions of bovine-4-sulphate standard.

40 µL of supernatant samples and standard dilutions were transferred to a 96-well plate before adding 250 µL of DMMB reagent into each well. Darkness was ensured due to light sensitivity of the reagent. The absorbance was measured at 595 nm using plate reader (FLUOstar OPTIMA reader, BMC LABTECH). The GAG production is then corrected for DNA synthesis and presented as GAG/DNA.

3.4.2.4 DNA Quantification

Hoechst 33258 working solution was made freshly by diluting the 1 µL of Hoechst stock solution (2 mg/mL; #861405, Sigma) with 10 mL of 2X saline sodium citrate buffer solution (SSC). Saline sodium citrate stock solution (20X) was prepared by dissolving 87.65 g of sodium chloride (#0241, Amresco) and 44.1 g of trisodium citrate (#0101, Amresco) in 480 mL of distilled water, and then adjusted to pH 7.0 with 1M sodium hydroxide or 1M hydrochloric acid. The solution was made up to 500 mL by adding distilled water. The 2X saline sodium citrate working solvent was made by diluting the stock solution with distilled water.

To prepare a DNA standard curve, serial dilutions of DNA standard (1 mg/mL; #D1501, Sigma) were performed (Figure 3.3). Linear regression analysis was conducted and only assays with correlation coefficient $R^2 \geq 0.95$ were accepted for downstream analysis. 40 µL of supernatant samples and DNA dilutions were distributed into each well of a black 96-well plate (Corning), followed by adding 200 µL of Hoechst working solution. The fluorescence was measured using plate reader (Ex: 355 nm; Em: 460 nm; FLUOstar OPTIMA reader, BMC LABTECH).

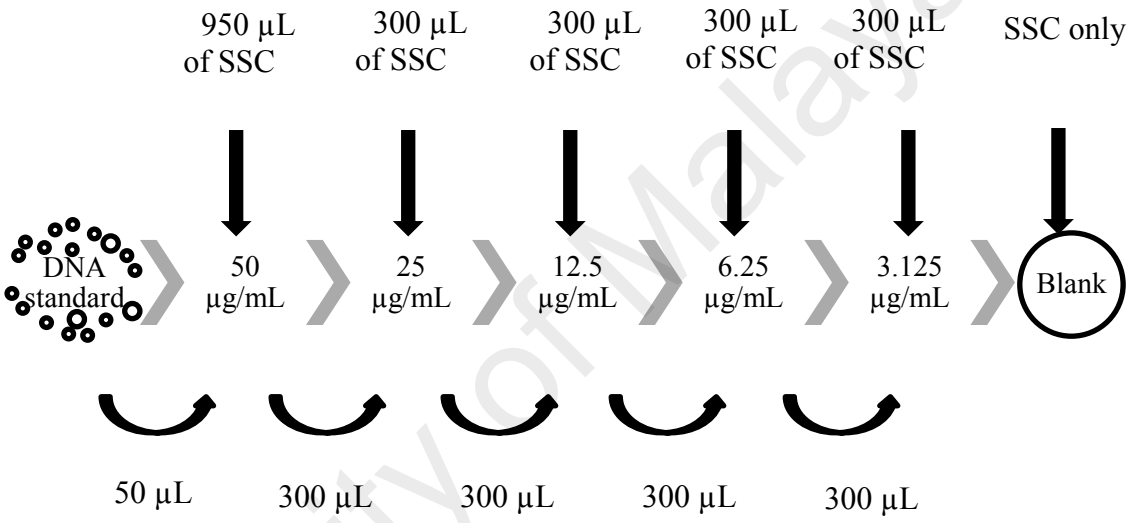

Figure 3.3: Schematic diagram of serial dilutions of DNA standard.

3.4.3 ADMSC

On Day 0, ADMSCs were seeded on substrates at a density of 1.2×10^4 cells/cm^2. At prescribed period (Day 1, Day 3, Day 7, and Day 14), the cell proliferation was measured by alamar blue assay. Culture medium was changed every 3 days. ADMSC basal medium was used unless otherwise stated. The immunohistochemical staining was performed to visualise the focal adhesion of ADMSC on substrates at early stage. The osteogenic potential of nanoislands was investigated by the changes in osteogenic gene expression of ADMSC through quantitative reverse-transcription polymerase chain reaction (RT-qPCR).

3.4.3.1 Focal Adhesion

The cells were seeded on the substrates at $5x10^3$ cells/cm^2 for 1 h prior to fixation with 4% paraformaldehyde for 20 min at room temperature. 4% paraformaldehyde was prepared earlier by dissolving 4 g of paraformaldehyde powder (#P6148, Sigma) into 100 mL of PBS. The mixture was heated at 60 ^oC after adding 1 mL of 1 M sodium hydroxide solution. After the mixture turned clear and cooled to room temperature, the pH was adjusted to 7.4 with 1 M hydrochloric acid. The mixture was filtered through a 0.45 µm filter to remove any particulate matter.

After fixation, the cells were washed twice with PBS and permeabilized with 0.1% Triton X-100 (#85111, Thermo Scientific) for 5 min at room temperature. Then, the cells were washed twice with PBS again. Blocking solution was applied for 30 min at room temperature. Blocking solution was prepared in advance by dissolving 1 g of bovine serum albumin (#0322, Amresco) into 100 mL of PBS and filtered through a 0.45 µm filter. Actin cytoskeleton and focal adhesion staining kit (#FAK100, Millipore) was used to study the focal adhesion of ADMSC on substrates at an early stage. The antibodies were diluted in blocking solution according to Table 3.2.

Table 3.2: **Dilution factor for antibodies.**

Antibody	Dilution
Anti-vinculin	1:250
Anti-mouse secondary antibody (AP124F, Millipore)	1: 100
Phalloidin	1:500
DAPI	1:500

The incubation of antibodies was performed at room temperature unless otherwise stated. The diluted anti-vinculin was incubated for 1 h and then washed thrice with PBS. The diluted anti-mouse secondary antibody and phalloidin were incubated simultaneously for 30 min and washed thrice with PBS for 5 min each. Nuclei counterstaining was performed with the incubation of DAPI for 5 min. The cells were washed thrice for 5 min each and then covered with PBS prior to visualisation with a confocal laser scanning microscope (Leica TCS SP5 II , Germany).

3.4.3.2 Cell Proliferation

The procedures were the same as described in the previous section (3.4.1.2) except that ADMSC basal medium was used.

3.4.3.3 Gene Expression

The ADMSCs were cultured on the control and nanostructured substrates in the presence of osteogenic medium. The osteogenic medium consisted of stromal medium, supplemented with 100 nM dexamethasone (#D4902, Sigma), 10 mM β-glycerophosphate (#G9891, Sigma), and 0.5 mM ascorbic acid-2-phosphate (#A8960, Sigma). The primers for osteo-lineage genes (RUNX2, OPN, BGLAP) and endogenous genes (HPRT1) were purchased from First BASE laboratories (Table 3.3).

Table 3.3: Primers used in RT-qPCR

Gene	Primers 5'→3'	PCR product (bp)
HPRT1	F: GAC AGG ACT GAA CGT CTT GC R: TCC AGC AGG TCA GCA AAG AA	110
RUNX2	F: CTA GGC GCA TTT CAG GTG C R: ACT GGC GGG GTG TAA GTA AA	139
OPN	F: GAA TTG CAG TGA TTT GCT TTT GC R: CTT GGA AGG GTC TGC TTT TCC	100
BGLAP	F: ATT GTG GCT CAC CCT CCA TC R: AGG GCT ATT TGG GGG TCA TC	119

(a) ***RNA Extraction***

RNeasy micro kit (#74004, Qiagen) was used for the RNA extraction in this study. Before the isolation of RNA, 4 volumes of ethanol were added to the buffer RPE to make working solution. For the preparation of DNase digestion, DNase stock solution was completed by injecting 550 µL of RNase-free water into the vial containing DNase I, to dissolve the lyophilized DNase. The cells can be lysed directly in the well plate or trypsinized and collected for cell lysis. Nevertheless, the cells should be lysed immediately with buffer RLT after harvesting to avoid undesirable changes in the gene expression. The cell lysate was collected in a microcentrifuge tube and vortexed to homogenize the lysate. The homogenized lysates were stored at -70 ^{o}C in the freezer (Forma, Thermo Scientific) until RNA extraction was carried out.

The frozen lysates were thawed quickly in a clean water bath at 37 ^{o}C. 1 volume of 70% ethanol was added to the lysate and mixed by pipetting. The sample was then

transferred to RNeasy MinElute spin column and centrifuged at 10,000 rpm for 15 s. All the centrifugation steps during RNA extraction were performed at room temperature. The flow-through was discarded. 350 µL of buffer RW1 was added to each RNeasy MinElute spin column and centrifuged at 10,000 rpm for 15 s to wash the spin column. RW1 was used as a washing buffer to remove biomolecules such as carbohydrates, protein, and fatty acids.

For DNase digestion, DNase I incubation mix (10 µL of DNase I stock solution and 70 µL buffer RDD) was added directly to the spin column. After 15 min, 350 µL of buffer RW1 was added to the spin column and centrifuged at 10,000 rpm for 15 s. The flow-through was discarded. The spin column was placed in a new collection tube provided by the kit. 500 µL of buffer RPE was added to the spin column and centrifuged at 10,000 rpm for 15 s. The flow-through was discarded. Buffer RPE was supplied as a concentrate and required dilution with ethanol before use. It was used to remove trace of salts on the column.

500 µL of 80% ethanol was added to the spin column. The spin column was centrifuged at 10,000 rpm for 2 min and the flow through was discarded. The spin column was then placed in a new collection tube and centrifuged at 12,000 rpm for 5 min with the lid being opened. Again, the spin column was placed in a new collection tube. 14 µL of RNase-free water was added directly to the spin column membrane and the column was centrifuged at 12,000 rpm for 1 min to elute the RNA. The RNA eluates were stored at -80^{o}C for downstream applications.

(b) ***RNA Quality Assessment***

The RNA purity was checked using a Nanodrop 2000 spectrophotometer (Thermo Scientific). Before measuring the purity of samples, a 'blank' was established using RNase free water. 1 µL of the RNase free water was placed onto the bottom pedestal

and the measurement was conducted. The purity of samples was also measured with the same procedure. After each measurement, the pedestals were gently wiped with laboratory wipe. Only RNA samples with high purity ($A_{260/280}$>1.8) were used for downstream applications.

The RNA integrity and concentration were evaluated using Experion RNA StdSens analysis kit and Experion automated electrophoresis system (Biorad, USA). The RNA stain, RNA loading buffer, and RNA gel were equilibrated to room temperature before use. The gel stain was filtered with a spin filter tube supplied by the kit and centrifuged at 4000 rpm for 10 min. Fresh gel-stain solution was prepared at a 65:1 ratio. The mixed solution was vortexed and kept from the light. RNA ladder and samples were thawed on ice, followed by denaturation at 70 ^{o}C for 2 min. The denatured ladder and samples were immediately cooled on ice for 5 min, spun down for 5 s, and stored on ice until analysis was carried out.

The LabChip required priming before loading the RNA ladder and samples. For priming the chip, 9 µL of filtered gel-stain solution was pipetted into the GS well and the chip was run at the priming station. The chip was considered properly primed when the glass chip appeared opaque. After successfully priming the chip, 9 µL of gel-stain solution and filtered gel were pipetted into GS well and G well respectively. 5 µL of loading buffer was loaded in each sample well and L well. 1 µL of RNA ladder and 1 µL of samples were pipetted into L well and each sample well respectively. The chip was vortexed in the Experion vortex station for 1 min, and then transferred to the chip platform of Experion electrophoresis station for analysis. Only RNA samples with good integrity score (>9) were to be used for downstream applications.

(c) ***Reverse transcription-quantitative polymerase chain reaction (RT-qPCR)***

After checking the purity and integrity of extracted RNA, the RNA was subjected to a reverse transcription process to synthesis cDNA. All the reactions were set up in 200 µL PCR tubes and a thermal cycler (S1000, Biorad, USA) was used for the incubation steps. The template RNA, gDNA removal mix, and reverse transcription enzyme (QuantiNova reverse transcription kit; #205413, Qiagen) were thawed on ice; meanwhile, the reverse transcription mix and RNase–free water were thawed at room temperature. Before conducting genomic DNA removal reactions, the components required were prepared according to Table 3.4. The genomic DNA removal reaction was set up on ice, subsequently incubated at 45 ^{o}C for 2 min, and kept on ice immediately. The components required for reverse transcription were also prepared according to Table 3.4 and kept on ice. After the genomic DNA removal reaction was completed, the RNA template was added to the reverse-transcription reaction, and incubated in the thermal cycler at 25 ^{o}C for 3 min and 45 ^{o}C for 10 min. To inactivate the reverse transcription enzyme, the reaction was incubated at 85 ^{o}C for 5 min.

Table 3.4: **Setup for genomic DNA removal reaction and reverse-transcription reaction**

Part I: Genomic DNA removal reaction	
Component	**Volume (µL)**
gDNA removal mix	2
Template RNA (100 ng/µL)	8
RNase-free water	5
Total volume per reaction	15
Part II Reverse-transcription reaction	
Reverse transcription master mix	1
Reverse transcription mix	4
Genomic DNA removal reaction from Part I	15
Total volume per reaction	20

A reaction mix for two-step PCR (QuantiNova SYBR Green PCR kit; #208054, Qiagen) was set up according to Table 3.5. The reaction mix was then dispensed into PCR plates and subjected to a cycling program in the real-time PCR system (StepOnePlus, Applied Biosystems). The cycler conditions were set up as follows: initial activation step at 95 ^{o}C for 2 min, denaturation at 95 ^{o}C for 5 s, and annealing/extension at 60 ^{o}C for 1 min.

Table 3.5: **Set up for qPCR reaction.**

Component	**Volume (µL)**
2x QuantiNova SYBR green master mix	10
QN ROX Reference Dye	2
Forward Primer (10 µM)	0.7 µM
Reverse Primer (10 µM)	0.7 µM
RNase-free water	3.2
Template DNA	2
Total volume per reaction	20

The expression of target genes was normalised to the expression of endogenous gene. The relative quantities of expressions were calculated using the comparative C_T approach. Also, the changes in osteogenic gene expression were shown relative to the control samples.

3.4.4 Statistical analysis

Throughout this study, the statistical differences between the control substrates and nanopatterned substrates were investigated by using Student's *t*-test. Statisitical significance in the differences is determined by $p < 0.05$ and indicated by *.

CHAPTER 4: RESULTS AND DISCUSSION

4.1 Optimisation of the Formation of Nanoislands on Miscut YSZ-(001)

This study examined the influence of annealing dwell time on the formation of self-assembled nanostructures on 6-degree and 10-degree miscut YSZ-(001) substrates by a simple annealing treatment. All samples were doped with GDC. At different dwell times (1, 3, 5, 10, and 15 h), the formation and alignment of nanostructures on the miscut substrates were observed. At shorter annealing times (<5 h) (Figure 4.1 (a-d)), the formation of nanostructures was poor. However, at longer annealing times (from 5 h to 15 h), the formation of nanostructures was clear and its morphology and alignment were anneal time dependent. The best annealing profile in this study was defined by the one that produced highest ratio of individual nanoislands with the highest order of alignment. Since an annealing profile temperature of 1100℃ held at 5 h and ramp rate of 10℃/min produced significantly improved formation of nanostructures on miscut substrates in terms of alignment and the number of individual nanoislands, the average sizes of nanoislands were calculated based on the nanostructures produced with this annealing profile. By comparing the substrates with different miscut angles, the nanoislands on 6-degree miscut substrates showed comparable average size (103.39 ± 24.26 nm) with the 10-degree miscut substrates (107.6 ± 26.7 nm). Increasing the dwell time did not improve the formation of individual nanoislands as more connected or merged islands are observed (Figure 4.1 (g-j)). Prolonged annealing no longer produced additional individual islands. The excessive thermal energy provided by prolonged annealing, increases the size of nanoislands since forming additional islands might not be favourable at this condition due to limited space, as individual islands have already fully occupied the miscut surface. Nucleation of new nanoislands between existing nanoislands might be difficult due to a repulsive interaction between the islands. Thus,

the continuos size expansion of individual nanoislands eventually resulted in the merging of individual nanoislands.

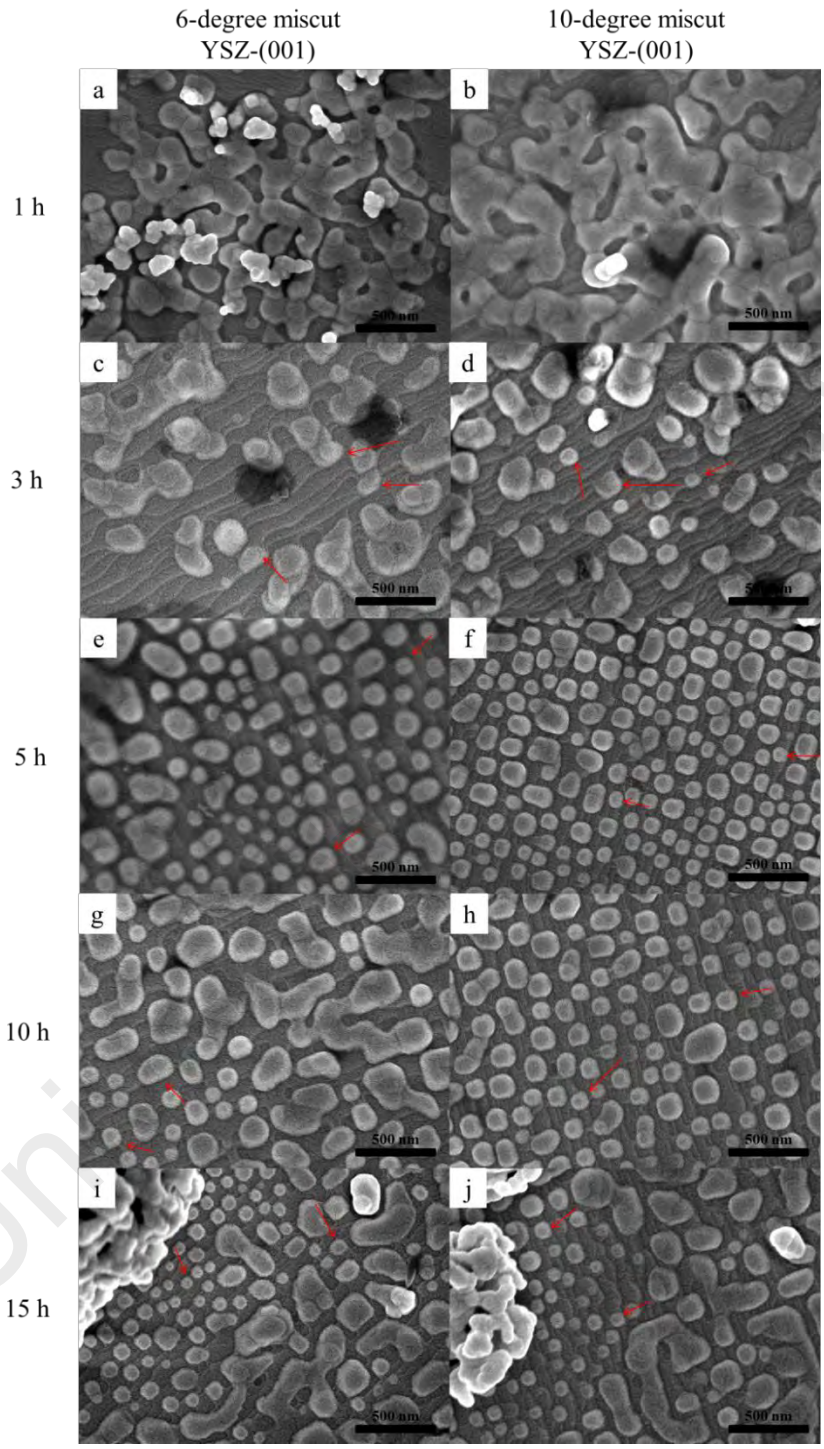

Figure 4.1: Formation of nanostructures on (a, c, e, g, i) 6-degree and (b, d, f, h, j) 10-degree miscut YSZ-(001) substrates, annealed at 1100℃ for (a,b) 1 h, (c, d) 3 h, (e, f) 5 h, (g, h) 10 h, and (i, j) 15 h at a ramp rate of 10℃/min.

The formation of nanoislands on YSZ substrate is a solid state reaction between the GDC powder and YSZ substrates. Similar to Ostwald ripening, in which larger island consuming the smaller island may occur but the main mechanism is coalescence of the nanoisland forming larger nanoislands and eventually lead to colonisation. When continuous heat energy is supplied, the nanoislands continuously grow to a point that the repulsive force between nanoislands is large enough to inhibit the growth of nanoislands. Further heating eventually causes the energy to surpass the repulsive force between nanoislands and lead to merging of nanoislands.

Further examination has shown that YSZ/GDC nanoislands formed on the substrates have a strong tendency to align along the miscut steps (Figure 4.1 (e-j)), especially the step edges (indicated by red arrows), as supported by Niu et al. (2017). The miscut steps have provided favourable nucleation sites at the edges to allow nucleation of nanoislands. A preference to align along the steps (indicated by red arrows) can also be seen clearly at lower annealing time (Figure 4.1(c) and Figure 4.1(d)), even though the shape of the surface structures were distorted compared to the nanoislands seen in Figure 4.1 (e) and Figure 4.1 (f). It is generally known that the driving force for mass transfer is the difference in chemical potential. The tendency to nucleate at the edge of step could be due to its low chemical potential since particles move from a region with high chemical potential to the region with low chemical potential.

According to Yang et al., although convex region (positive curvature) possesses the highest chemical potential, the highest strain relaxation opposes the contribution from the surface energy and decreases the chemical potential at that region. Thus, a local region with minimum chemical potential was formed in the most convex region (Yang, Liu, & Lagally, 2004). Additionally, the presence of substrate steps favoured heterogeneous step nucleation instead of homogenous nucleation due to higher binding

energy at the step edge as supported by Marsico et al. (1997), Roder et al. (1993), and Zhong et al. (2008). Hence, the binding energy at the step edge has made it a preferential site for nucleation.

A closer examination on the effect of degree of miscut on the formation of nanoisland, comparing substrates (6-degree and 10-degree miscut) with the same annealing time (Figure 4.1 (e) and 4.1 (f)), the spacing formed between nanoislands on 6-degree miscut substrate is wider than 10-degree miscut. The larger step width of 6-degree miscut substrate could be contributing to the wider space. In this study, it was reported that the nucleation of islands tends to occur at the edge, hence, it is not surprising to see the spacing between the nanoislands on 6-degree miscut is wider.

She and Wang (2009) have reported the lateral interaction is important for the ordering of nanostructure formation (She & Wang, 2009). In this study, it was shown that the periodicity of nanoislands formed on 10-degree miscut substrate is enhanced. This could be explained by the existence of stronger island-island interaction due to relatively narrower step on 10-degree miscut substrate. Since the nucleation of islands tends to occur at the edge, the narrower steps found on 10-degree miscut reduce the distance between islands. In other words, lateral interaction is stronger with a shorter distance between neighbouring islands.

In a separate study, when non-miscut YSZ-(001) was used as substrate, a significantly larger coverage of nanoislands is observed on miscut YSZ surface (Figure 4.1(e) and Figure 4.1(f)) compared to non-miscut YSZ surface (Figure 4.2(b)). Miscut surface could have lowered the nucleation barrier for the formation of nanoislands by providing steps, due to the more effective strain relief by deforming the underlying lattice near the edge, as supported by Kamins et al. (1999). The formation of nanoislands on non-miscut YSZ were not as distinguisable as compared to those formed

on miscut surface. Something worth mentioning, the alignment of nanoislands at 10 h annealing time for the non-miscut YSZ was observed along certain direction (indicated by red line) and it was presumed to be parallel to the <110> direction (Figure 4.2 (b)). This could be due to the elastic anisotropy of YSZ substrate in which the elastic modulus is the lowest along <110> direction on YSZ-(001). Elastic interaction has contributed to this phenomenon, as reported by Rauscher et al. (2008). According to Lau et al. (1977), local distortion of substrate lattice would result in the elastic interaction between two adsorbates to be repulsive. Without the lateral interaction (repulsive or attractive), distribution of nanostructures would be random. Lateral interaction is of particular interest in the formation of islands as it helps to enhance the order of nanostructures (She & Wang, 2009).

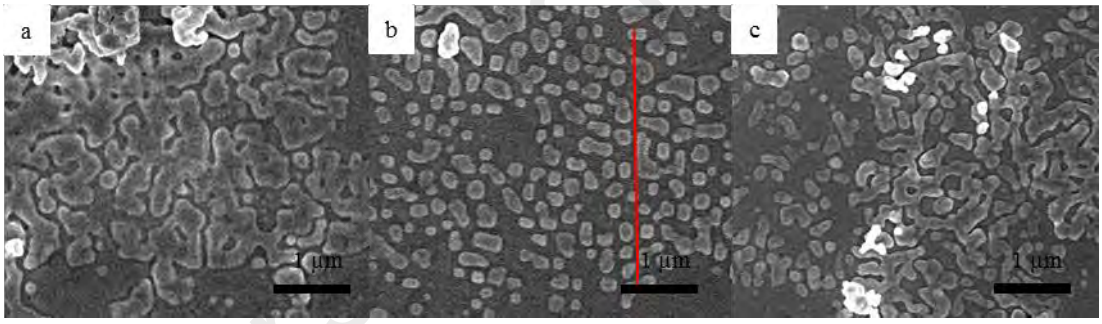

Figure 4.2: Formation of nanoislands on non-miscut YSZ-(001), annealed at 1100 °C for (a) 5 h, (b) 10 h, and (c) 15 h at a ramp rate of 10 °C/min.

Overall, the 10-degree miscut YSZ substrates annealed for 5 h have produced significantly ordered nanoislands and the coverage of individual nanoislands was more evident than that on 6-degree miscut. Hence, 10-degree miscut YSZ substrates annealed with this annealing profile will be fabricated for all the following experiments, with control samples produced from 10-degree miscut SZ substrates without heat treatment.

4.2 Characterisation of Nanoislands Formed on Miscut YSZ

In this experiment, 10-degree miscut YSZ substrates annealed for 5 h were prepared for further characterisation such as surface morphology, surface roughness, hydrophilicity, composition, and phase. The nanopatterned 10-degree miscut YSZ substrates (annealed for 5 h) will be referred as nanopatterned samples whereas the control samples (10-degree miscut YSZ substrates without heat treatment) will be referred as flat samples.

4.2.1 Evaluation of Surface Morphology of Nanopatterned Substrates

Figure 4.3 shows the surface morphology of the flat sample and nanopatterned sample in which nanoislands were absent on the control sample. On the nanopatterned samples, the size of the individual nanoislands was 107.6 ± 26.7 nm as reported previously. The spacing between the islands was 48.3 ± 20.7 nm.

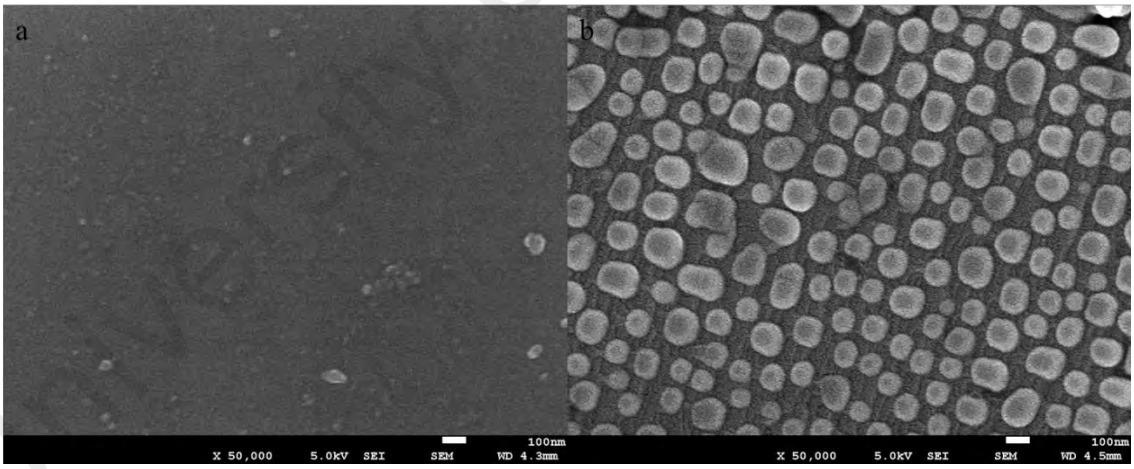

Figure 4.3: FESEM images of (a) flat sample and (b) nanopatterned sample.

4.2.2 Evaluation of Composition and Phase of Nanopatterned Samples

XRD results showed that the nanopatterned substrate was in cubic phase (Figure 4.4 (a)). The elements found in the nanopatterned substrate are stated in Figure 4.4 (b). The elemental composition consisted of gadolinium (Gd), cerium (Ce), oxygen (O), yttrium (Y), and zirconium (Zr) and this complied well with the XRD results obtained. Based

on Figure 4.4 (a), it is evident that the YSZ peak was found at 34.7 ^{o}, complying well with the (001) plane of the miscut substrate. In addition, the addition of GDC powder to YSZ miscut substrate caused no effect to the phase stability as no secondary phases were observed. This is important as the presence of secondary phases could affect the biocompatibility of the material.

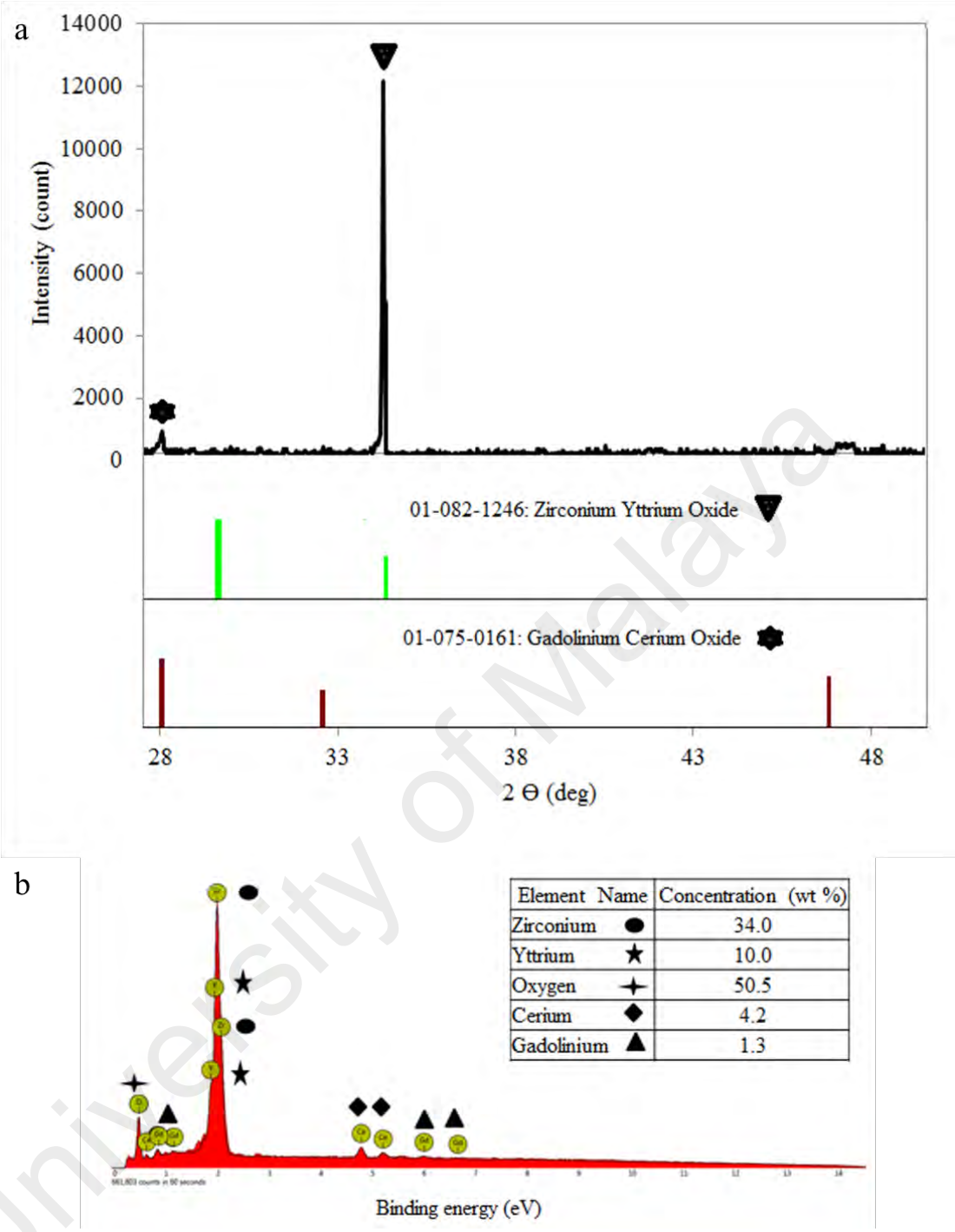

Figure 4.4: (a) XRD and (b) EDX results describing the phase stability and elemental composition of the nanopatterned samples.

4.2.3 Evaluation of Surface Roughness and Hydrophilicity of Nanopatterned Surface

The surface roughness R_a of the flat samples and nanopatterned samples was obtained by an AFM. The nanopatterned surface (R_a = 30.5 ± 2.1 nm) was expected

to be rougher than the flat surface (R_a = 17 ± 1.8 nm) due to the presence of nanoislands. The nanopatterned samples also presented a more hydrophilic surface than the control samples (84.8 ± 2.3°) as the water contact angles formed by sessile liquid drops on nanopatterned samples (51.7 ± 1.9°) were lower (Figure 4.5). Higher surface roughness leads to an increase in surface area thus enhancing the wettability of nanopatterned samples. Overall, the nanopatterned samples possessed an enhanced surface roughness and hydrophilicity in comparison with the control samples.

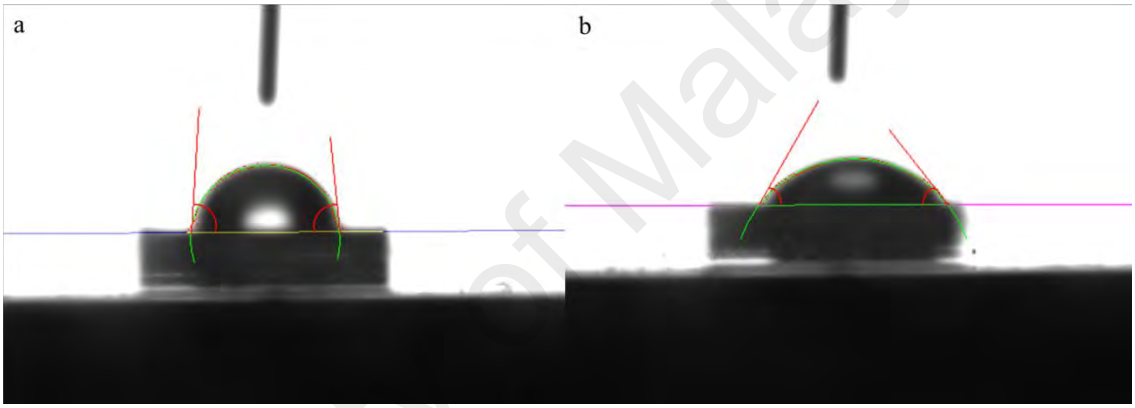

Figure 4.5: Water contact angle analysis of (a) flat samples and (b) nanopatterned samples.

4.3 *In Vitro* Study

It is imperative to ensure the biocompatibility of materials through a series of studies including *in vitro* tests, *in vivo* animal studies, and eventually clinical studies. Preliminary study of the biocompatibility of materials can be conducted through *in vitro* test before going into *in vivo* tests or clinical study. A satisfactory outcome obtained through these *in vitro* tests will assure the potential use of these nanostructured materials for biomaterial applications at an early developmental stage. In this study, osteoblasts, chondrocytes, and mesenchymal stem cells was chosen to study their cellular response on the nanopatterned samples in term of adhesion, proliferation, and

differentiation. Zirconia has demonstrated its potential as a biomaterial in dental and orthopaedic applications, and hence, it is of interest to investigate the interaction of osteoblasts, chondrocytes, and mesenchymal stem cells with the nanopatterned samples. This is because the adhesion of hard-tissue cells plays a key role in the sucesss of implant and biomaterials (Liu et al., 2007). Also, this study included the focal adhesion and proliferation of mesenchymal stem cells due to the fact that mesenchymal stem cells are also known to be initial colonisers of an implant surface (Gittens et al., 2013). The osteogenic potential of mesenchymal stem cells on nanopatterned samples was investigated as the differentiation of adherent cells towards the osteoblast lineage is important for the process of osseointegration (Mendonça, Mendonça, Aragao, & Cooper, 2008).

4.3.1 hFOB

4.3.1.1 Osteoblasts Adhesion

In order to establish a tight bond between the material and tissue, adequate cell adhesion is a key necessity for the subsequent differentiation process to take place and achieve the success of osseointegration. The formation of focal adhesion allows cell signal to transmit from the surrounding milieu into the cell through the cytoskeleton. These cell signalling events resulting from the cell adhesion and spreading will affect the following proliferation and differentiation process. Hence, it is of crucial importance to evaluate the biological impact of surface topography as the cell adhesion and spreading are highly responsive to the substrates they are in contact with (Sjöström, Lalev, Mansell, & Su, 2011).

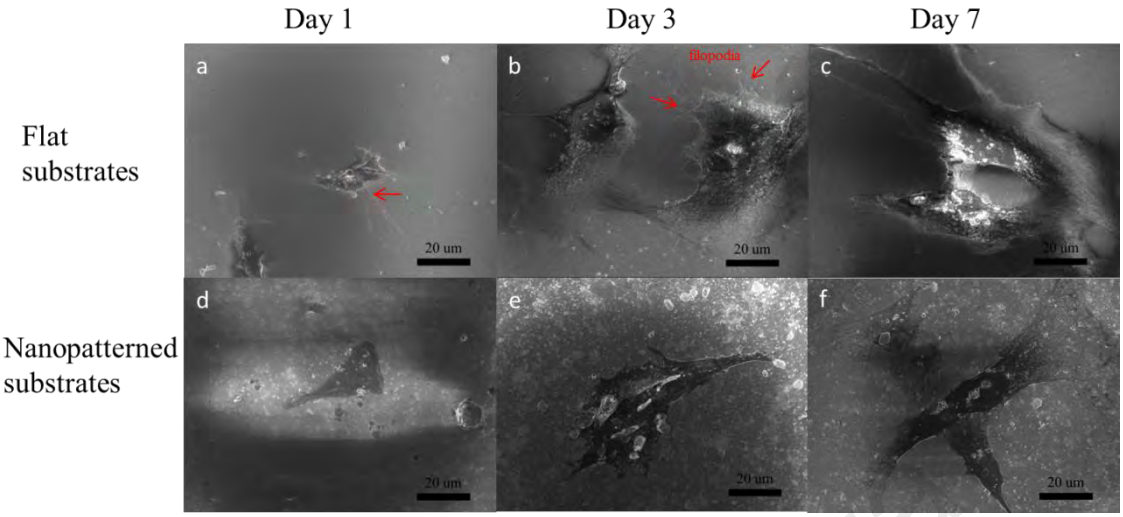

Figure 4.6: Scanning electron microscopic images of osteoblast adhesion on flat and nanopatterned samples at day 1, 3, and 7.

Based on Figure 4.6 (a), it can be seen that the osteoblasts were still in a rounded shape on the flat control surface at day 1. The filopodia extensions (indicated by red arrows) of the cells were also less intensive. Notably, the size of the cells was half that of those on the nanopatterned surface. This has indicated that the initial cell attachment was not as robust on the control samples in comparison with the nanopatterned samples. On the other hand, the cells on the nanopatterned surfaces at day 1 (Figure 4.6 (d)) were observed to be slightly spread and more elongated in size.

Due to the highly extensive coverage of nanostructures on the surface and some leftover GDC residues, it was difficult to capture the fine details of thin filopodia on the nanopatterned substrates. Nevertheless, the cells on nanopatterned samples were apparently more well-spread than those on flat control samples. In contrary to the cells on control samples which were evenly spread out and less elongated (Figure 4.6 (b)), the cells on nanopatterned samples appeared to be more elongated with extending lamellipodia protusions (Figure 4.6 (e)). The cells on nanopatterned samples have portrayed a stronger adhesion and conformation at different time interval even at day 7.

Overall, the quick spreading and flattening of cells indicated that the nanopatterned substrate is more compatible for cell growth.

According to Sjostrom et al. (2011), "the cells will actively sense the substrate, or the extra-cellular matrix covering the surface, for preferential adhering sites". The nanoislands on the surface in this study have been demonstrated to be a more favourable site for cell attachment for several likely factors. The distinctive cell performance in term of initial cell adhesion and spreading could be attributed to the presence of nanoislands which provide extensive gripping points for the cells to adhere to. On top of that, the presence of nanostructures also offered more surface area for cells to conform to the nanotopography. This again illustrates how topographical features are among the factors affecting cell behaviour on the material surface.

It is also known that cells receive topological cues from the surrounding in their microenvironment and respond to the cues. The surface roughness of bone has been reported to be 32 nm, being made up of nanophase hydroxyapatite with a size of 100 nm (Mendonça et al., 2008; Oh et al., 2006). As described earlier, the surface roughness of the nanopatterned samples in this study was 30.5±2.1 nm, which closely resembles that of natural bone; meanwhile, the size of nanoislands (107.6±26.7 nm) is also comparable to that of nanophase hydroxyapatite. In recent, researchers have been working on creating biomaterial that highly resembles or mimics the actual dynamic environment where cells reside. Not only do the surface nanofeatures allow mechanical interactions with cell receptors and regulate the cell behaviour, but they can also be perceived as microenvironment-like substances by the cells (An et al., 2013). The surface features and texture imposed by the nanoislands could have rendered the nanopatterned substrates to be more "microenvironment-like" than the flat control substrates. Thus, the nanopatterned surface appeared to be a more appealing site for cell growth.

4.3.1.2 Osteoblasts Proliferation

It is important to ascertain the cell growth on material in an attempt to investigate the cytocompatibility of the material. Materials with good biocompatibility allow cells to proliferate well and do not impede the cell viability. Figure 4.7 demonstrates an increased cell proliferation on both flat control and nanostructured samples. Both samples have shown considerable cell growth on the surfaces as indicated by the reduction of resazurin, particularly nanopatterned surfaces that outperformed the flat surfaces with a higher proliferation rate at all different time points.

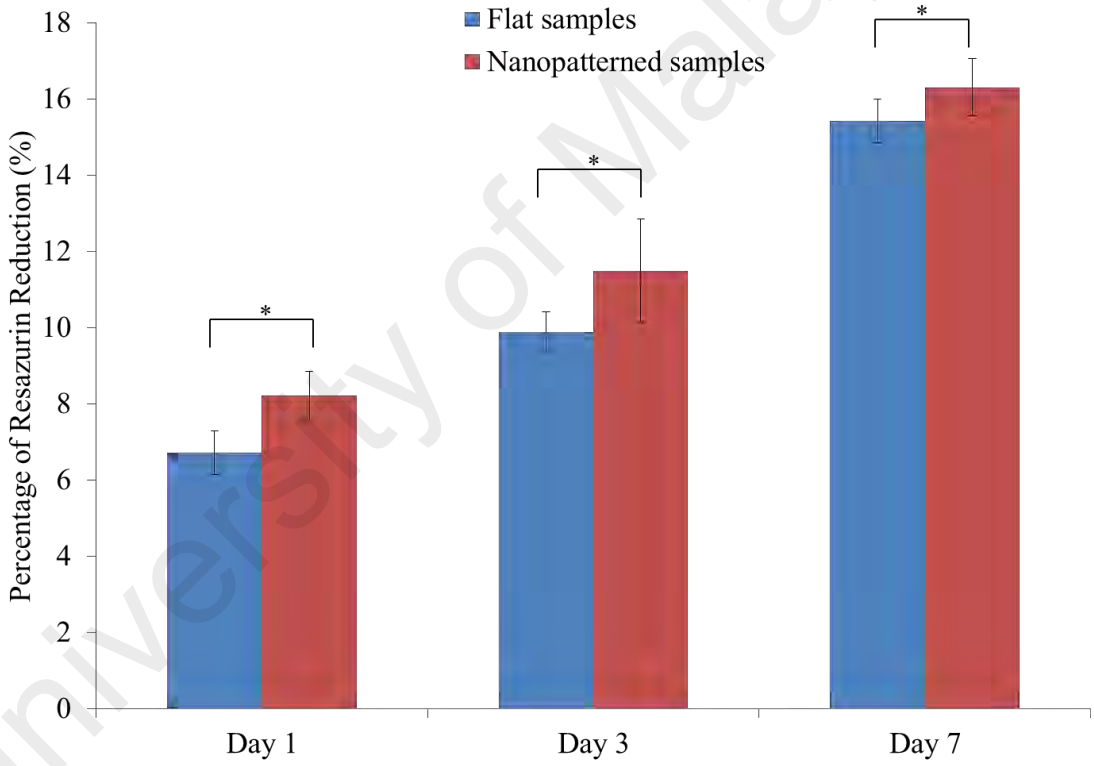

Figure 4.7: Cell proliferation on flat and nanopatterned samples (n=6) at different time points. Statistical significance is indicated by * at $p<0.05$.

On the basis of resazurin reduction, nanopatterned samples are seen to show a significantly higher cell proliferation rate at $p<0.05$ in comparison with the flat control samples at day 1,3, and 7. This implies that the nanopatterned samples have elicited

significant osteoblast growth at the surface. This finding also indicates that surface nanotopography exerts a certain level of influence in regulating the cell proliferation. Besides, the excellent initial cell attachment on the nanopatterned surfaces as discussed previously can also contribute to the subsequent proliferation. It is generally known that osteoblast preferred to adhere on rougher surface (Brett et al., 2004). Hence, the higher proliferation rate of osteoblasts on the nanopatterned samples in comparison to the flat sample may be due to the rougher surface imposed by nanopatterned samples.

Other than surface roughness, surface wettability has also been associated with the enhanced growth of osteoblasts. According to Mendoça et al. (2008) the surface wettability manipulates the protein-surface interaction which is involved in the cell adhesion. The interaction between protein and the material surface is an important aspect in the osseointegration process as the protein adsorption influences the subsequent cell behaviour in term of attachment and proliferation (Mendonça et al., 2008). For instance, the adsorbed extracellular matrix proteins on the biomaterial surfaces interact with the cell membrane receptor integrins which eventually affect the cellular response to the biomaterial (Intranuovo et al., 2010).

The nanopatterned samples possessed a considerable lower contact angle than the flat sample. In other words, the nanopatterned surface was more hydrophilic and had a higher wettability. Hence, previous results implied that osteoblasts tend to adhere and proliferate on a surface with higher hydrophilicity. Previous study by Frandsen et al. (2013) has also demonstrated the use of superhydrophilic nanotube-coated zirconia surface resulting in superior adhesion and integration of osteoblasts. Hence, nanotechnology can be a powerful tool to alter the surface topography at nanoscale and govern the cell growth at the surface.

4.3.1.3 ALP Activity and Mineralisation

ALP is known as a bone cell phenotypic marker which has often been used to examine the osteoblast differentiation and mineralisation in research. It is of importance to look into the mechanism underlying the formation of hard tissue, in order to enhance the feasibility of bone disease treatment and the development of functional bone biomaterials (Lim, Hansen, Siedlecki, Runt, & Donahue, 2005). ALP has long been noticeable for its role in the formation of hard tissue. Although the mechanism of the biological function of ALP is controversial, vigorous research has reaffirmed the role of ALP to be a reliable marker that indicates osteogenic activity. The expression of ALP in bone tissue takes place in the early stage of development and ALP is reported to be one of the first expressed functional genes during the calcification. Hence, these suggest that ALP is distinctly possible to be involved in the beginning of mineralisation process. In addition, this enzyme has been found to increase the local amount of inorganic phosphate, one of the mineralisation promoters. ALP has become a favoured marker to examine the osteoblast phenotype or maturity of the mineralisation process, due to the key role of ALP in osteogenesis and also the ease of conducting the assay (Golub & Boesze-Battaglia, 2007).

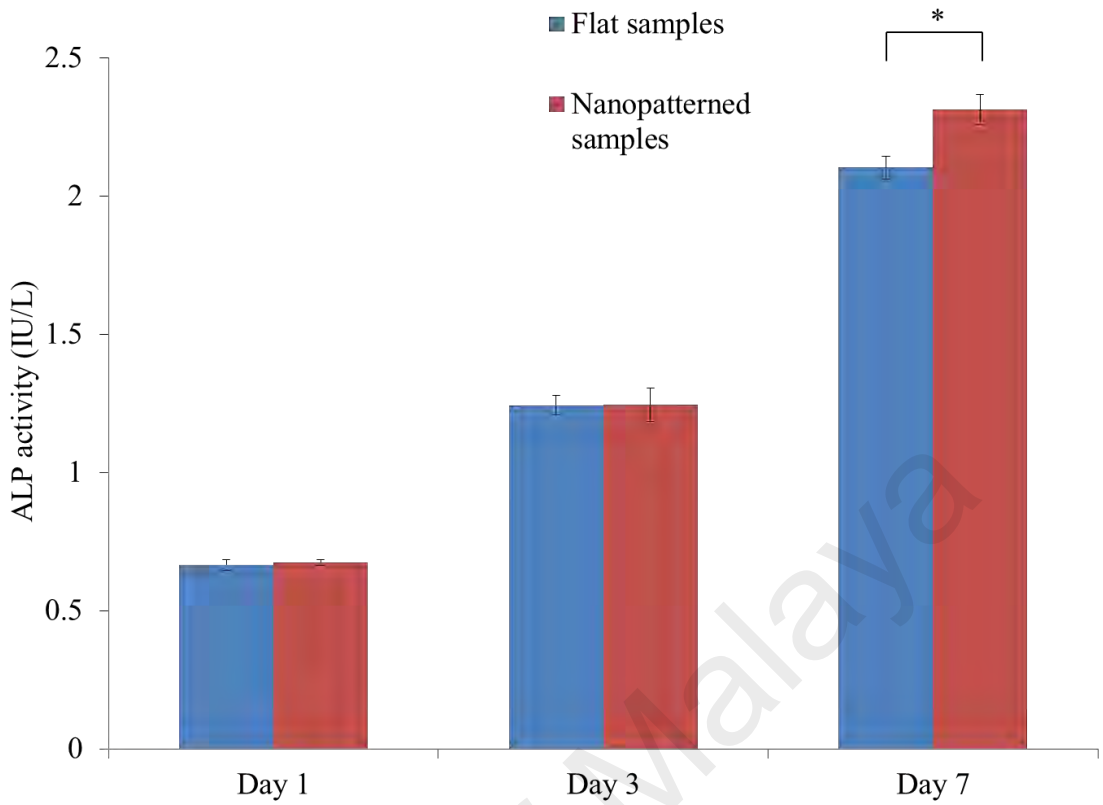

Figure 4.8: ALP activities on flat and nanopatterned samples (n=6) at day 1, 3, and 7. Statistical significance is indicated by * at p<0.05.

As seen on Figure 4.8, the ALP activity of osteoblast on nanopatterned samples was significantly higher than that on flat samples at day 7. It is very likely that the nanostructures have elicited the positive response of osteoblasts in which the osteoblast differentiation was significantly enhanced on the samples with nanostructures. According to Aparicio et al. (2002), a higher osteoblast differentiation with a lower osteoblast proliferation indicates a good cellular response. The proliferation of nanopatterned samples at day 7 was the highest among all but the increment in cell proliferation was not as outstanding as in those in the early stage. This can be explained by the reciprocal relationship between proliferation and differentiation in which an increase in osteoblast differentiation is often accompanied by a reduced proliferation (Aparicio, Gil, Planell, & Engel, 2002). When cells undergo a transition to a mature

state, they will become less proliferative and this leads to a decrease in cell number (Gittens et al., 2013).

It is evident that the nanostructures have shown to improve the osteoblast maturation through the higher ALP activity. The statistically significant higher ALP activity on nanopatterned samples appeared to illustrate an intriguing relationship between the osteoblasts and nanostructures. This observation is supported by the findings where ALP activity is proven to be substrate-dependent and the surface nanotopography may be influential in affecting the osteoblast phenotype (Lim et al., 2005). On the other hand, the enhanced osteoblast differentiation can also be due to the outstanding cell adhesion and proliferation as discussed earlier. Also, improved osteoblast differentiation has also been related to the initial cell spreading where enhanced cell spreading resulted in a greater level of differentiation (Sjöström et al., 2011).

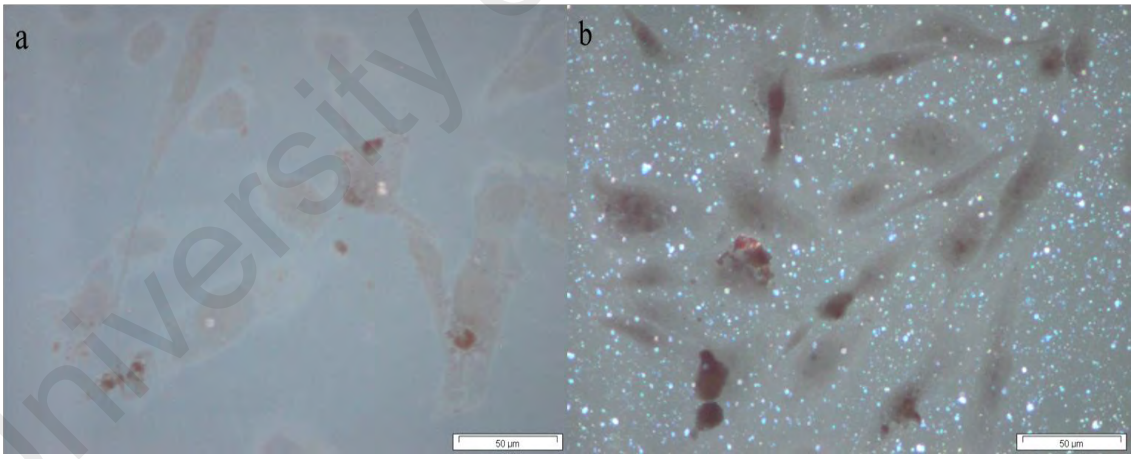

Figure 4.9: Alizarin red S staining of osteoblasts on (a) flat sample and (b) nanopatterned sample at day 7.

To examine the osteoblast differentiation and maturation through mineralisation activity, Alizarin red S staining was performed to stain the calcium deposits. Figure 4.9 has revealed the stained calcium deposits on flat sample and nanopatterned sample at day 7 in which more stained calcium deposits were observed on the nanopatterned

sample. This implied that the nanostructures promoted a higher mineralisation capability of osteoblasts and also provided a preferential site for the bone cells to mature. Also, the observed mineralisation as shown by the stained calcium deposits appeared to correlate well with the ALP activity judging from the significantly higher ALP activity on nanopatterned sample at day 7. In this study, the maturation of osteoblasts on nanopatterned samples has been testified through a higher mineralisation activity of osteoblasts. According to Frandsen et al. (2011), the ability of osteoblasts to carry out matrix mineralisation can gauge the cell maturation during the final event of osteogenesis. It is evident that the nanostructures imposed a positive influence on the bone cells considering that the stained mineralised matrix is more noticeable on the nanostructured surface.

The surface modification should be treated with importance as a means to improve the tissue reactivity toward the material and promote a positive cell-substrate interaction. In this study, the surface modification of material is conducted by introducing the nanotopographic features to the surface. Overall, a desirable cellular response has been exhibited by the osteoblasts as disclosed through the enhanced cell spreading, attachment, proliferation, and differentiation.

4.3.2 Primary Bovine Chondrocyte

4.3.2.1 Cell Adhesion

It is imperative to study the structure-property relationship between the implant and biomaterial properties to address the challenges of hard-tissue repair or replacement. On top of that, the adhesion of hard tissue cells such as osteoblast and chondrocytes plays an important role in the success of the designed implant (Liu et al., 2007). Based on recent findings, chondrocytes have shown a good affinity to the surface nanostructures, suggesting the potential use of the substrates for cartilaginous applications. It is also

recommended that bi-functional substrates should be developed for the growth of hard and soft tissues to benefit the patients with both bone and cartilage tissue damage (Tan, Dalilottojari, Pingguan-Murphy, Ahmad, & Akbar, 2014). This idea was also supported by Brammer et al. (2010) in which a dual-funtioning substrate is expected to encourage cartilage growth as well as aid osseointegration by providing adequate mechanical support.

The use of polymer scaffolds such as polyglycolic acid, polyethylene glycol hydrogels, and polylactic acid is commonly applied to study the *in vitro* expansion of chondrocytes (Brammer, Oh, Frandsen, Varghese, & Jin, 2010). However, the clinical application of these materials as bone/cartilage prosthesis has been limited due to their less compatible mechanical properties in comparison to the native tissue (Kay, Thapa, Haberstroh, & Webster, 2002). To our knowledge, very few studies have been conducted to study chondrocyte growth on surface-modified zirconia material. Hence, this study will provide a glimpse of the chondrocyte response towards the self-assembled nanostructures of the nanopatterned samples.

It can be observed that chondrocytes adhered well on both flat samples and nanopatterned samples at day 7, as seen in Figure 4.10. The chondrocyte growth was dense on both samples, indicating a good biocompatibility of the substrates. Also, cell-cell contact was complex, with cells overlaying each other over the surfaces. The intense filopodia morphology of chondrocytes showed tight anchorage to both substrates, which revealed that flat and nanopatterned samples possessed comparably appealing surfaces for chondrocyte attachment.

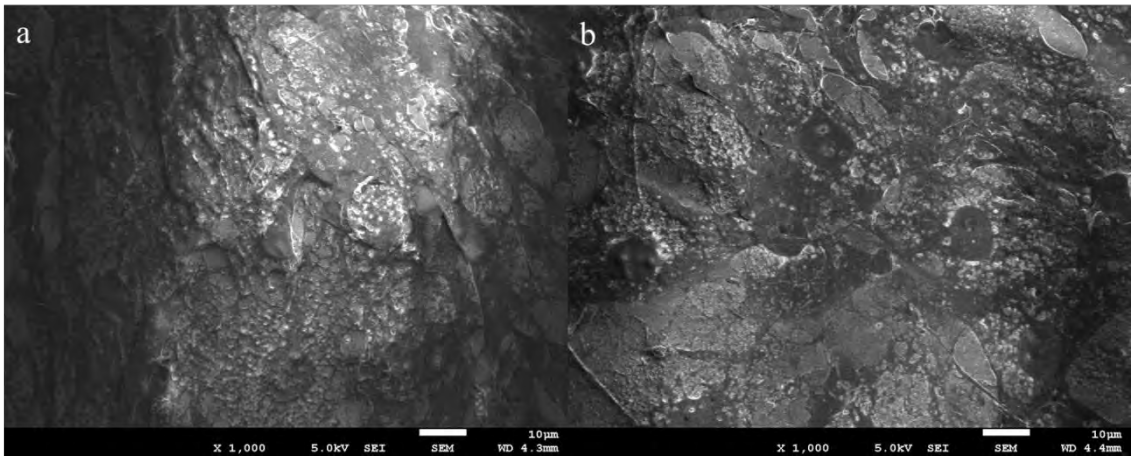

Figure 4.10: FESEM images of chondrocyte adhesion on (a) flat sample and (b) nanopatterned sample at day 7.

4.3.2.2 Chondrocytes Proliferation

Figure 4.11 illustrated a significantly enhanced cell proliferation on nanopatterned samples at day 3 and day 7.

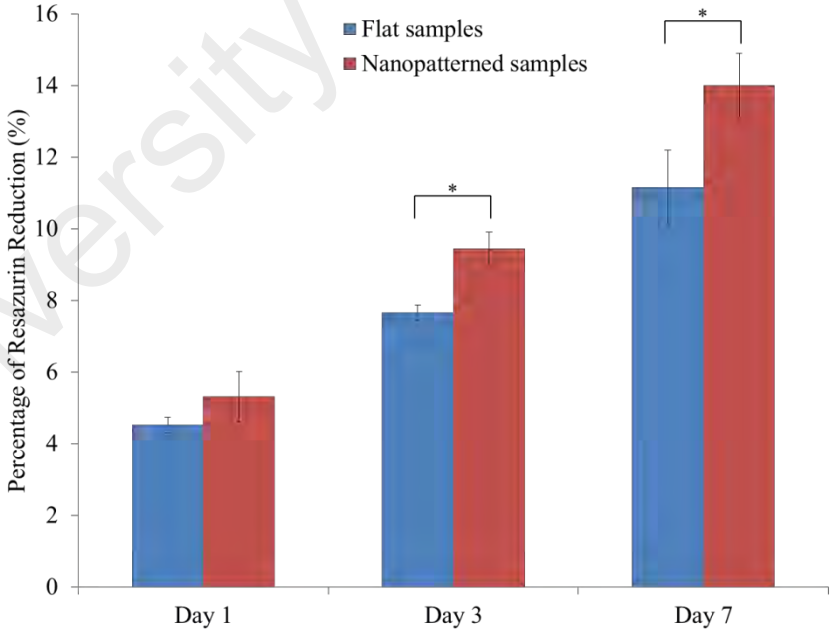

Figure 4.11: Chondrocyte proliferation on flat and nanopatterned samples (n=3) at day 1, 3, and 7. Statistical significance is indicated by * at $p<0.05$.

This result is in good agreement with other published results which concluded that increased nanometer roughness enhance the chondrocyte adhesion and proliferation (Burns, Yao, & Webster, 2009; Jun, Park, & Webster, 2002). It is known that cartilage formation and functionality are highly dependant on chondrocytes. However, due to the low repair capacity of the cartilage, cartilage defects could be challenging as the source of chondrocytes is in short supply and the cell isolation for the autologous chondrocyte implantation is invasive. Also, the expansion of chondrocytes in culture would eventually result in dedifferentiation of the chondrocytes (Prittinen et al., 2014). Jun et al. (2002) has presented the idea of using synthetic biomaterials which boost the chondrocyte adhesion and growth for cartilage regeneration. Hence, the good adhesion and significantly up-regulated proliferation of chondrocytes on nanopatterned samples depicted its promising prospects for cartilaginous application.

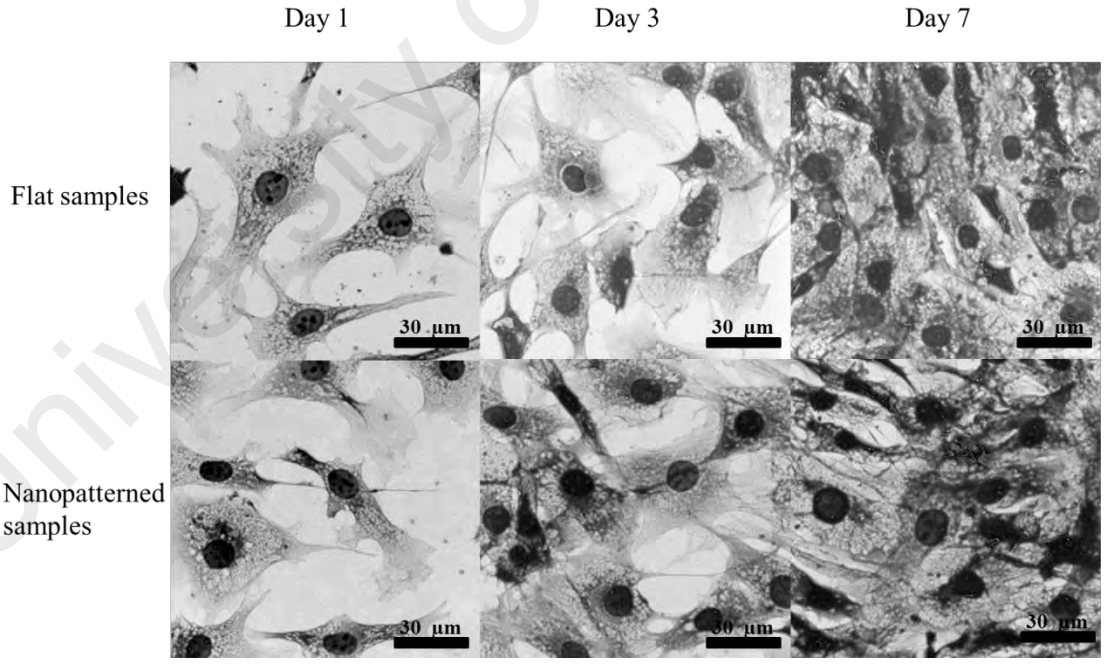

Figure 4.12: SEM images of cell growth on flat and nanopatterned samples at day 1, 3, and 7.

The chondrocytes growth on flat and nanopatterned samples was observed and the cells depicted a rather rounded or polygonal morphology as seen in Figure 4.12. Although cell flattening and spreading often indicate a positive cellular response where the evidence of an outstanding cell adhesion is convincing, these may not be the case for chondrocytes. It should be noted that chondrocytes have a round characteristic shape and the loss of chondrocytic phenotype can be determined by the transformation of a rounded shape of cells into a fibroblastic morphology. In other words, changes in the cell shape will eventually affect the phenotypic expression of chondrocytes (Brammer et al., 2010).

The nanostructured surface was believed to have up-regulated the performance of chondrocytes as the proliferation rate was significantly higher and yet the characteristic morphology was perceived to be well-preserved. This might be attributed to the sensitivity of chondrocytes to external stimulation and they received excitations from the nanostructures to organise their cell morphology for growth and attachment (Chen, Lin, Wang, & Tseng, 2013). The expansion of chondrocytes starts after being isolated from the extracellular matrix, but the chondrocyte dedifferentiation occurs simultaneously resulting in the change of the cell morphology and the loss of cartilage-specific function (Brandt, Michler, Vogel, & Henning, 2010). Thus, despite the observed adhesion and proliferation of chondrocytes, probe the GAG production was further probe which is a distinctive feature of chondrogenic differentiation in the following section.

4.3.2.3 GAG/DNA quantification

As reported by Chen et al. (2013), although mesenchymal stem cells (MSCs) have been utilised to solve the scarce source of chondrocytes by inducing the MSCs to chondrocytes, the adhesion force and stiffness of these differentiated cells are different

from the original chondrocytes. Thus, it is worth investigating chondrocyte behaviour and their interaction with designed biomaterials, since the use of chondrocytes could be a more appropriate choice at times for cartilaginous application. The positive chondrocyte growth reported in this study has shed some light on the use of the materials.

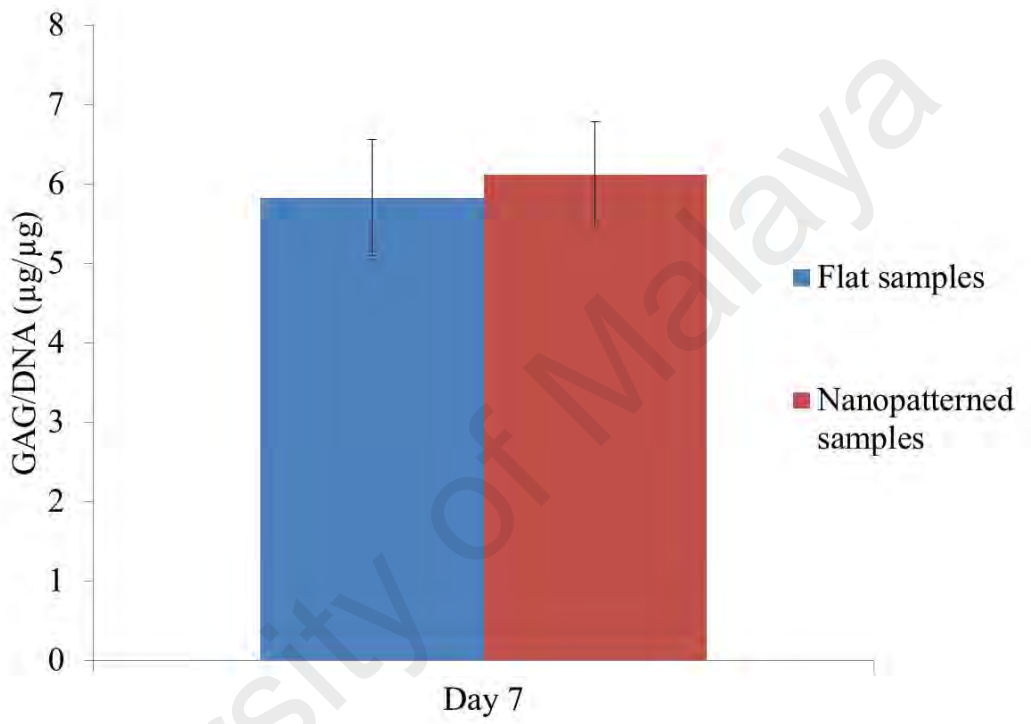

Figure 4.13: GAG/DNA ratio on flat and nanopatterned samples at day 7.

On the other hand, it is also important to ensure the dedifferentiation of chondrocytes did not take place, which can be examined by the appearance of fibroblast looking cells as discussed previously and also its ability to produce proteoglycans (Prittinen et al., 2014). The GAG/DNA production is observed to be higher on nanopatterned samples than that on flat samples (Figure 4.13). However, the difference is not statistically significant at $p<0.05$ indicating that this surface nanofeature alone might not be sufficient to meet the needs of chondrocytes to reside in a 3D environment. This statement can be supported by the findings in which GAG was found to be the highest

in 3D cultures than in 2D cultures, and 2D cultures were deemed to be a better choice for chondrocyte proliferation (Caron et al., 2012). A recent study by Prittinen et al. (2014) has also concluded the influence of isolation from the native environment on chondrocytes where the chondrogenic differentiation can hardly be driven even if the cells form a 3D extracellular matrix. Hence, further efforts are needed to address the necessity of chondrocytes to maintain their phenotype and enhance the differentiation process.

4.3.3 ADMSC

4.3.3.1 Characterization of ADMSC

Mesenchymal stem cells (MSC) are a population of stem cells showing properties of self-renewal and multipotent differentiation *in vitro*. They were isolated from adult bone marrow initially and were later discovered in almost all adult tissues, including adipose tissue and dermis. They have also been found in peripheral blood and solid organs (Baer & Geiger, 2012). The International Society for Cellular Therapy (ISCT) has proposed three minimal criteria to define MSC for labscale and pre-clinical studies:

> "First, MSC must be plastic-adherent when maintained in standard culture conditions using tissue culture flasks. Second, ≥ 95% of the MSC population must express CD105, CD73 and CD90, as measured by flow cytometry. Additionally, these cells must lack expression (≤ 2% positive) of CD45, CD34, CD14 or CD11b, CD79a or CD19 and HLA class II. Third, the cells must be able to differentiate to osteoblasts, adipocytes and chondroblasts under standard in vitro differentiating conditions." (Dominici, 2006, p. 316)

ADMSCs used in this study were isolated from the infrapatellar fat pads which were discarded after knee surgery. The infrapatellar fat pad is also known as Hoffa's fat pad, a highly vascularised and innervated structure that is located at the anterior knee

compartment (Dragoo, Johnson, & McConnell, 2012). They are often surgically removed to enhance the visualisation of surgical treatment sites or for the treatment of Hoffa's disease during arthroscopy or total knee arthroplasty (Koh & Choi, 2012)

(a) *Tri-lineage Differentiation*

The isolated ADMSCs were cultured in osteogenic, chondrogenic, adipogenic differentiation media respectively for the inspection of their multilineage differentiation capacity. The positively stained ADMSCs in different *in vitro* differentiation assays have demonstrated their ability to differentiate towards multiple lineages as shown in Figure 4.14-4.16.

i Osteogenic Differentiation

Alizarin red S staining is a common technique used to examine the mineralisation activity of osteoblasts, due to its ability to bind to calcium salts (Birmingham et al., 2012). The stained mineral deposits were observed on the cells cultured in osteogenesis differentiation medium. This observations made indicated that the ADMSCs have been osteogenically differentiated. In comparison, the control sample remained unstained under the microscope.

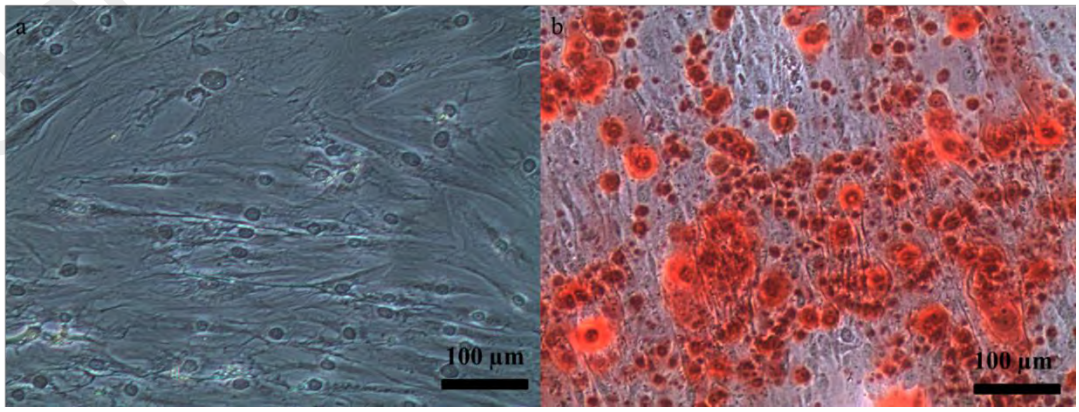

Figure 4.14: Alizarin red S staining of ADMSC cultured in (a) basal medium and (b) osteogenic differentiation medium.

ii Chondrogenic Differentiation

Safranin O dye was used to stain the sulfated proteoglycans which were synthesised by the chondrogenic-differentiated ADMSCs (Lee et al., 2004). Figure 4.15 has illustrated successful chondrogenic differentiation of ADMSC with the use of differentiation media. The orange-red complex showed the presence of accumulated cartilage extracellular matrix. The cells also appeared to be polygonal or rounded in shape, which is different from the characteristic spindle-like shape of ADMSCs.

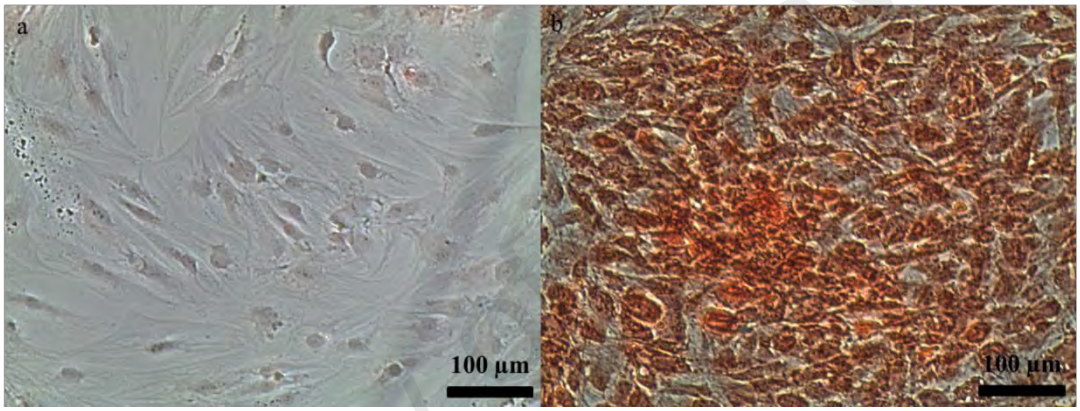

Figure 4.15: Safranin O staining of ADMSC cultured in (a) basal medium and (b) chondrogenic differentiation medium.

iii Adipogenic Differentiation

Oil-red O staining was used to visualise the production of neutral lipid vacuoles (Lee et al., 2004). The presence of lipid droplets was indicated by the bright red stains observed in Figure 4.16.

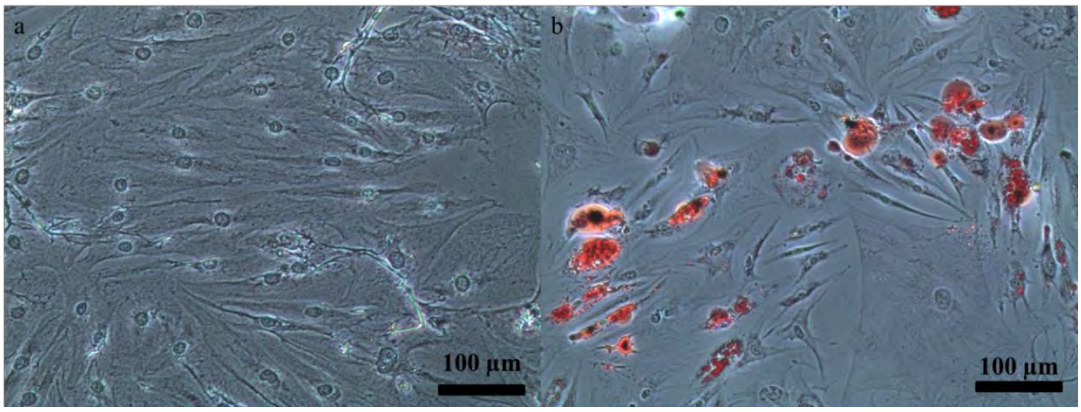

Figure 4.16: Oil red O staining of ADMSC cultured in (a) basal medium and (b) adipogenic differentiation medium.

(b) ***Flow Cytometry***

The isolated ADMSCs (N=3) on early passage (passage 2) were used for flow cytometric analysis whereas the commercial ADMSC was used as a positive control (Figure 4.17). The characterisation of isolated samples has been successfully completed by flow cytometric evaluation. For both control and isolated samples, the phenotype of ADMSCs has been defined by the ≥ 95% expression of cell surface markers CD90, CD73, and CD105, along with the absence or ≤ 2% expression of hematopoietic lineage markers (PE hMSC negative cocktail).

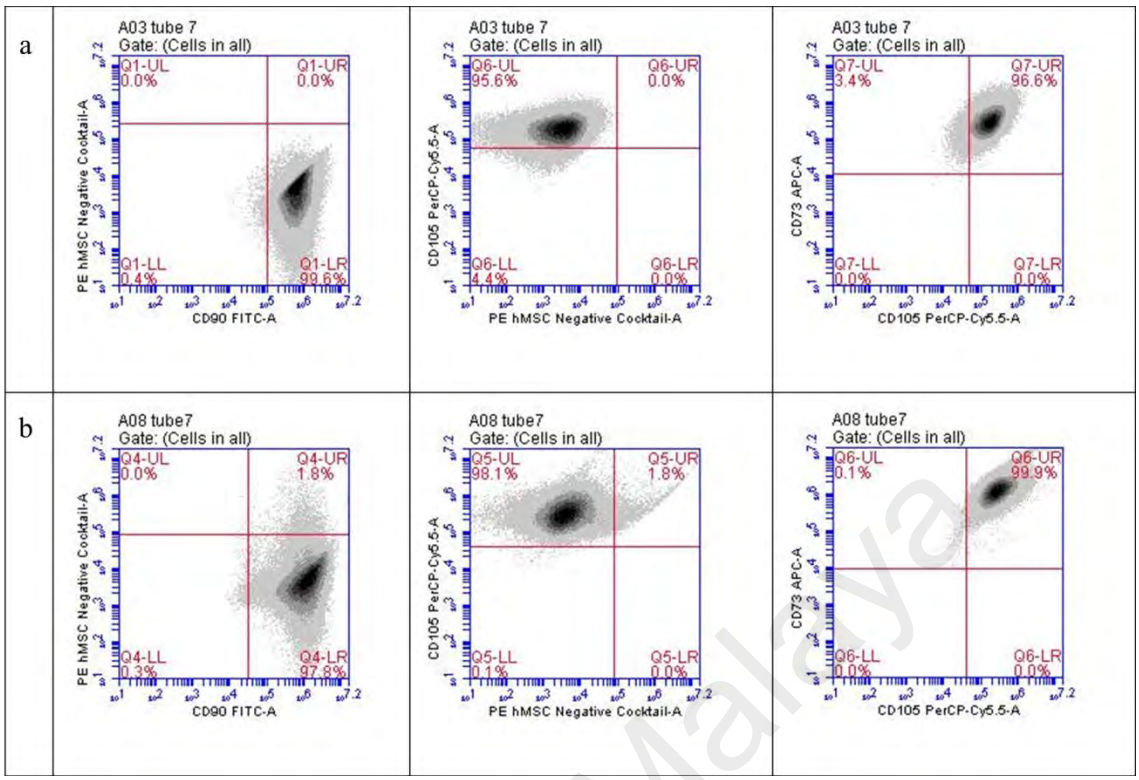

Figure 4.17: Flow cytometric analysis of (a) commercial ADMSC and (b) representative isolated ADMSCs.

4.3.3.2 Focal Adhesion

It is evident that the cell-ECM interaction modulates the cell behaviour, gene expression, and signal transduction. Focal adhesions which connect the ECM to the cytoskeleton, allow signaling pathway to take place through the mechanical force interaction between the cell and ECM. With the coordination of cytoskeleton, the transmission of mechanical signals from ECM to nucleus occurs by means of integrin receptors (Yim, Darling, Kulangara, Guilak, & Leong, 2010). Researchers have conducted several investigations into how nanotopography affects the focal adhesion and cell behaviour of mesenchymal stem cells, results believed to be invaluable for tissue engineering applications (Sjöström et al., 2009; Yim et al., 2010).

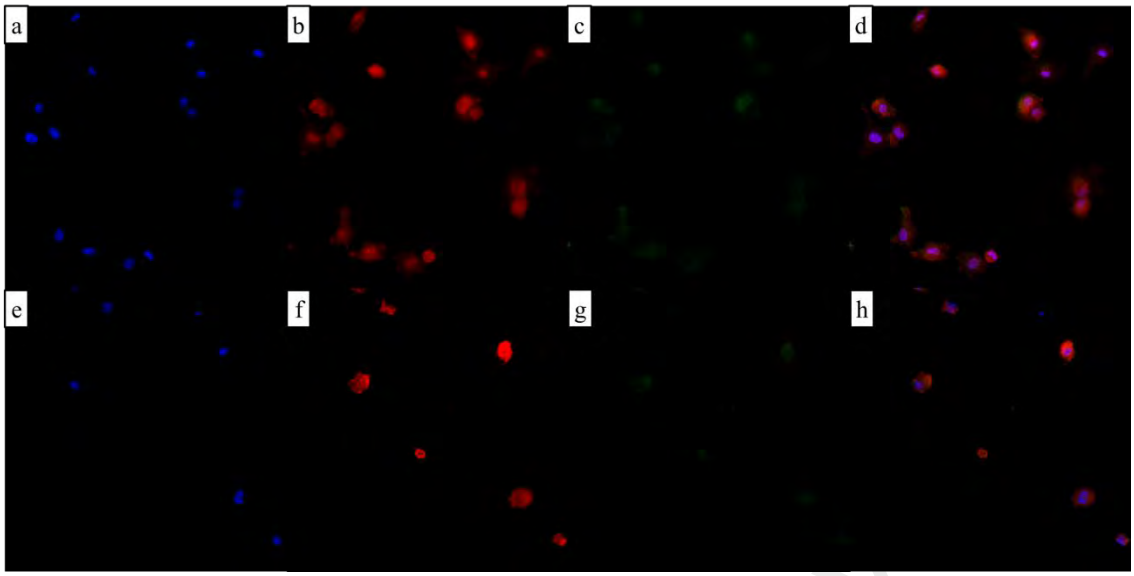

Figure 4.18: Confocal fluorescence imaging of (a,e) nuclei counterstaining, (b,f) F-actin, and (c,g) focal contacts of ADMSC cultured on (a-d) nanostructured substrate and (e-h) control substrate for 1 h; (d,h) An overlaid monochrome images of (a,e), (b,f), and (c,g).

Immunofluorescence images of ADMSCs after 1 h of incubation on both control and nanopatterned samples are depicted in Figure 4.18. The number of adherant cells was noticeably greater on the nanopatterned samples, demonstrated by a higher number of fluorescent-labelled nuclei on the surface (Figure 4.18a). Actin cytoskeleton is known to be a dynamic structure involved in cell organisation and it is linked to the cell junctions. There are two forms of actin: G-actin and F-actin which are monomeric globular and polymeric filamentous respectively. Actin regulates the cell shape, movement, and phagocytosis, along with intercellular communication and organelle distribution (Navarro-Garcia, Serapio-Palacios, Ugalde-Silva, Tapia-Pastrana, & Chavez-Dueñas, 2012).

The stained F-actin on the nanopatterned surface appeared to be distributed widely (Figure 4.18b) whereas blob-like stains were observed on the control surface (Figure 4.18f). The actin cytoskeleton on the nanopatterned surface was more spread and the

cells were identified to be less rounded in shape than those on the control surface. Although the cells were not highly expanded to form spindle-shape yet on the nanopatterned surface, their cytoskeletons seemed to be more well-organised compared to those on control surface. This showed that the cells conformed to the nanostructured surface rapidly, being highly responsive to the subjected topographical cues. The weaker motility of cells on the control surface was indicated by the less prominent actin cytoskeleton, which explains the rather rounded cell shape and less spread morphology.

The main role of focal adhesion is to initiate signaling pathways and to regulate integrin function (Wozniak, Modzelewska, Kwong, & Keely, 2004). During cell migration, proliferation and differentiation, the mechanical coupling with the ECM and cells can be achieved via focal adhesions. Further, they serve to transmit the force between cytoskeleton and the ECM (Oakes & Gardel, 2014).

The focal points were observed to be denser on the nanopatterned sample (Figure 4.18c). This observation revealed that the initial adhesion of ADMSC was highly promoted due to the presence of nanostructures. The presence of nanostructures has supported the cells to form a larger contact with the material surface. According to Sjöström et al. (2009), enhanced adhesions are correlated to improved direct and indirect mechanotransductive signaling as a result of increased cytoskeleton tension, alterations in focal adhesion assembly and up-regulated cytoskeletal contractility. The formation of focal adhesions has been reported to influence the osteogenic differentiation of MSC, despite the underlying mechanism behind is vague (Sjöström et al., 2009).

4.3.3.3 Cell Proliferation

It is highly likely that the cell proliferation at early stage would be higher on nanopatterned samples as the initial attachment has been demonstrated to be notably

enhanced. Hence, the proliferation as depicted (Figure 4.19) has supported the previous observation on the cell interaction with the surface topography. ADMSCs have shown statistically-significant up-regulated growth on day 1, 7, and even 14. This finding is noteworthy as one of the characteristic properties of MSC is their ability to self-replicate, in other words, proliferate (Xin, Hussain, & Mao, 2007). This study has also demonstrated that not only did the nanopatterned substrates show a satisfactory *in vitro* cytocompatibility with the different types of cell sources, but also promoted their proliferation rate.

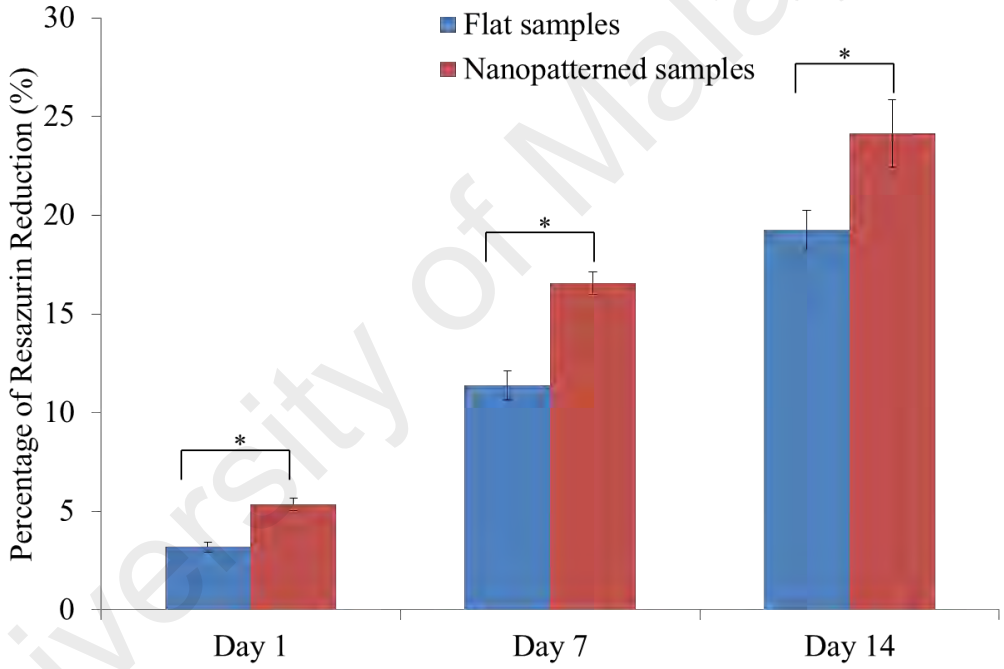

Figure 4.19: ADMSC proliferation on flat and nanopatterned samples (n=3) at day 1, 7, and 14. Statistical significance is indicated by * at $p<0.05$

4.3.3.4 Osteogenic Gene Expression

Mesenchymal stem cells exist in blood, bone marrow, and other tissues, and they are the first type of cells to colonise the material surface following an implantation. With the cues from chemo-attractant molecules, the peripheral MSCs travel through the blood clot to colonise the implant. The differentiation of MSCs is likely to be influenced by

the surface properties of the implant and eventually affect the nature of the surrounding tissue (Lavenus et al., 2011). Hence, the surface properties of implant material have been investigated with the object of developing a more ideal material to carry out this function.

According to Zhao et al. (2012), previous studies have suggested that the cell shape and focal adhesion are manipulated by the surface topographies, which eventually direct the cell fate through changes in the gene expression. These changes in gene expression could be attributed to the force transmission through the cytoskeleton that caused distortion in the cell nucleus. Also, well spread MSCs were reported to have a higher tendency to differentiation towards the osteogenic lineage, as the cells conformed better to the micro/nano topographies which promoted higher skeletal tension and mechanotranduction (Zhao, Liu, Wu, Zhang, & Chu, 2012). A similar observation was noted in the study of Seon et al. (2011) in which high cytoskeletal tension in the MSCs has resulted in osteogenic differentiation through an upregulation of osteogenic genes due to the mechanotransduction pathway.

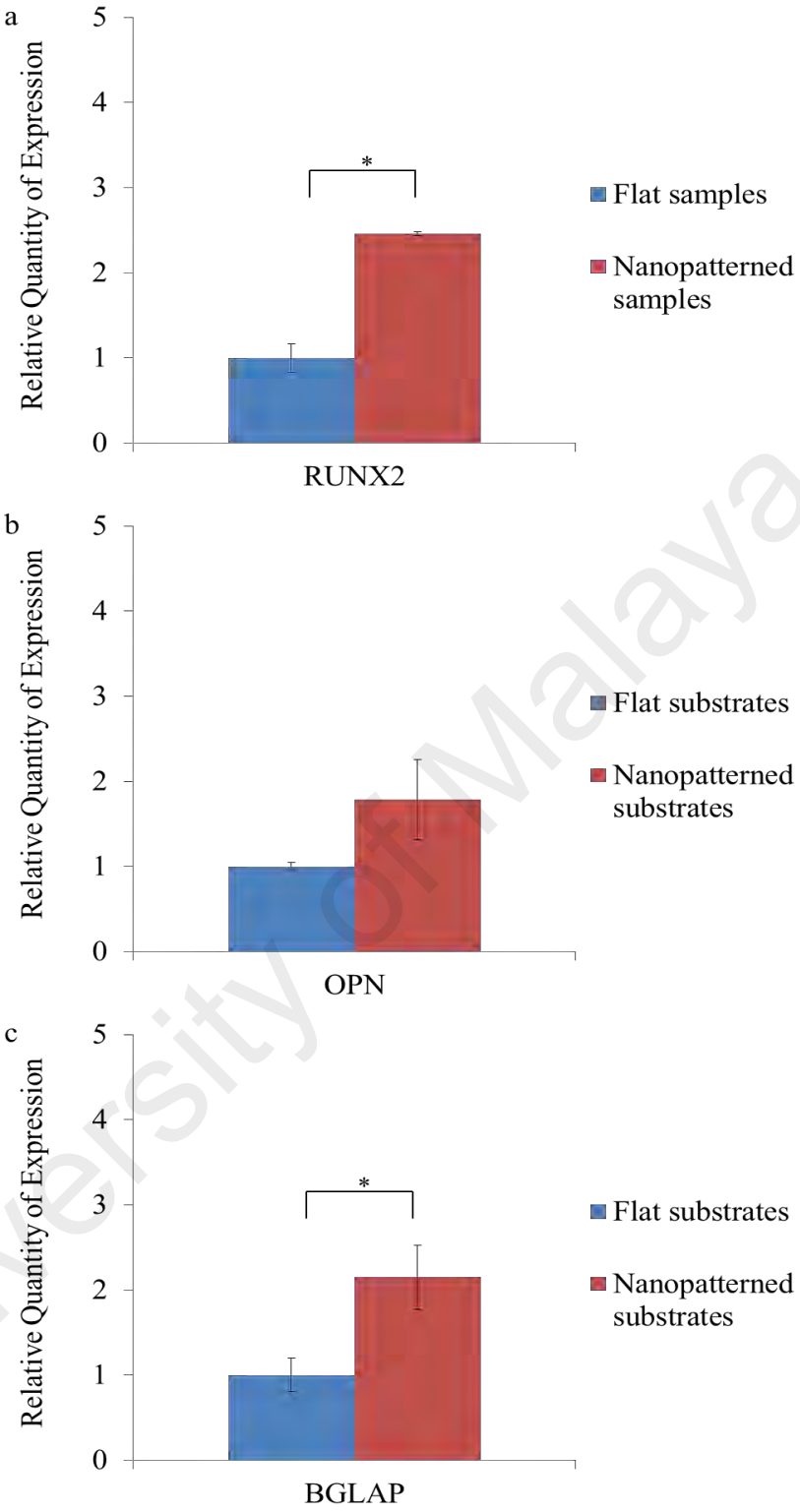

Figure 4.20 qPCR gene expression of osteogenic markers (a) RUNX2, (b) OPN, and (c) BGLAP.

Investigation of the osteogenic potential of nanostructures was conducted in the presence of osteogenic supplements such as dexamethasone, β-glycerophosphate, and

ascorbic acid-2-phosphate. This is because bare zirconia material is usually inert, and hence, lacks osteoinductive properties. Nevertheless, the use of both osteogenic medium and nanostructures could provide a synergetic effect in the osteoblastic differentiation of MSCs on the nanopatterned samples.

In this study, it was shown that increase of expression of RUNX2 gene in nanopatterned samples was higher than that of other target genes (Figure 4.20). RUNX2, the transcriptional activator of osteoblast differentiation, has been reported to greatly promote the differentiation of MSCs towards osteogenic lineage in the early stages (de Peppo et al., 2014; Polini, Pisignano, Parodi, Quarto, & Scaglione, 2011). Further, the effect of nanostructures in fostering a higher proliferation on the nanopatterned samples could have contributed to the upregulation of the RUNX2 gene. De Peppo et al. (2014) has reported that there is a correlation of RUNX2 expression with cell proliferation. This could be due to a specific cadherin-mediated cell-cell interaction and gap junctions involved in the osteogenic differentiation of cells. Another study has demonstrated a positively correlated relationship between osteogenic differentiation and cell-cell contact (Tang, Peng, & Ding, 2010). The higher proliferation rate on nanopatterned samples could have contributed to the greater cell-cell contact which eventually up-regulated the osteogenic differentiation. RUNX2 is also known to promote the production of bone specific extracellular matrix such as osteopontin and osteocalcin (You et al., 2010). The presence of osteocalcin and osteopontin were indicated by BGLAP and OPN respectively. In this study, it was found that OPN and BGLAP genes were found at a higher level on the nanopatterned samples compared to control samples (Figure 4.20). OPN and BGLAP have been commonly used in studies to individually represent early and late osteogenic differentiation marker (Lavenus et al., 2011; Peng, Wu, Zheng, Xu, & Yu, 2012).

The cells are believed to be in an early stage of differentiation as the fold change in RUNX2 expression was much higher compared to those of OPN and BGLAP. Although the expression of BGLAP signified a late stage of osteoblast differentiation, it was viewed as an early apperance of the late differentiation marker as the RUNX2 and osteocalcin gene can be expressed simultaneously before the mature osteoblast phase (Peng et al., 2012). Further, the early occurrence of BGLAP expression may be stimulated by the presence of nanostructures.

CHAPTER 5: CONCLUSIONS AND FUTURE PERSPECTIVES

5.1 Conclusions

Surface modification of materials has been a popular practice in industry and research to enhance certain desirable characteristics or features to fulfill the demands of intended applications. In this study, self-assembled nanoislands was produced by utilising a simple annealing treatment with powder-suspension-based method to explore the cellular response to surface nanotopography. In summary, the objectives of the study have been achieved as follows:

This study has demonstrated that with the use of miscut surface, the alignment and coverage of nanoislands were significantly improved compared to that of non-miscut surface. Interaction between the nanostructures and steps provided by miscut substrates has been demonstrated to be affected by miscut angles and dwell time. The *in vitro* study has also shown that the cells have responded positively to the nanopatterned samples in general. Overall, osteoblasts have shown great adhesion and bone maturation at an early stage on the nanostructured samples. The nanopatterned samples have shown a greater initial osteoblasts adhesion as the cells were more well-spread in the initial stage of development. This was attributed to the higher surface area and availability of extensive anchorage points provided by the nanoislands. The bone cells cultured on the nanopatterned samples also gave rise to significantly improved ALP activity at day 7, which complied well with the formation of the mineralised matrix observed through staining. These are the evidences of an improved osteoblast functionality as elicited by the fabricated nanostructures. In short, the surface modification technique has increased the surface roughness and wettability, which in turn promoted osteoblast functionality in terms of proliferation and differentiation.

It can be concluded that the cytocompatibility of the nanopatterned samples is supported at the cellular level. This is because not only did the presence of nanostructure improve the proliferation rate of osteoblasts, but it also up-regulated those of chondrocytes and mesenchymal stem cells. Nanotopographical cues have significantly improved chondrocytes proliferation in this study, but not the differentiation process. Hence, the ability of nanopattern material in 2D culture system to maintain the chondrocytes phenotype is questionable in long term. Although the sign of fibroblastic appearance of chondrocytes is not readily noticeable at an early stage, the absence of statistical significance in the GAG production has implied that further measurements are required to address the need of improving chondrocyte functionality in 2D cultures.

The ADMSCs have illustrated significantly-improved focal adhesion on the nanostructured surface with well-organised cytoskeleton in comparison with the less spreading cytoskeleton on the untreated surface. Other than improving the osteoblast function on nanostructured substrates, it is of interest to probe the osteogenic potential of nanostructures in directing stem cell fate, as the differentiation of mesenchymal stem cells into osteoblasts plays a key role in the success of osseointegration. It can be concluded that the presence of nanostructures has stimulated an early stage of differentiation of ADMSCs and the osteogenic markers were up-regulated in general.

In conclusion, miscut step provided preferential nucleation sites and lowered nucleation barriers for the formation of nanoislands. Significant alignment of nanoislands on the miscut surface could also be attributed to the high binding energy and minimum local chemical potential at the step edge. Miscut surfaces have provided an efficient and effective way to produce ordered nanoislands. Additionally, with the flexibility of depositing source with simple powder suspension method, this study has

shown that self-assembly of nanoislands on miscut substrates is a promising technique to fulfil the needs of industrial production, namely to achieve large scale production at the lowest possible cost.

5.2 Future works

Several suggestions have been made for further improvement to the fabrication of self-assembled nanostructures in this study. With the use of sputtering techniques and lithography, the location and quantification of source deposition can be more accurate and precise. This would allow a more in-depth study of the mechanism of formation of self-assembled nanostructures in ceramic oxide material systems. Another suggestion for the improvement of nanoisland alignment is to conduct pre-annealing treatment on the miscut substrates alone before the substrates were used for the self-assembly of nanostructures (Niu et al., 2017). Step bunching, which would result in wider terrace, can be achieved by annealing the miscut surfaces. A more developed morphology of steps on the substrate is believed to enhance the order and alignment of nanostructures.

Future work can also explore on the versatility of using various types of dopant source to fabricate nanoislands with different sizes, morphologies, and compositions. Ansari et al. (2013) have illustrated self-assembled nanoislands fabricated with the use of europium oxide (Eu_2O_3) as dopant source. This suggests the possibility of using other oxide dopants for different morphologies of nanostructures by tuning the annealing profiles.

On top of that, the potential contribution of nanostructures can also be dedicated for biosensor, pattern transfer and tissue engineering applications. The good mechanical properties of YSZ substrates have made them suitable for us as a mold or stamp to transfer a nanopattern to other materials, in particular, to polymers. The pattern of YSZ/GDC nanoislands has been successfully transferred to three different types of

polymers: polydimethlysiloxane (PDMS), polystyrene (PS), and ethyleneglycol dimethacrylate (EGDMA) (Zimmerman, Rauscher, Ellis, Boukany, & Lee, 2009). This can be further extended to other types of materials, including hydrogels. In fact, patterned hydrogels have been developed for various biomedical applications such as cell culture and scaffolds. Also, by exploring other annealing profiles or other YSZ substrates with different crystallographic orientation, different morphologies of the nanostructures can be obtained to study the response of cells towards different patterns. For example, nanobars are formed on (110)-oriented YSZ substrates instead of nanoislands (Aminuddin et al., 2016).

Satisfactory results have been obtained to demonstrate the potential of nanopatterned substrates as a biocompatible material. It should be noted that the osteoblast differentiation and osteogenic differentiation of ADMSCs will continue to progress and the late differentiation is not reflected in this study. However, these results provide insight into future development of nanopatterned material to fulfill different requirement for different applications. This work can be improved by incorporating new study to investigate the signalling pathway involved in the cell functions and the influence of nanostructures on cellular behaviour in depth, in which gene expression analysis and immunoblot analysis of protein expression can be comprehensively conducted. Also, quantitative analysis is preferred to allow a more precise comparison of the results obtained.

According to Mendonça et al. (2008), one of the great challenges in exploring the influence of surface topography lies in the difficulty of excluding the other factors such as surface charge or chemistry. These surface qualities are closely associated with the created topography. Hence, the effect of these factors is worth investigation to deepen understanding of the underlying mechanism on the cellular response to cues from

designed materials. In addition, the surface properties of the substrate can also be enhanced through combination of different approaches. For example, the immobilisation of the BMPs to the material surface can be applied to enhance the osteoinductivity of substrate (Chiara et al., 2012).

Lastly, future work should also include comparison of the performance of nanopatterned substrates in this study to other types of nanostructured materials. This is to thoroughly examine and inspect the performance variation from various aspects. Ultimately, the outcome of assessment on these innovative materials could be advantageous for the advancement of new biomaterial design.

REFERENCES

Aboushelib, M. N., Kleverlaan, C. J., & Feilzer, A. J. (2007). Selective infiltration-etching technique for a strong and durable bond of resin cements to zirconia-based materials. *The Journal of Prosthetic Dentistry, 98*(5): 379-388.

Aboushelib, M. N., Osman, E., Jansen, I., Everts, V., & Feilzer, A. J. (2013). Influence of a nanoporous zirconia implant surface of on cell viability of human osteoblasts. *Journal of Prosthodontics, 22*(3): 190-195.

Aita, H., Hori, N., Takeuchi, M., Suzuki, T., Yamada, M., Anpo, M., & Ogawa, T. (2009). The effect of ultraviolet functionalization of titanium on integration with bone. *Biomaterials, 30*(6): 1015-1025.

Akagawa, Y., Ichikawa, Y., Nikai, H., & Tsuru, H. (1993). Interface histology of unloaded and early loaded partially stabilized zirconia endosseous implant in initial bone healing. *The Journal of Prosthetic Dentistry, 69*(6): 599-604.

Albee, F. H. (1920). Studies in bone growth: triple calcium phosphate as a stimulus to osteogenesis. *Annals of Surgery, 71*(1): 32.

Albrektsson, T., Zarb, G., Worthington, P., & Eriksson, A. R. (1986). The long-term efficacy of currently used dental implants: a review and proposed criteria of success. *The International Journal of Oral & Maxillofacial Implants, 1*(1): 11-25.

Aminuddin, N. I., Ahmad, R., Ansari, H. M., Mohd. Zain, N., Akbar, S. A., & Pingguan-Murphy, B. (2016). Human fetal osteoblast cell response to self-assembled nanostructures on YSZ-(110) single crystal substrates. *Materials & Design, 94*: 274-279.

An, J., Chua, C. K., Yu, T., Li, H., & Tan, L. P. (2013). Advanced nanobiomaterial strategies for the development of organized tissue engineering constructs. *Nanomedicine, 8*(4): 591-602.

Angelova, N., & Hunkeler, D. (1999). Rationalizing the design of polymeric biomaterials. *Trends in Biotechnology, 17*(10): 409-421.

Ansari, H. M., Dixit, V., Zimmerman, L. B., Rauscher, M. D., Dregia, S. A., & Akbar, S. A. (2013). Self assembly of nanoislands on YSZ-(001) surface: a mechanistic approach toward a robust process. *Nano Letters, 13*(5): 2116-2121.

Anselme, K., Davidson, P., Popa, A. M., Giazzon, M., Liley, M., & Ploux, L. (2010). The interaction of cells and bacteria with surfaces structured at the nanometre scale. *Acta Biomaterialia, 6*(10): 3824-3846.

Aparicio, C., Gil, F., Planell, J., & Engel, E. (2002). Human-osteoblast proliferation and differentiation on grit-blasted and bioactive titanium for dental applications. *Journal of Materials Science: Materials in Medicine, 13*(12): 1105-1111.

Att, W., Takeuchi, M., Suzuki, T., Kubo, K., Anpo, M., & Ogawa, T. (2009). Enhanced osteoblast function on ultraviolet light-treated zirconia. *Biomaterials, 30*(7): 1273-1280.

Baer, P. C., & Geiger, H. (2012). Adipose-derived mesenchymal stromal/stem cells: tissue localization, characterization, and heterogeneity. *Stem Cells International, 2012*.

Balza, J. C., Zujur, D., Gil, L., Subero, R., Dominguez, E., Delvasto, P., & Alvarez, J. (2013). *Sandblasting as a surface modification technique on titanium alloys for biomedical applications: abrasive particle behavior.* Paper presented at the IOP Conference Series: Materials Science and Engineering.

Barnes, D., Johnson, S., Snell, R., & Best, S. (2012). Using scratch testing to measure the adhesion strength of calcium phosphate coatings applied to poly (carbonate urethane) substrates. *Journal of the Mechanical Behavior of Biomedical Materials, 6*: 128-138.

Bavbek, A. B., Ozcan, M., & Eskitascioglu, G. (2014). Radioactive potential of zirconium-dioxide used for dental applications. *Journal of Applied Biomaterials & Functional Materials, 12*(1): 35-40.

Becher, P. F., Hsueh, C. H., Angelini, P., & Tiegs, T. N. (1988). Toughening Behavior in Whisker‐Reinforced Ceramic Matrix Composites. *Journal of the American Ceramic Society, 71*(12): 1050-1061.

Bettinger, C. J., Zhang, Z., Gerecht, S., Borenstein, J. T., & Langer, R. (2008). Enhancement of in vitro capillary tube formation by substrate nanotopography. *Advanced Materials, 20*(1): 99-103.

Birmingham, E., Niebur, G., McHugh, P., Shaw, G., Barry, F., & McNamara, L. (2012). Osteogenic differentiation of mesenchymal stem cells is regulated by osteocyte and osteoblast cells in a simplified bone niche. *European Cells & Materials 23*: 13-27.

Bohner, M. (2001). Physical and chemical aspects of calcium phosphates used in spinal surgery. *European Spine Journal, 10*(2): S114-S121.

Bose, S., Banerjee, A., Dasgupta, S., & Bandyopadhyay, A. (2009). Synthesis, Processing, Mechanical, and Biological Property Characterization of Hydroxyapatite Whisker‐Reinforced Hydroxyapatite Composites. *Journal of the American Ceramic Society, 92*(2): 323-330.

Bosetti, M., Vernè, E., Ferraris, M., Ravaglioli, A., & Cannas, M. (2001). In vitro characterisation of zirconia coated by bioactive glass. *Biomaterials, 22*(9): 987-994.

Boyne, A., Rauscher, M. D., Dregia, S. A., & Wang, Y. (2011). Surface island formation with localized stresses. *Scripta Materialia, 64*(8): 705-708.

Brammer, K. S., Oh, S., Frandsen, C. J., Varghese, S., & Jin, S. (2010). Nanotube surface triggers increased chondrocyte extracellular matrix production. *Materials Science and Engineering: C, 30*(4): 518-525.

Brandt, J., Michler, G., Vogel, J., & Henning, S. (2010). *Nanostructured materials for skeletal repair.* Paper presented at the Macromolecular symposia.

Brett, P. M., Harle, J., Salih, V., Mihoc, R., Olsen, I., Jones, F. H., & Tonetti, M. (2004). Roughness response genes in osteoblasts. *Bone, 35*(1): 124-133.

Burdick, J. A., & Mauck, R. L. (2010). *Biomaterials for tissue engineering applications: a review of the past and future trends*. New York: Springer Science & Business Media.

Burns, K., Yao, C., & Webster, T. J. (2009). Increased chondrocyte adhesion on nanotubular anodized titanium. *Journal of Biomedical Materials Research Part A, 88*(3): 561-568.

Caron, M., Emans, P., Coolsen, M., Voss, L., Surtel, D., Cremers, A., . . . Welting, T. (2012). Redifferentiation of dedifferentiated human articular chondrocytes: comparison of 2D and 3D cultures. *Osteoarthritis and Cartilage, 20*(10): 1170-1178.

Castner, D. G., & Ratner, B. D. (2002). Biomedical surface science: Foundations to frontiers. *Surface Science, 500*(1): 28-60.

Chen, T.-J., Lin, T.-Y., Wang, Y.-L., & Tseng, F.-G. (2013). *Increased proliferation of primary chondrocyte cells by nanostructure and cycling mechanical stimulation on PDMS cell chip.* Paper presented at the Micro Electro Mechanical Systems (MEMS), 2013 IEEE 26th International Conference on.

Chevalier, J. (2006). What future for zirconia as a biomaterial? *Biomaterials, 27*(4): 535-543.

Chevalier, J., & Gremillard, L. (2009). Ceramics for medical applications: A picture for the next 20 years. *Journal of the European Ceramic Society, 29*(7): 1245-1255.

Chiara, G., Letizia, F., Lorenzo, F., Edoardo, S., Diego, S., Stefano, S., . . . Barbara, Z. (2012). Nanostructured biomaterials for tissue engineered bone tissue reconstruction. *International Journal of Molecular Sciences, 13*(1): 737-757.

Chokshi, A. H. (1990). An evaluation of the grain-boundary sliding contribution to creep deformation in polycrystalline alumina. *Journal of Materials Science, 25*(7): 3221-3228.

Chrcanovic, B. R., Leão, N. L. C., & Martins, M. D. (2013). Influence of different acid etchings on the superficial characteristics of Ti sandblasted with Al2O3. *Materials Research, 16*(5): 1006-1014.

Chrcanovic, B. R., & Martins, M. D. (2014). Study of the influence of acid etching treatments on the superficial characteristics of Ti. *Materials Research, 17*(2): 373-380.

Conrad, H. J., Seong, W. J., & Pesun, I. J. (2007). Current ceramic materials and systems with clinical recommendations: a systematic review. *The Journal of Prosthetic Dentistry, 98*(5): 389-404.

Crnogorac, F., Witte, D. J., Xia, Q., Rajendran, B., Pickard, D. S., Liu, Z., . . . Kamins, T. I. (2007). Nano-graphoepitaxy of semiconductors for 3D integration. *Microelectronic Engineering, 84*(5): 891-894.

Cutright, D. E., Bhaskar, S. N., Brady, J. M., Getter, L., & Posey, W. R. (1972). Reaction of bone to tricalcium phosphate ceramic pellets. *Oral Surgery, Oral Medicine, Oral Pathology, 33*(5): 850-856.

Davison, N. L., ten Harkel, B., Schoenmaker, T., Luo, X., Yuan, H., Everts, V., . . . de Bruijn, J. D. (2014). Osteoclast resorption of beta-tricalcium phosphate controlled by surface architecture. *Biomaterials, 35*(26): 7441-7451.

De Aza, P. N., De Aza, A. H., & De Aza, S. (2005). Crystalline bioceramic materials. *Bulletin of the Spanish Society of Ceramics and Glass, 44*(3): 135-145.

De Groot, K., De Putter, C., Smitt, P., & Driessen, A. (1981). Mechanical failure of artificial teeth made of dense calcium hydroxyapatite. *Science of Ceramics, 11*: 433-437.

de Peppo, G. M., Agheli, H., Karlsson, C., Ekström, K., Brisby, H., Lennerås, M., . . . Olsson, E. (2014). Osteogenic response of human mesenchymal stem cells to well-defined nanoscale topography in vitro. *International Journal of Nanomedicine, 9*: 2499.

Depprich, R., Ommerborn, M., Zipprich, H., Naujoks, C., Handschel, J., Wiesmann, H.-P., . . . Meyer, U. (2008). Behavior of osteoblastic cells cultured on titanium and structured zirconia surfaces. *Head & Face Medicine, 4*(1): 1.

Dominici, M., Le Blanc, K., Mueller, I., Slaper-Cortenbach, I., Marini, F., Krause, D., . . . Horwitz, E. (2006). Minimal criteria for defining multipotent mesenchymal stromal cells. The International Society for Cellular Therapy position statement. *Cytotherapy, 8*(4): 315-317.

Dorozhkin, S. V. (2013). Calcium orthophosphates in dentistry. *Journal of Materials Science: Materials in Medicine, 24*(6): 1335-1363.

Dragoo, J. L., Johnson, C., & McConnell, J. (2012). Evaluation and treatment of disorders of the infrapatellar fat pad. *Sports Medicine, 42*(1): 51-67.

Dubotzky, A., & Kruger, B. (2001). *Evaluation of alternative preparation methods for failure analysis at modern chip-and package technologies.* Paper presented at the International Symposium for Testing and Failure Analysis.

Ercan, B., Khang, D., Carpenter, J., & Webster, T. J. (2013). Using mathematical models to understand the effect of nanoscale roughness on protein adsorption for improving medical devices. *International Journal of Nanomedicine, 8*(Suppl 1): 75.

Faia-Torres, A. B., Guimond-Lischer, S., Rottmar, M., Charnley, M., Goren, T., Maniura-Weber, K., . . . Neves, N. M. (2014). Differential regulation of osteogenic differentiation of stem cells on surface roughness gradients. *Biomaterials, 35*(33): 9023-9032.

Fielding, G. A., Bandyopadhyay, A., & Bose, S. (2012). Effects of silica and zinc oxide doping on mechanical and biological properties of 3D printed tricalcium phosphate tissue engineering scaffolds. *Dental Materials, 28*(2): 113-122.

Forster, A., Ungvári, K., Györgyey, Á., Kukovecz, Á., Turzó, K., & Nagy, K. (2014). Human epithelial tissue culture study on restorative materials. *Journal of Dentistry, 42*(1): 7-14.

Foston, M., Hubbell, C., Park, D. Y., Cook, F., Tezuka, Y., & Beckham, H. W. (2012). Surface Modification by Electrostatic Self‐Assembly Followed by Covalent Fixation. *Angewandte Chemie International Edition, 51*(8): 1849-1852.

Frandsen, C. J., Brammer, K. S., Noh, K., Connelly, L. S., Oh, S., Chen, L.-H., & Jin, S. (2011). Zirconium oxide nanotube surface prompts increased osteoblast functionality and mineralization. *Materials Science and Engineering: C, 31*(8): 1716-1722.

Frandsen, C. J., Noh, K., Brammer, K. S., Johnston, G., & Jin, S. (2013). Hybrid micro/nano-topography of a TiO 2 nanotube-coated commercial zirconia femoral knee implant promotes bone cell adhesion in vitro. *Materials Science and Engineering: C, 33*(5): 2752-2756.

Gadegaard, N., Martines, E., Riehle, M., Seunarine, K., & Wilkinson, C. D. W. (2006). Applications of nano-patterning to tissue engineering. *Microelectronic Engineering, 83*(4): 1577-1581.

Gago, R., Vázquez, L., Cuerno, R., Varela, M., Ballesteros, C., & Albella, J. M. (2002). Nanopatterning of silicon surfaces by low-energy ion-beam sputtering: dependence on the angle of ion incidence. *Nanotechnology, 13*(3): 304.

Gao, C., Deng, Y., Feng, P., Mao, Z., Li, P., Yang, B., . . . Peng, S. (2014). Current progress in bioactive ceramic scaffolds for bone repair and regeneration. *International Journal of Molecular Sciences, 15*(3): 4714-4732.

Gehrke, S. A. (2013). Analysis of Bone Tissue Healing around Titanium Implant Surface Treated with Tio Sandblasted after Three and Six Weeks Used Different Histological Methods-a Study in Rabbits. *Science Journal of Medicine and Clinical Trials, 2013*.

Ghrebi, S., Hamilton, D. W., Douglas Waterfield, J., & Brunette, D. M. (2013). The effect of surface topography on cell shape and early ERK1/2 signaling in macrophages; linkage with FAK and Src. *Journal of Biomedical Materials Research Part A, 101*(7): 2118-2128.

Gittens, R. A., Olivares-Navarrete, R., Cheng, A., Anderson, D. M., McLachlan, T., Stephan, I., . . . Rupp, F. (2013). The roles of titanium surface

micro/nanotopography and wettability on the differential response of human osteoblast lineage cells. *Acta Biomaterialia, 9*(4): 6268-6277.

Golub, E. E., & Boesze-Battaglia, K. (2007). The role of alkaline phosphatase in mineralization. *Current Opinion in Orthopaedics, 18*(5): 444-448.

Goriainov, V., Cook, R., Latham, J. M., Dunlop, D. G., & Oreffo, R. O. (2014). Bone and metal: An orthopaedic perspective on osseointegration of metals. *Acta biomaterialia, 10*(10): 4043-4057.

Govindarajan, T., & Shandas, R. (2014). A survey of surface modification techniques for next-generation shape memory polymer stent devices. *Polymers, 6*(9): 2309-2331.

Griffin, M. F., Butler, P. E., Seifalian, A. M., & Kalaskar, D. M. (2015). Control of stem cell fate by engineering their micro and nanoenvironment. *World Journal of Stem Cells, 7*(1): 37.

Gristina, A. G. (1987). Biomaterial-centered infection: microbial adhesion versus tissue integration. *Science, 237*(4822): 1588-1595.

Grzelczak, M., Vermant, J., Furst, E. M., & Liz-Marzán, L. M. (2010). Directed self-assembly of nanoparticles. *ACS Nano, 4*(7): 3591-3605.

Hanawa, T. (2002). Evaluation techniques of metallic biomaterials in vitro. *Science and Technology of Advanced Materials, 3*(4): 289-295.

Hao, L., & Lawrence, J. (2003a). CO2 laser modification of the wettability characteristics of a magnesia partially stabilized zirconia bioceramic. *Journal of Physics D: Applied Physics, 36*(11): 1292.

Hao, L., & Lawrence, J. (2003b). Effects of CO 2 laser irradiation on the wettability and human skin fibroblast cell response of magnesia partially stabilised zirconia. *Materials Science and Engineering: C, 23*(5): 627-639.

Hao, L., & Lawrence, J. (2004). On the role of CO2 laser treatment in the human serum albumin and human plasma fibronectin adsorption on zirconia (MGO‐PSZ) bioceramic surface. *Journal of Biomedical Materials Research Part A, 69*(4): 748-756.

Hao, L., Ma, D. R., Lawrence, J., & Zhu, X. (2005). Enhancing osteoblast functions on a magnesia partially stabilised zirconia bioceramic by means of laser irradiation. *Materials Science and Engineering: C, 25*(4): 496-502.

Hauser-Gerspach, I., Vadaszan, J., Deronjic, I., Gass, C., Meyer, J., Dard, M., . . . Mauth, C. (2012). Influence of gaseous ozone in peri-implantitis: bactericidal efficacy and cellular response. An in vitro study using titanium and zirconia. *Clinical Oral Investigations, 16*(4): 1049-1059.

Helmer, J. D., & Driskell, T. D. (1969). *Research on bioceramics.* Paper presented at the Symposium on Use of Ceramics as Surgical Implants. South Carolina (USA): Clemson University.

Helmus, M. N., Gibbons, D. F., & Cebon, D. (2008). Biocompatibility: meeting a key functional requirement of next-generation medical devices. *Toxicologic Pathology, 36*(1): 70-80.

Hempel, U., Hefti, T., Kalbacova, M., Wolf‐Brandstetter, C., Dieter, P., & Schlottig, F. (2010). Response of osteoblast‐like SAOS‐2 cells to zirconia ceramics with different surface topographies. *Clinical Oral Implants Research, 21*(2): 174-181.

Herman, H. (1988). Plasma spray deposition processes. *MRS Bulletin, 13*(12): 60-67.

Hong, M. H., Huang, S. M., Luk'yanchuk, B. S., & Chong, T. C. (2003). Laser assisted surface nanopatterning. *Sensors and Actuators A: Physical, 108*(1): 69-74.

Hoshing, U. A., Suvarna Patil, A. M., & Bandekar, S. D. (2014). Comparison of shear bond strength of composite resin to enamel surface with laser etching versus acid etching: An in vitro evaluation. *Journal of Conservative Dentistry, 17*(4): 320.

Hsu, S. K., Hsu, H. C., Ho, W. F., Yao, C. H., Chang, P. L., & Wu, S. C. (2014). Biomolecular modification of zirconia surfaces for enhanced biocompatibility. *Thin Solid Films, 572*: 91-98.

Intranuovo, F., Favia, P., Sardella, E., Ingrosso, C., Nardulli, M., d'Agostino, R., & Gristina, R. (2010). Osteoblast-like cell behavior on plasma deposited micro/nanopatterned coatings. *Biomacromolecules, 12*(2): 380-387.

Iwaya, Y., Machigashira, M., Kanbara, K., Miyamoto, M., Noguchi, K., Izumi, Y., & Ban, S. (2008). Surface properties and biocompatibility of acid-etched titanium. *Dental Materials Journal, 27*(3): 415-421.

Jaffe, W. L., & Scott, D. F. (1996). Current concepts review-total hip arthroplasty with hydroxyapatite-coated prostheses. *Journal of Bone and Joint Surgery: American Volume, 78*(12): 1918-1934.

Jones, J. R., Gentleman, E., & Polak, J. (2007). Bioactive glass scaffolds for bone regeneration. *Elements, 3*(6): 393-399.

Jun, G., Park, K., & Webster, T. (2002). *Nanostructured and aligned scaffold material for articular cartilage regeneration.* Paper presented at the Engineering in Medicine and Biology, 2002. 24th Annual Conference and the Annual Fall Meeting of the Biomedical Engineering Society EMBS/BMES Conference, 2002. Proceedings of the Second Joint.

Kamins, T., Williams, R. S., & Basile, D. (1999). Self-aligning of self-assembled Ge islands on Si (001). *Nanotechnology, 10*(2): 117.

Kawahara, H., Hirabayashi, M., & Shikita, T. (1980). Single crystal alumina for dental implants and bone screws. *Journal of Biomedical Materials Research, 14*(5): 597-605.

Kay, S., Thapa, A., Haberstroh, K. M., & Webster, T. J. (2002). Nanostructured polymer/nanophase ceramic composites enhance osteoblast and chondrocyte adhesion. *Tissue Engineering, 8*(5): 753-761.

Khan, W. S., Rayan, F., Dhinsa, B. S., & Marsh, D. (2011). An osteoconductive, osteoinductive, and osteogenic tissue-engineered product for trauma and orthopaedic surgery: how far are we? *Stem Cells International, 2012*.

Kiang, J. D., Wen, J. H., del Álamo, J. C., & Engler, A. J. (2013). Dynamic and reversible surface topography influences cell morphology. *Journal of Biomedical Materials Research Part A, 101*(8): 2313-2321.

Kimura, Y., Matsuzaka, K., Yoshinari, M., & Inoue, T. (2012). Initial attachment of human oral keratinocytes cultured on zirconia or titanium. *Dental Materials Journal, 31*(3): 346-353.

Klinge, B., & Meyle, J. (2006). Soft‐tissue integration of implants. *Clinical Oral Implants Research, 17*(S2): 93-96.

Knosp, H., Holliday, R. J., & Corti, C. W. (2003). Gold in dentistry: alloys, uses and performance. *Gold Bulletin, 36*(3): 93-102.

Ko, H. C., Han, J.-S., Bächle, M., Jang, J. H., Shin, S. W., & Kim, D. J. (2007). Initial osteoblast-like cell response to pure titanium and zirconia/alumina ceramics. *Dental Materials, 23*(11): 1349-1355.

Kobune, K., Miura, T., Sato, T., Yotsuya, M., & Yoshinari, M. (2014). Influence of plasma and ultraviolet treatment of zirconia on initial attachment of human oral keratinocytes: Expressions of laminin γ 2 and integrin β 4. *Dental Materials Journal, 33*(5): 696-704.

Koh, Y.-G., & Choi, Y.-J. (2012). Infrapatellar fat pad-derived mesenchymal stem cell therapy for knee osteoarthritis. *The Knee, 19*(6): 902-907.

Kohal, R. J., Bächle, M., Att, W., Chaar, S., Altmann, B., Renz, A., & Butz, F. (2013). Osteoblast and bone tissue response to surface modified zirconia and titanium implant materials. *Dental Materials, 29*(7): 763-776.

Kokubo, T., Ito, S., Huang, Z. T., Hayashi, T., Sakka, S., Kitsugi, T., & Yamamuro, T. (1990). Ca, P‐rich layer formed on high‐strength bioactive glass‐ceramic A‐W. *Journal of Biomedical Materials Research, 24*(3): 331-343.

Kokubo, T., Kushitani, H., Ohtsuki, C., Sakka, S., & Yamamuro, T. (1992). Chemical reaction of bioactive glass and glass-ceramics with a simulated body fluid. *Journal of Materials Science: Materials in Medicine, 3*(2): 79-83.

Kokubo, T., & Takadama, H. (2006). How useful is SBF in predicting in vivo bone bioactivity? *Biomaterials, 27*(15): 2907-2915.

Kono, M., Aita, H., Ichioka, Y., Kado, T., Endo, K., & Koshino, H. (2015). NaOCl-mediated biofunctionalization enhances bone-titanium integration. *Dental Materials Journal, 34*(4): 537-544.

Langer, R., & Vacanti, J. P. (1993). Tissue engineering. *Science, 260*(5110): 920-926.

Langhoff, J. D., Voelter, K., Scharnweber, D., Schnabelrauch, M., Schlottig, F., Hefti, T., . . . Von Rechenberg, B. (2008). Comparison of chemically and pharmaceutically modified titanium and zirconia implant surfaces in dentistry: a study in sheep. *International Journal of Oral and Maxillofacial Surgery, 37*(12): 1125-1132.

Laranjeira, M. S., Carvalho, Â., Pelaez-Vargas, A., Hansford, D., Ferraz, M. P., Coimbra, S., . . . Monteiro, F. J. (2014). Modulation of human dermal microvascular endothelial cell and human gingival fibroblast behavior by micropatterned silica coating surfaces for zirconia dental implant applications. *Science and Technology of Advanced Materials, 15*(2): 025001.

Lau, K., & Kohn, W. (1977). Elastic interaction of two atoms adsorbed on a solid surface. *Surface Science, 65*(2): 607-618.

Lavenus, S., Berreur, M., Trichet, V., Pilet, P., Louarn, G., & Layrolle, P. (2011). Adhesion and osteogenic differentiation of human mesenchymal stem cells on titanium nanopores. *European Cells & Materials, 22*(84): e96.

Lawrence, J., & Li, L. (1999). Wettability characteristics of an Al2O3/SiO2-based ceramic modified with CO2, Nd: YAG, excimer and high-power diode lasers. *Journal of Physics D: Applied Physics, 32*(10): 1075.

Lawrence, J., & Li, L. (2001). Modification of the wettability characteristics of polymethyl methacrylate (PMMA) by means of CO 2, Nd: YAG, excimer and high power diode laser radiation. *Materials Science and Engineering: A, 303*(1): 142-149.

Lawrence, J., & Li, L. (2002). On the mechanisms of wetting characteristics modification for selected metallic materials by means of high power diode laser radiation. *Journal of Laser Applications, 14*(2): 107-113.

Lawrence, J., Li, L., & Spencer, J. T. (1999). Diode laser modification of ceramic material surface properties for improved wettability and adhesion. *Applied Surface Science, 138*: 388-393.

Lazzara, R. J., Testori, T., Trisi, P., Porter, S. S., & Weinstein, R. L. (1999). A human histologic analysis of osseotite and machined surfaces using implants with 2 opposing surfaces. *International Journal of Periodontics & Restorative Dentistry, 19*(2).

Lee, O. K., Kuo, T. K., Chen, W.-M., Lee, K.-D., Hsieh, S.-L., & Chen, T.-H. (2004). Isolation of multipotent mesenchymal stem cells from umbilical cord blood. *Blood, 103*(5): 1669-1675.

Lim, J. Y., & Donahue, H. J. (2007). Cell sensing and response to micro-and nanostructured surfaces produced by chemical and topographic patterning. *Tissue Engineering, 13*(8): 1879-1891.

Lim, J. Y., Hansen, J. C., Siedlecki, C. A., Runt, J., & Donahue, H. J. (2005). Human foetal osteoblastic cell response to polymer-demixed nanotopographic interfaces. *Journal of the Royal Society Interface, 2*(2): 97-108.

Linkevicius, T., & Apse, P. (2008). Influence of abutment material on stability of peri-implant tissues: a systematic review. *International Journal of Oral & Maxillofacial Implants, 23*(3).

Liu, X., Lim, J. Y., Donahue, H. J., Dhurjati, R., Mastro, A. M., & Vogler, E. A. (2007). Influence of substratum surface chemistry/energy and topography on the human fetal osteoblastic cell line hFOB 1.19: phenotypic and genotypic responses observed in vitro. *Biomaterials, 28*(31): 4535-4550.

Liu, X. H., Wu, L., Ai, H. J., Han, Y., & Hu, Y. (2015). Cytocompatibility and early osseointegration of nanoTiO 2-modified Ti-24 Nb-4 Zr-7.9 Sn surfaces. *Materials Science and Engineering: C, 48*: 256-262.

Liu, Y. T., Lee, T. M., & Lui, T. S. (2013). Enhanced osteoblastic cell response on zirconia by bio-inspired surface modification. *Colloids and Surfaces B: Biointerfaces, 106*: 37-45.

Losquadro, W. D., Tatum, S. A., Allen, M. J., & Mann, K. A. (2009). Polylactide-co-glycolide fiber–reinforced calcium phosphate bone cement. *Archives of Facial Plastic Surgery, 11*(2): 104-109.

Lu, W., & Sastry, A. M. (2007). Self-assembly for semiconductor industry. *IEEE Transactions on Semiconductor Manufacturing, 20*(4): 421-431.

MacManus‐Driscoll, J. L. (2010). Self‐assembled heteroepitaxial oxide nanocomposite thin film structures: designing interface‐induced functionality in electronic materials. *Advanced Functional Materials, 20*(13): 2035-2045.

Mai, R., Kunert-Keil, C., Grafe, A., Gedrange, T., Lauer, G., Dominiak, M., & Gredes, T. (2012). Histological behaviour of zirconia implants: an experiment in rats. *Annals of Anatomy-Anatomischer Anzeiger, 194*(6): 561-566.

Marsico, V., Blanc, M., Kuhnke, K., & Kern, K. (1997). Discrete row growth at vicinal surfaces. *Physical Review Letters, 78*(1): 94.

Mendes, P. M., Jacke, S., Critchley, K., Plaza, J., Chen, Y., Nikitin, K., . . . Fitzmaurice, D. (2004). Gold nanoparticle patterning of silicon wafers using chemical e-beam lithography. *Langmuir, 20*(9): 3766-3768.

Mendonça, G., Mendonça, D. B., Aragao, F. J., & Cooper, L. F. (2008). Advancing dental implant surface technology–from micron-to nanotopography. *Biomaterials, 29*(28): 3822-3835.

Meyers, M. A., Mishra, A., & Benson, D. J. (2006). Mechanical properties of nanocrystalline materials. *Progress in Materials Science, 51*(4): 427-556.

Mills, A., & Crow, M. (2008). A study of factors that change the wettability of titania films. *International Journal of Photoenergy*.

Morra, M. (2006). Biochemical modification of titanium surfaces: peptides and ECM proteins. *European Cells & Materials, 12*: 1-15.

Munz, D., & Fett, T. (2013). *Ceramics: mechanical properties, failure behaviour, materials selection* (Vol. 36): Springer Science & Business Media.

Namgung, S., Baik, K. Y., Park, J., & Hong, S. (2011). Controlling the growth and differentiation of human mesenchymal stem cells by the arrangement of individual carbon nanotubes. *ACS Nano, 5*(9): 7383-7390.

Navarro-Garcia, F., Serapio-Palacios, A., Ugalde-Silva, P., Tapia-Pastrana, G., & Chavez-Dueñas, L. (2012). Actin cytoskeleton manipulation by effector proteins secreted by diarrheagenic Escherichia coli pathotypes. *BioMed Research International, 2013*.

NIH. (1982). Clinical applications of biomaterials. *NIH Consensus Statement, 4*(5): 1-19.

Niinomi, M. (2008). Metallic biomaterials. *Journal of Artificial Organs, 11*(3): 105-110.

Niu, Z., Ansari, H. M., Chowdhury, E. A., Dregia, S. A., & Akbar, S. A. (2017). Step faceting and the self-assembly of nanoislands on miscut YSZ(001) surfaces. *Applied Surface Science, 407*: 192-196.

Nothdurft, F. P., Fontana, D., Ruppenthal, S., May, A., Aktas, C., Mehraein, Y., . . . Kaestner, L. (2015). Differential behavior of fibroblasts and epithelial cells on structured implant abutment materials: a comparison of materials and surface topographies. *Clinical Implant Dentistry and Related Research, 17*(6): 1237-1249.

O'Brien, F. J. (2011). Biomaterials & scaffolds for tissue engineering. *Materials Today, 14*(3): 88-95.

Oakes, P. W., & Gardel, M. L. (2014). Stressing the limits of focal adhesion mechanosensitivity. *Current Opinion in Cell Biology, 30*: 68-73.

Ogawa, R., Ogawa, H., Oki, A., Hashioka, S., & Horiike, Y. (2007). Fabrication of nano-pillar chips by a plasma etching technique for fast DNA separation. *Thin Solid Films, 515*(12): 5167-5171.

Ogawa, T. (2014). Ultraviolet photofunctionalization of titanium implants. *International Journal of Oral & Maxillofacial Implants, 29*(1).

Oh, S., Daraio, C., Chen, L. H., Pisanic, T. R., Finones, R. R., & Jin, S. (2006). Significantly accelerated osteoblast cell growth on aligned TiO2 nanotubes. *Journal of Biomedical Materials Research Part A, 78*(1): 97-103.

Omar, O., Lennerås, M., Svensson, S., Suska, F., Emanuelsson, L., Hall, J., . . . Thomsen, P. (2010). Integrin and chemokine receptor gene expression in implant-adherent cells during early osseointegration. *Journal of Materials Science: Materials in Medicine, 21*(3): 969-980.

Pae, A., Lee, H., Kim, H. S., Kwon, Y. D., & Woo, Y. H. (2009). Attachment and growth behaviour of human gingival fibroblasts on titanium and zirconia ceramic surfaces. *Biomedical Materials, 4*(2): 025005.

Pae, A., Lee, H., Noh, K., & Woo, Y. H. (2014). Cell attachment and proliferation of bone marrow-derived osteoblast on zirconia of various surface treatment. *The Journal of Advanced Prosthodontics, 6*(2): 96-102.

Pardun, K., Treccani, L., Volkmann, E., Li Destri, G., Marletta, G., Streckbein, P., . . . Rezwan, K. (2015). Characterization of Wet Powder‐Sprayed Zirconia/Calcium Phosphate Coating for Dental Implants. *Clinical Implant Dentistry and Related Research, 17*(1): 186-198.

Pardun, K., Treccani, L., Volkmann, E., Streckbein, P., Heiss, C., Destri, G. L., . . . Rezwan, K. (2015). Mixed zirconia calcium phosphate coatings for dental implants: tailoring coating stability and bioactivity potential. *Materials Science and Engineering: C, 48*: 337-346.

Parikh, K., Rao, S., Ansari, H., Zimmerman, L., Lee, L., Akbar, S., & Winter, J. (2012). Ceramic nanopatterned surfaces to explore the effects of nanotopography on cell attachment. *Materials Science and Engineering: C, 32*(8): 2469-2475.

Park, J., & Lakes, R. S. (2007). *Biomaterials: an introduction*. New York: Springer Science & Business Media.

Park, J. Y., Shin, D. H., Choi, J. S., & Kim, K. H. (2013). Metallic discoloration on the right shin caused by titanium alloy prostheses in a patient with right total knee replacement. *Annals of Dermatology, 25*(3): 356-359.

Pelaez-Vargas, A., Gallego-Perez, D., Magallanes-Perdomo, M., Fernandes, M. H., Hansford, D. J., De Aza, A. H., . . . Monteiro, F. J. (2011). Isotropic micropatterned silica coatings on zirconia induce guided cell growth for dental implants. *Dental Materials, 27*(6): 581-589.

Peng, F., Wu, H., Zheng, Y., Xu, X., & Yu, J. (2012). The effect of noncoherent red light irradiation on proliferation and osteogenic differentiation of bone marrow mesenchymal stem cells. *Lasers in Medical Science, 27*(3): 645-653.

Pettit, R. K., Weber, C. A., Kean, M. J., Hoffmann, H., Pettit, G. R., Tan, R., . . . Horton, M. L. (2005). Microplate Alamar blue assay for Staphylococcus epidermidis biofilm susceptibility testing. *Antimicrobial Agents and Chemotherapy, 49*(7): 2612-2617.

Piconi, C., & Maccauro, G. (1999). Zirconia as a ceramic biomaterial. *Biomaterials, 20*(1): 1-25.

Pimpin, A., & Srituravanich, W. (2011). Review on micro-and nanolithography techniques and their applications. *Engineering Journal, 16*(1): 37-56.

Planell, J. A., Best, S. M., Lacroix, D., & Merolli, A. (2009). *Bone repair biomaterials*. North America: CRC Press.

Polini, A., Pisignano, D., Parodi, M., Quarto, R., & Scaglione, S. (2011). Osteoinduction of human mesenchymal stem cells by bioactive composite scaffolds without supplemental osteogenic growth factors. *PloS One, 6*(10): e26211.

Prittinen, J., Jiang, Y., Ylärinne, J. H., Pakkanen, T. A., Lammi, M. J., & Qu, C. (2014). Chondrocyte behavior on nanostructured micropillar polypropylene and polystyrene surfaces. *Materials Science and Engineering: C, 43*: 424-431.

Psarra, E., König, U., Ueda, Y., Bellmann, C., Janke, A., Bittrich, E., . . . Uhlmann, P. (2015). Nanostructured biointerfaces: nanoarchitectonics of thermoresponsive polymer brushes impact protein adsorption and cell adhesion. *ACS Applied Materials & Interfaces, 7*(23): 12516-12529.

Rauscher, M. D., Boyne, A., Dregia, S. A., & Akbar, S. A. (2008). Self‐Assembly of Pseudoperiodic Arrays of Nanoislands on YSZ‐(001). *Advanced Materials, 20*(9): 1699-1705.

Röder, H., Brune, H., Bucher, J.-P., & Kern, K. (1993). Changing morphology of metallic monolayers via temperature controlled heteroepitaxial growth. *Surface Science, 298*(1): 121-126.

Rubinstein, A. I., Sabirianov, R. F., & Namavar, F. (2014). Enhanced cell growth by nanoengineering zirconia to stimulate electrostatic fibronectin activation. *Nanotechnology, 25*(6): 065101.

Ruoslahti, E., & Pierschbacher, M. D. (1987). New perspectives in cell adhesion: RGD and integrins. *Science, 238*(4826): 491-497.

Sabir, M. I., Xu, X., & Li, L. (2009). A review on biodegradable polymeric materials for bone tissue engineering applications. *Journal of Materials Science, 44*(21): 5713-5724.

Salernitano, E., & Migliaresi, C. (2003). Composite materials for biomedical applications: a review. *Journal of Applied Biomaterials & Biomechanics, 1*(1): 3-18.

Sammons, R. L., Lumbikanonda, N., Gross, M., & Cantzler, P. (2005). Comparison of osteoblast spreading on microstructured dental implant surfaces and cell behaviour in an explant model of osseointegration. *Clinical Oral Implants Research, 16*(6): 657-666.

Sandhaus, S. (1967). Bone implants and drills and taps for bone surgery. *British Patent, 1*(083): 769.

Sandhyarani, M., Rameshbabu, N., & Venkateswarlu, K. (2014). Fabrication, characterization and in-vitro evaluation of nanostructured zirconia/hydroxyapatite composite film on zirconium. *Surface and Coatings Technology, 238*: 58-67.

Sansone, V., Pagani, D., & Melato, M. (2013). The effects on bone cells of metal ions released from orthopaedic implants. A review. *Clinical Cases in Mineral and Bone Metabolism, 10*(1): 34-40.

Sartoretto, S. C., Alves, A. T. N. N., Resende, R. F. B., Calasans-maia, J., Granjeiro, J. M., & Calasans-maia, M. D. (2015). Early osseointegration driven by the surface chemistry and wettability of dental implants. *Journal of Applied Oral Science, 23*(3): 279-287.

Sawase, T., Jimbo, R., Baba, K., Shibata, Y., Ikeda, T., & Atsuta, M. (2008). Photo‐induced hydrophilicity enhances initial cell behavior and early bone apposition. *Clinical Oral Implants Research, 19*(5): 491-496.

Schwarz, F., Herten, M., Sager, M., Wieland, M., Dard, M., & Becker, J. (2007). Histological and immunohistochemical analysis of initial and early osseous integration at chemically modified and conventional SLA® titanium implants: Preliminary results of a pilot study in dogs. *Clinical Oral Implants Research, 18*(4): 481-488.

Sennerby, L., Dasmah, A., Larsson, B., & Iverhed, M. (2005). Bone Tissue Responses to Surface‐Modified Zirconia Implants: A Histomorphometric and Removal Torque Study in the Rabbit. *Clinical Implant Dentistry and Related Research, 7*(s1): s13-s20.

She, H., & Wang, B. (2009). Analysis of the Vertical and Lateral Interactions in a Multisheet Array of InAs/GaAs Quantum Dots. *Journal of Materials Science & Technology*(25): 677-680.

Sheikh, Z., Najeeb, S., Khurshid, Z., Verma, V., Rashid, H., & Glogauer, M. (2015). Biodegradable materials for bone repair and tissue engineering applications. *Materials, 8*(9): 5744-5794.

Shetty, S., Puthukkat, N., Bhat, S. V., & Shenoy, K. K. (2014). Short implants: A new dimension in rehabilitation of atrophic maxilla and mandible. *Journal of Interdisciplinary Dentistry, 4*(2): 66.

Shoichet, M. S. (2009). Polymer scaffolds for biomaterials applications. *Macromolecules, 43*(2): 581-591.

Shu, Y., Ou, G., Wang, L., Zou, J., & Li, Q. (2011). Surface modification of titanium with heparin-chitosan multilayers via layer-by-layer self-assembly technique. *Journal of Nanomaterials, 2011*: 2.

Šimůnek, A., Kopecká, D., & Strnad, J. (2004). Reduced healing time of Impladent Implants. *Quintessenz, 13*.

Sjöström, T., Dalby, M. J., Hart, A., Tare, R., Oreffo, R. O., & Su, B. (2009). Fabrication of pillar-like titania nanostructures on titanium and their interactions with human skeletal stem cells. *Acta Biomaterialia, 5*(5): 1433-1441.

Sjöström, T., Lalev, G., Mansell, J. P., & Su, B. (2011). Initial attachment and spreading of MG63 cells on nanopatterned titanium surfaces via through-mask anodization. *Applied Surface Science, 257*(10): 4552-4558.

Smith, L. (1963). Ceramic-plastic material as a bone substitute. *Archives of Surgery, 87*(4): 653-661.

Song, Y. G., & Cho, I. H. (2014). Characteristics and osteogenic effect of zirconia porous scaffold coated with β-TCP/HA. *The Journal of Advanced Prosthodontics, 6*(4): 285-294.

Soon, G., Pingguan-Murphy, B., Lai, K. W., & Akbar, S. A. (2016). Review of zirconia-based bioceramic: Surface modification and cellular response. *Ceramics International, 42*(11): 12543-12555.

Stadlinger, B., Hennig, M., Eckelt, U., Kuhlisch, E., & Mai, R. (2010). Comparison of zirconia and titanium implants after a short healing period. A pilot study in minipigs. *International Journal of Oral and Maxillofacial Surgery, 39*(6): 585-592.

Stanic, V., Aldini, N. N., Fini, M., Giavaresi, G., Giardino, R., Krajewski, A., . . . Bossi, M. P. (2002). Osteointegration of bioactive glass-coated zirconia in healthy bone: an in vivo evaluation. *Biomaterials, 23*(18): 3833-3841.

Su, Y. F., Lin, C. C., Huang, T. H., Chou, M. Y., Yang, J. J., & Shie, M. Y. (2014). Osteogenesis and angiogenesis properties of dental pulp cell on novel injectable tricalcium phosphate cement by silica doped. *Materials Science and Engineering: C, 42*: 672-680.

Tan, A., Dalilottojari, A., Pingguan-Murphy, B., Ahmad, R., & Akbar, S. (2014). In vitro chondrocyte interactions with TiO 2 nanofibers grown on Ti–6Al–4V substrate by oxidation. *Ceramics International, 40*(6): 8301-8304.

Tang, J., Peng, R., & Ding, J. (2010). The regulation of stem cell differentiation by cell-cell contact on micropatterned material surfaces. *Biomaterials, 31*(9): 2470-2476.

Tengvall, P., & Lundström, I. (1992). Physico-chemical considerations of titanium as a biomaterial. *Clinical Materials, 9*(2): 115-134.

Teo, A. J. T., Mishra, A., Park, I., Kim, Y. J., Park, W. T., & Yoon, Y. J. (2016). Polymeric Biomaterials for Medical Implants and Devices. *ACS Biomaterials Science & Engineering, 2*(4): 454-472.

Tiwari, A., & Nordin, A. N. (2014). *Advanced biomaterials and biodevices*. New Jersey: John Wiley & Sons.

Torricelli, P., Verné, E., Brovarone, C. V., Appendino, P., Rustichelli, F., Krajewski, A., . . . Giavaresi, G. (2001). Biological glass coating on ceramic materials: in vitro evaluation using primary osteoblast cultures from healthy and osteopenic rat bone. *Biomaterials, 22*(18): 2535-2543.

Tran, P. A., Sarin, L., Hurt, R. H., & Webster, T. J. (2009). Opportunities for nanotechnology-enabled bioactive bone implants. *Journal of Materials Chemistry, 19*(18): 2653-2659.

Tredici, I. G., Sebastiani, M., Massimi, F., Bemporad, E., Resmini, A., Merlati, G., & Anselmi-Tamburini, U. (2016). Low temperature degradation resistant nanostructured yttria-stabilized zirconia for dental applications. *Ceramics International, 42*(7): 8190-8197.

Tuna, T., Wein, M., Swain, M., Fischer, J., & Att, W. (2015). Influence of ultraviolet photofunctionalization on the surface characteristics of zirconia-based dental implant materials. *Dental Materials, 31*(2): e14-e24.

Ueno, T., Tsukimura, N., Yamada, M., & Ogawa, T. (2011). Enhanced bone-integration capability of alkali-and heat-treated nanopolymorphic titanium in micro-to-nanoscale hierarchy. *Biomaterials, 32*(30): 7297-7308.

Wan, Y., Hu, D., Xiong, G., Li, D., Guo, R., & Luo, H. (2015). Directional fluid induced self-assembly of oriented bacterial cellulose nanofibers for potential biomimetic tissue engineering scaffolds. *Materials Chemistry and Physics, 149*: 7-11.

Wang, J., & Shaw, L. L. (2009). Nanocrystalline hydroxyapatite with simultaneous enhancements in hardness and toughness. *Biomaterials, 30*(34): 6565-6572.

Weiss, P. (1945). Experiments on cell and axon orientation in vitro: the role of colloidal exudates in tissue organization. *Journal of Experimental Zoology, 100*(3): 353-386.

Wennerberg, A., & Albrektsson, T. (2009). Effects of titanium surface topography on bone integration: a systematic review. *Clinical Oral Implants Research, 20*(s4): 172-184.

Whitesides, G. M., & Grzybowski, B. (2002). Self-assembly at all scales. *Science, 295*(5564): 2418-2421.

Williams, D. F. (2009). On the nature of biomaterials. *Biomaterials, 30*(30): 5897-5909.

Wilson, C. J., Clegg, R. E., Leavesley, D. I., & Pearcy, M. J. (2005). Mediation of biomaterial-cell interactions by adsorbed proteins: a review. *Tissue Engineering, 11*(1-2): 1-18.

Wozniak, M. A., Modzelewska, K., Kwong, L., & Keely, P. J. (2004). Focal adhesion regulation of cell behavior. *Biochimica et Biophysica Acta (BBA)-Molecular Cell Research, 1692*(2): 103-119.

Xin, X., Hussain, M., & Mao, J. J. (2007). Continuing differentiation of human mesenchymal stem cells and induced chondrogenic and osteogenic lineages in electrospun PLGA nanofiber scaffold. *Biomaterials, 28*(2): 316-325.

Yang, B., Liu, F., & Lagally, M. G. (2004). Local strain-mediated chemical potential control of quantum dot self-organization in heteroepitaxy. *Physical Review Letters, 92*(2): 025502.

Yang, Y., Kim, K. H., & Ong, J. L. (2005). A review on calcium phosphate coatings produced using a sputtering process—an alternative to plasma spraying. *Biomaterials, 26*(3): 327-337.

Yasuno, K., Kakura, K., Taniguchi, Y., Yamaguchi, Y., & Kido, H. (2014). Zirconia implants with laser surface treatment: peri-implant bone response and enhancement of osseointegration. *Journal of Hard Tissue Biology, 23*(1): 93-100.

Yim, E. K., Darling, E. M., Kulangara, K., Guilak, F., & Leong, K. W. (2010). Nanotopography-induced changes in focal adhesions, cytoskeletal organization, and mechanical properties of human mesenchymal stem cells. *Biomaterials, 31*(6): 1299-1306.

You, M.-H., Kwak, M. K., Kim, D.-H., Kim, K., Levchenko, A., Kim, D.-Y., & Suh, K.-Y. (2010). Synergistically enhanced osteogenic differentiation of human mesenchymal stem cells by culture on nanostructured surfaces with induction media. *Biomacromolecules, 11*(7): 1856-1862.

Yugeswaran, S., Yoganand, C. P., Kobayashi, A., Paraskevopoulos, K. M., & Subramanian, B. (2012). Mechanical properties, electrochemical corrosion and in-vitro bioactivity of yttria stabilized zirconia reinforced hydroxyapatite coatings prepared by gas tunnel type plasma spraying. *Journal of the Mechanical Behavior of Biomedical Materials, 9*: 22-33.

Zeng, H., & Lacefield, W. R. (2000). The study of surface transformation of pulsed laser deposited hydroxyapatite coatings. *Journal of Biomedical Materials Research, 50*(2): 239-247.

Zhang, B., Kwok, C. T., Cheng, F. T., & Man, H. C. (2011). Fabrication of nano-structured HA/CNT coatings on Ti6Al4V by electrophoretic deposition for biomedical applications. *Journal of Nanoscience and Nanotechnology, 11*(12): 10740-10745.

Zhao, G., Schwartz, Z., Wieland, M., Rupp, F., Geis‐Gerstorfer, J., Cochran, D. L., & Boyan, B. D. (2005). High surface energy enhances cell response to titanium substrate microstructure. *Journal of Biomedical Materials Research Part A, 74*(1): 49-58.

Zhao, L., Liu, L., Wu, Z., Zhang, Y., & Chu, P. K. (2012). Effects of micropitted/nanotubular titania topographies on bone mesenchymal stem cell osteogenic differentiation. *Biomaterials, 33*(9): 2629-2641.

Zhao, P., Zhao, S., Zhao, T. R., Ren, X. H., Wang, F., & Chen, X. N. (2012). *Hydroxyapatite whisker effect on strength of calcium phosphate bone cement.* Paper presented at the Advanced Materials Research.

Zheng, C. Y., Nie, F. L., Zheng, Y. F., Cheng, Y., Wei, S. C., & Valiev, R. Z. (2011). Enhanced in vitro biocompatibility of ultrafine-grained titanium with hierarchical porous surface. *Applied Surface Science, 257*(13): 5634-5640.

Zhong, D., Hirtz, M., Wang, W., Dou, R., Chi, L., & Fuchs, H. (2008). Kinetics of island formation in organic film growth. *Physical Review B, 77*(11): 113404.

Zhong, J., & Greenspan, D. C. (2000). Processing and properties of sol–gel bioactive glasses. *Journal of Biomedical Materials Research, 53*(6): 694-701.

Zimmerman, L. B., Rauscher, M., Ellis, J., Boukany, P., & Lee, L. J. (2009). Nanoimprinting using self-assembled ceramic nanoislands. *Nanotechnology, 21*(4): 045304.

LIST OF PUBLICATIONS

1. Soon, G., Pingguan-Murphy, B., Lai, K. W., & Akbar, S. A. (2016). Review of zirconia-based bioceramic: Surface modification and cellular response. *Ceramics International*, *42*(11), 12543-12555.
2. Soon, G., Pingguan-Murphy, B., & Akbar, S. A. (2017). Modulation of osteoblast behavior on nanopatterned yttria-stabilized zirconia surfaces. *Journal of the Mechanical Behavior of Biomedical Materials*, *68*, 26-31.